



ISSN 1854-0171

ACTA GEOTECHNICA SLOVENICA

2015/1
VOL. 12

- A three-dimensional static numerical model of a complex underground structure in high squeezing ground
- Influence of the virtual strain rate of non-cohesive granular media on the discrete element method
- Implementation and verification of a geosynthetic-soil interface constitutive model in the Geogrid element of FLAC_{3D}
- Analysis of a dilatometer test in over-consolidated sediments, basin of the Duero river, Spain
- Relationship between the compressive and tensile strengths of lime-treated clay containing coconut fibres
- New computational models for better predictions of the soil-compression index



Ustanovitelji

Founders

Univerza v Mariboru, Fakulteta za gradbeništvo
University of Maribor, Faculty of Civil Engineering

Univerza v Ljubljani, Fakulteta za gradbeništvo in geodezijo
University of Ljubljana, Faculty of Civil and Geodetic Engineering

Univerza v Ljubljani, Naravoslovnotehniška fakulteta
University of Ljubljana, Faculty of Natural Sciences and Engineering
Slovensko geotehniško društvo
Slovenian Geotechnical Society

Društvo za podzemne in geotehniške konstrukcije
Society for Underground and Geotechnical Constructions

Izdajatelj

Publisher

Univerza v Mariboru, Fakulteta za gradbeništvo
University of Maribor, Faculty of Civil Engineering

Odgovorni urednik

Editor-in-Chief

Bojana Dolinar University of Maribor

Uredniki

Co-Editors

Jakob Likar	University of Ljubljana
Janko Logar	University of Ljubljana
Borut Macuh	University of Maribor
Ana Petkovšek	University of Ljubljana
Stanislav Škrabl	University of Maribor
Bojan Žlender	University of Maribor

Posvetovalni uredniki

Advisory Editors

Heinz Brandl	Vienna University of Technology
Chandrakant. S. Desai	University of Arizona
Pedro Seco e Pinto	National Laboratory of Civil Engineering

Lektor

Proof-Reader

Paul McGuinness

Naklada

Circulation

300 izvodov - issues

Cena

Price

25 EUR/letnik - 25 EUR/vol.; (50 EUR for institutions/za institucije)

Tisk

Print

Tiskarna Saje

Revija redno izhaja dvakrat letno. Članki v reviji so recenzirani s strani priznanih mednarodnih strokovnjakov. Baze podatkov v katerih je revija indeksirana: SCIE - Science Citation Index Expanded, JCR - Journal Citation Reports / Science Edition, ICONDA - The international Construction database, GeoRef. Izid publikacije je finančno podprla Javna agencija za raziskovalno dejavnost Republike Slovenije iz naslova razpisa za sofinanciranje domačih periodičnih publikacij.

Uredniški odbor

Editorial Board

Amin Barari	Aalborg University
Theodoros Hatzigogos	Aristotle University of Thessaloniki
Vojkan Jovičič	IRGO-Ljubljana, President of the SloGeD
Rolf Katzenbach	Technical University Darmstadt
Nasser Khalili	The University of New South Wales, Sydney
Bojan Majes	University of Ljubljana
Svetlana Melentijevic	RodioKronsa, Soletanche-Bachy Group, Spain
Borut Petkovšek	Slovenian National Building and Civil Engineering Institute
Mihael Ribičič	University of Ljubljana
César Sagaseta	University of Cantabria
Patrick Selvadurai	McGill University
Stephan Semprich	University of Technology Graz
Devendra Narain Singh	Indian Institute of Technology, Bombay
Abdul-Hamid Soubra	University of Nantes
Kiichi Suzuki	Saitama University
Antun Szavits-Nossan	University of Zagreb
Kosta Urumović	Croatian geological survey
Ivan Vaniček	Czech Technical University in Prague

Naslov uredništva

Address

ACTA GEOTECHNICA SLOVENICA
Univerza v Mariboru, Fakulteta za gradbeništvo
Smetanova ulica 17, 2000 Maribor, Slovenija
Telefon / Telephone: +386 (0)2 22 94 300
Faks / Fax: +386 (0)2 25 24 179
E-pošta / E-mail: ags@uni-mb.si

Spletni naslov

web Address

<http://www.fg.uni-mb.si/journal-ags/>

The journal is published twice a year. Papers are peer reviewed by renowned international experts. Indexation data bases of the journal: SCIE - Science Citation Index Expanded, JCR - Journal Citation Reports / Science Edition, ICONDA - The international Construction database, GeoRef. The publication was financially supported by Slovenian Research Agency according to the Tender for co-financing of domestic periodicals.

Uvodnik	Editorial	2
<i>T. M. Čebašek & J. Likar</i> Tridimenzionalni statični numerični model kompleksnega podzemnega objekta v zelo iztisljivi hribini	<i>T. M. Čebašek & J. Likar</i> A three-dimensional static numerical model of a complex underground structure in high squeezing ground	4
<i>K. Suzuki</i> Vpliv virtualne stopnje specifične deformacije nekohezivnega zrnatega medija na metodo diskretnih elementov	<i>K. Suzuki</i> Influence of the virtual strain rate of non-cohesive granular media on the discrete element method	16
<i>W. Haimin in drugi</i> Implementacija in verifikacija kon- stitutivnega modela vmesne plo- skve geosintetik-zemljina v ele- mentu Geogrid programa FLAC ^{3D}	<i>W. Haimin et al.</i> Implementation and verification of a geosynthetic-soil interface constitutive model in the Geogrid element of FLAC ^{3D}	26
<i>F. E. Sánchez</i> Analiza preiskave z dilato- metrom v prekonsolidiranih sedimentih, kotlina reke Duero v Španiji	<i>F. E. Sánchez</i> Analysis of a dilatometer test in over-consolidated sediments, basin of the Duero river, Spain	36
<i>V. Anggraini et al.</i> Povezava med tlačno in natezno trdnostjo z apnom obdelanih glin, ki vsebujejo kokosova vlakna	<i>V. Anggraini et al.</i> Relationship between the compressive and tensile strengths of lime-treated clay containing coconut fibres	48
<i>A. Demir</i> Novi računski model za boljše napoved kompresijskega indeksa zemljine	<i>A. Demir</i> New computational models for better predictions of the soil-compression index	58
Navodila avtorjem	Instructions for authors	70

Neposredno pred izdajo decembrske številke revije Acta Geotechnica Slovenica smo prejeli žalostno vest o smrti prof.dr. Milana Maksimovića, člana uredniškega odbora revije AGS od začetka njenega izhajanja. Prof. Maksimović je s kritičnimi recenzijami prispevkov veliko doprinesel h kvaliteti revije. V zahvalo mu zato posvečamo ta Uvodnik, v katerem podajamo kratek oris njegovega dela. Posredovali so nam ga prijatelji prof. Maksimovića, prof.dr. Ludvik Trauner, prof.dr. Radomir Folić in dr. Nenad Šušić.



Prof. Maksimović se je rodil leta 1941 v Mladenovu v Srbiji. Po zaključeni Gradbeni fakulteti se je leta 1965 zaposlil v podjetju Energo-projekt-hidroinženiring, biroju za geotehniko. Specializiral se je za inženirsko seizmologijo, znanje s tega področja pa pridobival na Politehniko v Milanu in na Inštitutu za preskušanje modelov in konstrukcij v Bergamu. Magistriral je na

Imperial College v Londonu leta 1971. V okviru doktorskega raziskovanja je kot Fulbright-ov štipendist leta 1975 opravil specializacijo za numerične metode v geotehniko na Ohio State University v Columbus-u. Leta 1978 je doktoriral na Fakulteti gradbenih znanosti v Zagrebu pod mentorstvom prof.dr. Ervina Nonveiller-ja, leto kasneje pa se zaposlil na Gradbeni fakulteti v Beogradu. Zaradi svoje izjemne sposobnosti je hitro napredoval do naziva rednega profesorja za predmet Mehanika tal. Vse do upokojitve leta 2006 je bil predstojnik Katedre za gradbeno geotehniko.

Ukvarjal se je s temeljnimi vidiki mehanike zemljin in kamnin, temeljenjem inženirskih objektov, sanacijami plazov, projektiranjem zemeljskih nasipov in številnimi drugimi geotehničnimi problemi. Sodeloval je v velikem številu pomembnih projektov in pri izdelavi različnih izvedenskih mnenj doma in v tujini (Egipt, Jordanija, Libija, Gvajana, Gabon, Irak, Zambija, Zimbabve, Tanzanija, Turčija, Peru, Dubaj). Bil je dolgoletni predsednik Srbskega društva za mehaniko tal in geotehniško inženirstvo ter aktivni član v Zvezi gradbenih inženirjev Srbije. Znana je njegova knjiga Mehanika tal. Njen prvi natis je zagledal luč sveta 1995, peti leta 2014. Je avtor velikega števila objavljenih in citiranih strokovnih in

znanstvenih prispevkov v domačih in tujih publikacijah. Bil je odličen programer in avtor mnogih programskih paketov z uporabnostjo v širokem spektru geotehniškega inženirstva.

Profesor Maksimović je bil velik strokovnjak, znanstvenik in univerzitetni učitelj, ki je s svojo pronicljivo kritično mislijo več desetletij bogatil mednarodno gradbeno in geotehniško sfero. Njegov doprinos in območje delovanja na področju geotehniko visoko cenijo ugledni strokovnjaki.

Prof.dr. Milan Maksimović je umrl 15. novembra v Beogradu. Dne 24. novembra 2014 je bil posmrtno promoviran za Rednega člana Inženirske akademije Srbije.

Bojana Dolinar
Glavna urednica

Just before the publication of the December issue of *Acta Geotechnica Slovenica* we received the sad news about the death of Prof. Dr Milan Maksimović, a member of our Editorial board from the very first publication. Prof. Maksimović made significant contributions to the quality of the journal with his critical reviews. Therefore, we would like to devote this editorial to him. His friends, Prof. Dr Ludvik Trauner, Prof. Dr Radomir Folić and Dr Nenad Šušić, contributed a short overview of his work.



Prof. Maksimović was born in 1941 in Mladenovo, Serbia. After graduating from the Faculty of Civil Engineering, he joined the company Energoprojekt-hidroinženiring, in the office for geotechnics, in 1965. During his specialization in engineering seismology, he developed his knowledge at Polytechnics in Milan and at the Institute for Model and Structural

Testing in Bergamo. He obtained his Master's degree from Imperial College in London in 1971. As part of his doctoral research he specialized in numerical methods in geotechnics at Ohio State University in Columbus as a Fulbright scholar in 1975. In 1978 he graduated from the Faculty of Civil Engineering in Zagreb with a doctorate under the mentorship of Prof. Dr Ervin Nonveiller, and a year later he was employed at the Faculty of Civil Engineering in Belgrade. Due to his exceptional talents he was rapidly promoted to Professor for Soil Mechanics. Until his retirement in 2006, he was the Head of the Chair for Construction Geotechnics.

He was involved in the basic perspectives of soil and stone mechanics, the foundation of engineering objects, landslide sanitation, the design of earth dikes and many other geotechnical problems. He cooperated in numerous important projects and provided various expert opinions at home and worldwide (Egypt, Jordan, Libya, Guiana, Gabon, Iraq, Zambia, Zimbabwe, Tanzania, Turkey, Peru, and Dubai). He was a president of the Serbian Society for Soil Mechanics and Geotechnical Engineering for many years and an active member of Serbian Association of Civil Engineers. His renowned book *Soil Mechanics* was first published in 1995, with the fifth edition in 2014. He is the author of numerous published and cited technical

and scientific articles in domestic and foreign publications. He was an excellent programmer and the author of many software packages, applicable to a wide spectrum of geotechnical engineering.

Prof. Maksimović was a superb expert, scientist and university teacher, who was improving the international construction and geotechnical sphere for decades. His contribution and activity in geotechnics is highly respected by distinguished experts.

Prof. Dr Milan Maksimović died on 15 November 2014 in Belgrade. He was posthumously promoted to be a regular member of the Academy of Engineering Sciences of Serbia on 24 November 2014.

Bojana Dolinar
Editor-in-chief

TRIDIMENZIONALNI STATIČNI NUMERIČNI MODEL KOMPLEKSNEGA PODZEMNEGA OBJEKTA V ZELO IZTISLJIVI HRIBINI

Tina Marolt Čebašek (vodilni avtor)

Univerza v Ljubljani,
Naravoslovnotehniška fakulteta
Aškerčeva 12, 1000 Ljubljana, Slovenija
E-pošta: tina.marolt@ogr.ntf.uni-lj.si

Jakob Likar

Univerza v Ljubljani,
Naravoslovnotehniška fakulteta
Aškerčeva 12, 1000 Ljubljana, Slovenija
E-pošta: jakob.likar@ogr.ntf.uni-lj.si

Ključne besede

zelo iztisljiva hribina, numerični model, podzemni objekti, deformacije, popustljiv podporni element

Izvleček

V predstavljeni raziskavi je ocena zelo iztisljive hribine potrjena tako z empiričnimi kot polempiričnimi teorijami. Zelo iztisljive hribine so pogosto prisotne v geološki zgradbi skupaj z malo do srednje iztisljivimi plastmi, v katerih poteka gradnja podzemnih prostorov v večjih globinah, zato izvedene raziskave geomehanskih lastnosti niso ločene za vsako hribinsko kategorijo posebej. Da bi bili ugotovljeni temeljni geomehanski vplivi med vertikalnim jaškom, silosom in dovozno jamsko progo, je bil izdelan tridimenzionalni statični numerični model za kompleksen sistem navedenih podzemnih prostorov, ki se nahaja v večji globini v zelo iztisljivih hribinskih plasteh. Za zagotovitev stabilnih razmer gradnje kompleksnega sistema podzemnih prostorov je bil v 3D-modelu upoštevan podporni sistem iz obloge iz brizganega betona z vključenimi popustljivimi elementi. Ti so v splošnem dovolj popustljivi, da absorbirajo deformacijsko energijo s stiskanjem pri relativno konstantni napetosti in nepovratni deformaciji. S 3D-simulacijo izkopa in vgradnje podpornih elementov, ki je upoštevala popustljiv podporni sistem, je bilo dokazano, da reaktivne sile v popustljivem podpornem sistemu ustrezajo še dovoljenim pomikom ostenja analiziranih podzemnih prostorov. Rezultati poglobljenih geomehanskih simulacij obnašanja kompleksa podzemnih objektov v zelo iztisljivi hribini so osnova za pravočasno ukrepanje pri povečanih deformacijah za preprečitev porušitve obloge iz brizganega betona. Analize, ki so bile narejene s poudarkom na medsebojnem učinkovanju med popustljivimi elementi in oblogo iz brizganega betona v zelo iztisljivem hribinskem mediju, so osnova za izvedbo kakovostnega načrtovanja kompleksnih podzemnih prostorov v zelo zahtevnih geotehničnih razmerah.

A THREE-DIMENSIONAL STATIC NUMERICAL MODEL OF A COMPLEX UNDER- GROUND STRUCTURE IN HIGH SQUEEZING GROUND

Tina Marolt Čebašek (corresponding author)

University of Ljubljana,
Faculty of Natural Sciences and Engineering
Aškerčeva 12, 1000 Ljubljana, Slovenia
E-mail: tina.marolt@ogr.ntf.uni-lj.si

Jakob Likar

University of Ljubljana,
Faculty of Natural Sciences and Engineering
Aškerčeva 12, 1000 Ljubljana, Slovenia
E-mail: jakob.likar@ogr.ntf.uni-lj.si

Keywords

high squeezing ground, numerical model, underground structures, deformations, yielding support element

Abstract

The present study assesses high squeezing ground confirmed by empirical and semi-empirical theories. High squeezing ground is often present in underground constructions at great depths, but it is hardly ever researched separately from light and fair squeezing ground. A three-dimensional, static numerical model is developed for a complex underground structure consisting of a shaft, a silo, and a mine roadway at great depth, which is certainly in high squeezing ground. Furthermore, a solution for the entire structure based on shotcrete with incorporated yielding elements is provided. The yielding elements, in general, absorb the strain energy by compressing at a relatively constant stress, but without rebounding. A three-dimensional, static numerical model of a support system with incorporated yielding elements is established in order to demonstrate that the presented forces are under control. Therefore, a failure of the lining is avoided because the stresses in the shotcrete lining are below its load-bearing capacity. It can be concluded that yielding elements incorporated in the shotcrete lining play an important role in the support solution in high squeezing ground.

1 INTRODUCTION

The common view is that the excavation of underground structures through squeezing ground conditions is a very slow and hazardous process because the rock mass around the opening loses its inherent strength under the influence of the *in-situ* stresses [1]. Deformation can terminate during the construction or continue over a long period of time [2]. This study focuses on high squeezing ground conditions, confirmed by the theories of many authors [3,4,5,6,7,8]. The prediction of squeezing has also been made using experimental and critical stress methods [4]. Nowadays, research tends to focus on fairly and severe squeezing ground, but the main purpose of this paper is to explain and find a complete support solution for high and very heavy squeezing grounds. The challenge of this paper is the construction of shaft, silo, and a mine roadway through a rock mass with a low rock-mass quality value Q and a low uniaxial compressive strength σ_{cmass} . Various design options have been proposed and applied in Alpine tunnels [9]. The recent innovative technological developments in a yielding support system were implemented and proven in tunneling projects [10]. In this paper a three-dimensional, static numerical model of the structure in high squeezing grounds is created and the present study offers possible yielding support measures for high squeezing ground.

2 A REVIEW OF THE INDICATIONS OF HIGH SQUEEZING GROUND CONDITIONS

The high squeezing ground conditions are determined by two empirical approaches and four semi-empirical approaches in order to be certain that the structure is located in high squeezing ground.

Potential tunnel squeezing problems have been discussed by several authors and their definitions used in this study are listed below. In Singh's approach, based on an evaluation of squeezing and non-squeezing conditions, as in this case, the squeezing degree is not defined, but is based on the rock-mass quality Q and the overburden height H [8]. For the squeezing conditions the value should satisfy the equation $H \gg 350 Q^{1/3}$. Furthermore, it is established that the tangential stress failure may be double the *in-situ* stress p_0 . In other words, the rock-mass uniaxial compressive strength σ_{cmass} can be calculated as follows [11]:

$$\sigma_{cmass} = 0.7\gamma Q^{1/3} \text{ [MPa] for } Q < 10. \quad (1)$$

where γ is the rock-mass unit weight (MN/m^3) and Q is the rock-mass quality.

This equation is also logically justified when the rock mass quality Q is obtained soon after excavation in nearly dry, weak rock masses. This equation also explains why the squeezing criterion is found to be independent of the uniaxial compressive strength and so its correction is not needed [1,4,10].

Goel explained a theory that is based on the rock-mass number and considers the overburden height H and the tunnel diameter B [5]. The degree of squeezing is defined as high squeezing at 5% of the normalized tunnel squeezing ε_t . See Table 1.

Jethwa included the data on the degree of squeezing in relation to the ratio of the rock-mass uniaxial compressive strength σ_{cm} and the *in-situ* stress p_0 . The solution of the type behaviour is described as highly squeezing only when the degree of squeezing is less than 0.4 [7]. See Table 1.

Aydan's criterion assumed that the rock-mass uniaxial compressive strength σ_{cmass} and the uniaxial compressive strength of the intact rock are the same σ_c [3]. The squeezing level is described as heavy squeezing when the ratio of the peak tangential strain ε_p at the periphery of the tunnel and the elastic strain limit ε_e , also known as the elastic state ς , is greater than the ratio of the critical

strain limit ε_s and the elastic strain limit ε_e , but lower than the ratio of the residual strain limit ε_r and the elastic strain limit ε_e (see Table 1). The strain limits are explained in Figure 1. In order to simplify the comparison of the different theories, it is considered that a heavy squeezing condition corresponds to a high squeezing condition.

Barton's criterion is similar to Ayden's, and the squeezing level is described by the squeezing index SI . The very heavy squeezing condition corresponds to values greater than 5 and the heavy squeezing condition corresponds to values between 3 and 5 [4] (see Table 1). According to the uniaxial compressive strength, the intact rock is assumed to be 1 MPa. The SI corresponds to the ratio between the observed, or the expected, strain and the critical strain. Several levels of squeezing based on the ratio between the expected strain and the critical strain:

$$SI = \frac{\frac{u}{r_0}}{\varepsilon_{cr}} \quad (2)$$

where u is the radial closure, ε_{cr} is the critical strain and r_0 is the radius of the opening.

The values of the critical strains are obtained from the numerical modelling in this study, but they could also be obtained from actual monitoring. In order to simplify the comparison of different theories, it is considered that a heavy squeezing condition corresponds to a high squeezing condition.

Finally, Hoek's approach is used for the evaluation of squeezing problems. It is considered that very severe squeezing problems occur when the tunnel strain ε_t is between 5% and 10%, and extreme squeezing problems occur when the tunnel strain ε_t is larger than 10% [7]. In order to simplify the comparison of the different theories, it is considered that very severe squeezing problems correspond to a high squeezing condition.

The presented approaches are limited to a high and a very heavy squeezing condition, and they are presented Table 1.

2.1 Squeezing classification

The potential squeezing problems of the mine roadway are evaluated using Equation 3, and the ultimate support pressure in the squeezing ground condition is evaluated according to Equation 3, where in this study a rock-mass

Table 1. Review of approaches.

	Empirical approach		Semi-empirical approach			
	Singh	Goel	Jethwa	Aydan	Barton	Hoek
HS	-	$\varepsilon_t > 5\%$ of B	$\sigma_{cm}/p_0 < 0.4$	$\varepsilon_s/\varepsilon_e < \zeta < \varepsilon_r/\varepsilon_e$	$3 < SI \leq 5$	$5\% < \varepsilon_t < 10\%$
VHS	-	-	-	$\varepsilon_r/\varepsilon_e < \zeta$	$5 < SI$	$10\% < \varepsilon_t$
S	$H \gg 350 Q^{1/3}$	$\varepsilon_t > 1\%$ of B	$\sigma_{cm}/p_0 < 2$	$1 < \zeta$	$1 < SI$	$1\% < \varepsilon_t$

HS – high squeezing, VHS – very heavy squeezing, S – squeezing

quality Q with $SRF=1$ and the correction factor f for the tunnel closure obtained for a high degree of squeezing is used [12,13,14].

$$\varepsilon_t = 0.15 \left(1 - \frac{p_i}{p_0} \right) \frac{\sigma_{cm} \left[\frac{3p_i + 1}{p_0} \right] \left(\frac{3.8p_i + 0.54}{p_0} \right)}{p_0} \quad (3)$$

where ε_t is the tunnel strain, p_i is the support pressure, σ_{cm} is the rock-mass uniaxial compressive strength, and p_0 is the *in-situ* stress.

$$p_{sq} = \left[\frac{f}{30} \right] \cdot 10 \left[\frac{H^{0.6} \left(\frac{B}{2} \right)^{0.1}}{50 \cdot N^{0.33}} \right] r \quad (4)$$

where p_{sq} is the estimated ultimate support pressure in the squeezing ground conditions, f is the correction factor for the tunnel closure, N is the rock-mass number, H is the overburden height, B is the diameter of the tunnel, and r is the correlation coefficient.

It is important to precisely evaluate the degree of squeezing because underground construction in the squeezing

ground is very demanding due to the difficulty in making a reliable prediction in the design stage. For the study of the squeezing potential a program in MATLAB is written, where the squeezing classification is based on empirical equations and inequalities from Table 1 and other model characteristics obtained from the numerical modeling and laboratory tests. The final results are presented in Table 2.

2.3 Laboratory testing and rock description

The properties of the model material are defined by a laboratory test that was carried out by testing specimens in order to analyse the strength and the strain behaviour under a uniaxial stress state, where ε_p is the peak strain limit, ε_s is the critical strain limit, ε_e is the elastic strain limit, ε_r is the residual strength limit, σ_p is the peak stress, and σ_r is the residual stress (Figure 1). Generally, very weak to weak sedimentary rocks with a typical uniaxial strength between 1 MPa and 3 MPa are presented at the investigated depths (Figure 2). The uniaxial compression tests were carried out using an electronically controlled hydraulic press with a capacity of 1150 kN. The velocity during the test was 1 mm/min. The vertical displacements and the normal force were measured and the numerical modeling is conducted with the same force-strain behavior as shown in Figure 1. For modelling a three-dimensional, static numerical model the results of one specimen are used for reasons of simplicity.

Table 2. Analysis of the selected data.

Structure	Overburden height (m)	<i>In-situ</i> stress (MPa)	Empirical approach		Semi-empirical approach			
			Singh	Goel	Jethwa	Aydan	Barton	Hoek
Shaft	448	9.86	S	VHS	HS	VHS	VHS	HS _p
Mine roadway	468	10.30	S	VHS	HS	HS	VHS	HS _p
Silo	484.5	10.66	S	VHS	HS	HS	VHS	HS _p
Shaft	500	11	S	VHS	HS	HS	VHS	HS _p

HS – high squeezing, VHS – very heavy squeezing, S – squeezing, index p refers to problems.

Due to the geological conditions given in Figure 1, the squeezing level is obtained from critical strains. The

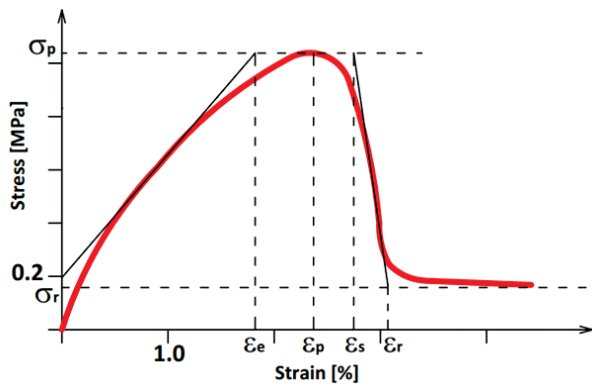


Figure 1. Strain limits of the subjected high squeezing ground.

typical uniaxial compressive strength is 1.25 MPa, the rock-mass quality Q is 0.16, and the unit weight is 22 kN/m^3 .

For each sample from Figure 2 the squeezing index is provided. It is clear from Figure 3 that the upper part of the shaft is under very heavy squeezing conditions and the other parts of the underground structures are under high squeezing conditions. This is also summarized in Table 2.

It is obvious from Figure 3 that the squeezing level of the investigated samples is relatively high, and for that reason it can be concluded that the three-dimensional, static numerical model is set in high to very heavy squeezing ground. These results suggest the need for further research and modelling.

	Lithology	Description	Sample No.	Ground Type (GT)	Behavior Type (BT)	Density (g/m ³)	Moisture (%)	UCS (MPa)	Shear strength (MPa)	Poisson's ratio	
425	Intercalations of claystone and andesite layers.		97			2.42	4.83	2.39	1.20	0.25	
430			98			2.21	7.24	1.98	0.99		
435			99			2.22	3.87				
440			100			2.29	10.29	1.42	0.71		
445			101			2.15	4.64				
450			102			2.28	5.29	3.32	1.66		
455	Gray micaceous in part silty sandstone with marl matrix and cracks and with intermediate siltstone layers.		103	GT - 7	BT3 BT9 BT10	2.38	1.83	1.92	0.96	0.21	
460			104			2.42	2.45	1.28	0.64		
465			105			2.34	7.36	1.11	0.56		
470			107			2.51	3.82	3.06	1.53		
475			108			2.35	4.43	4.68	2.34		
480			109			2.46	6.37	1.50	0.75		0.26
485			110			2.44	4.10	2.50	1.25		
490			111	2.58	2.44	2.56	1.33				
495											
500			112	2.38	3.66	2.6	1.24				
505			113	2.48	3.66	3.67	1.84	0.23			
510	114	2.34	6.65	3.97	1.99						
515	115	2.39	6.94	1.25	2.05						
520	116	2.41	4.59	1.06	2.53						

Figure 2. Geological conditions.

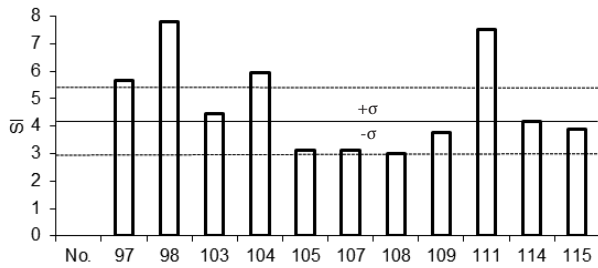


Figure 3. The squeezing level of the investigated samples.

3 A THREE-DIMENSIONAL, STATIC NUMERICAL MODEL

3.1 The Model

The analyses are carried out in order to identify the critical strains and stresses using the Midas GTS (Geotechnical and Tunnel Analysis system) software, which also enables modelling of unconventional interconnections in underground structures [15]. This is the main reason why it is used in this issue. Finite-element software and a three-dimensional, static numerical model of the study are established. The numerical analyses are performed

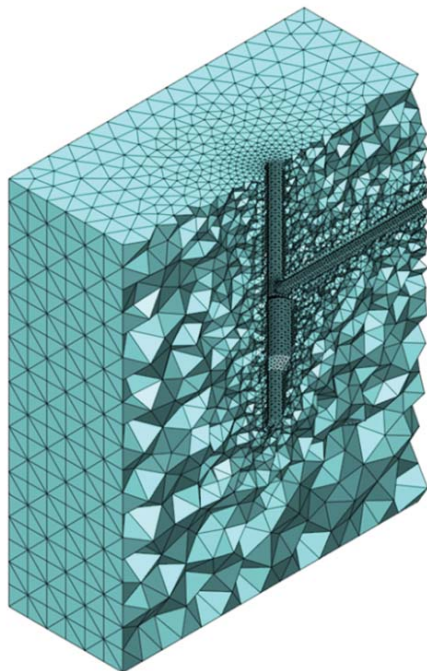


Figure 4. The mesh of a 3D computation model that is divided into 406,990 elements and 68,658 nodes.

on an idealised shaft, a silo, and a mine roadway in the idealized high squeezing grounds. The complex underground structure is excavated to a depth between 427.3 m and 519 m. In all the analyses and calculations the time development of the ground pressure of the high squeezing ground is not taken into account. It is included as a final maximum ground pressure, which is applied on the primary shotcrete lining of the shaft.

The total size of the model is 120 m × 100 m × 150 m (Figure 4) and the input parameters are presented in Table 3. The high squeezing ground is simulated by specific, four-noded, tetrahedron elements with Mohr-Coulomb's ideal elastic-plastic constitutive material model. Furthermore, a von Mises yield criterion is used for the yielding elements, and shotcrete is simulated by plane triangular elements with Mohr-Coulomb's ideal elastic-plastic constitutive material model. Ultimately, all the elements are connected into the discretization points. The horizontal movement is limited on the sides; the vertical and horizontal movements are limited on the bottom; and the top of the model is a free surface. The length of the mine roadway is 60 m and the diameter is 4.6 m. It is positioned 466.9 m below the surface; the shaft's diameter is 6.4 m; the silo is placed at a depth between 474 m and 495 m, and its diameter is 10 m.

The process is simulated in 36 stages; the shaft dipping (sinking) and the mine roadway excavation begin at the same time. The mine roadway's excavation is conducted from the edge in the direction of the silo. During the first stage, the primary stress state condition is analysed; during the second-stage excavation a 3-m-long excavation step is simulated; and in the third stage the next excavation step follows and is of the same length as in the previous step. Meanwhile, the primary lining in the second stage is being applied and the characteristics of the primary lining are used for applying young shotcrete. Simultaneously, the yielding elements are being installed in a three-dimensional, static numerical model with incorporated yielding elements. During the fourth stage the third excavation step is simulated and the installation of the primary lining with young shotcrete characteristics is described as well. At the same time, the yielding elements are being installed in a three-dimensional, static numerical model with incorporated yielding elements. At that point in the second phase, the characteristics of the hardening shotcrete are considered. The process of excavating and supporting is repeated until stage 36. The explanation of this process is presented in Figure 5, and the characteristics of model, in Table 3. A numerical simulation without yielding elements is carried out in the same sequences, but the yielding elements are omitted.

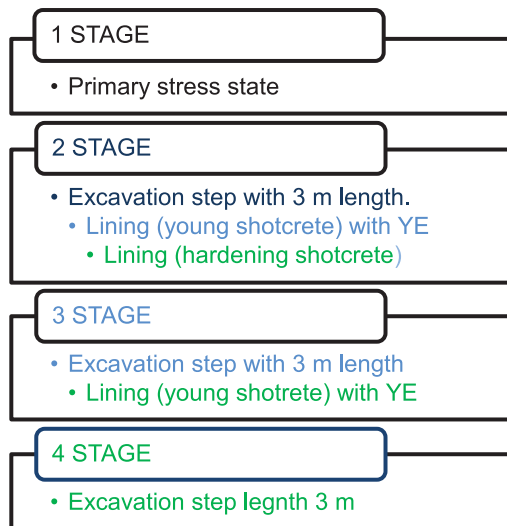


Figure 5. Explanation of stages to the point when the process starts repeating until the 36th stage.

The shaft sinking was stopped at stage 16, and this is 474 m below the surface. The mine roadway’s excavation continued in three isolated stages. The shaft and the mine roadway were connected at stage 19. Finally, the silo and the last part of shaft sinking were implemented.

3.2 Displacements

The displacements of the nodes in the model without the yielding elements’ integration are analysed in Figure 6. The nodes are placed on the shotcrete lining and their displacements vs. stages are investigated in the shaft at stage 7, which is 448 m below the surface; in the mine roadway at stage 10, which is 468 m below the surface; and in the silo at stage 24, which is 484.5 m below the surface. The approximate location of the nodes for a better visualisation can be seen in Figure 9, and these nodes are investigated in the model without the yielding elements’ integration.

Table 3. Details of the reference case.

	Squeezing ground	Young shotcrete	Hardening shotcrete	Yielding element
Modulus of elasticity (MPa)	700	3 000	20 000	150
Unit Weight (MN/m ³)	0.022	0.025	0.025	0.0785
Poisson’s ratio	0.3	0.2	0.2	0.3
Model Type	Mohr-Coulomb’s ideal elastic-plastic			Von Mises
Uniaxial compressive strength (MPa)	1.25	10	32	-
Yield stress (MPa)	-	-	-	4.5
Thickness (m)	-	0.25	0.25	0.25

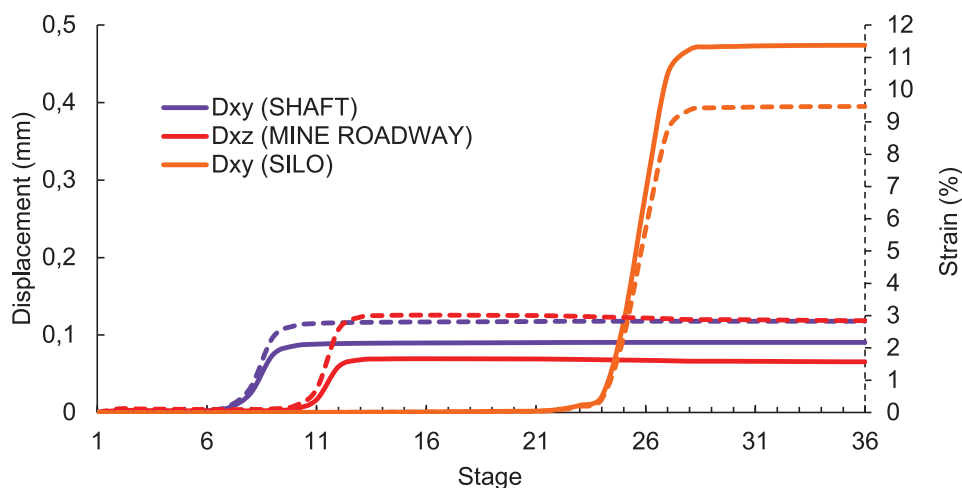


Figure 6. The tunnel shotcrete lining deformation against the stages and values indicate the movement towards the centre of the mine roadway, the shaft, and the silo.

It is considered that the shotcrete lining can withstand 1% of strain deformation; higher deformations lead to a collapse [10,16]. It is clear from Figure 6 that the maximum strain deformation of the shotcrete is exceeded and amounts to 2.85% in the mine roadway, 2.92% in the shaft, and 9.48% in the silo. This means that the shotcrete is an inappropriate support solution when dealing with high squeezing ground.

In addition, the stability of the shaft, the silo, the mine roadway, and the wall rock are investigated with a numerical method; this is a three-dimensional structure and requires three-dimensional modelling for a proper understanding. The displacements actually occur at the periphery of the openings and may be obtained for the shaft, as well as for the silo with displacements in the XY

direction (Figure 7, Figure 8) and for the mine roadway with displacements in the XZ direction (Figure 7).

It should be noted that the critical strain is an anisotropic property and it is different in different points at the periphery of the openings. The expected critical strain at the periphery of the openings depends on the size and the shape of the openings, as well as on the *in-situ* stress state, and on the rock-mass properties. A simulation is made in 3D conditions, and displacements of 116 mm in the wall rock of the shaft and the mine roadway are usually expected (Figure 7). These displacements are incomparably lower than the displacements in the wall rock of the silo. For this reason, Figure 8 shows the displacements towards the end of the simulation. It is clear that displacements of 539 mm occur at this point.

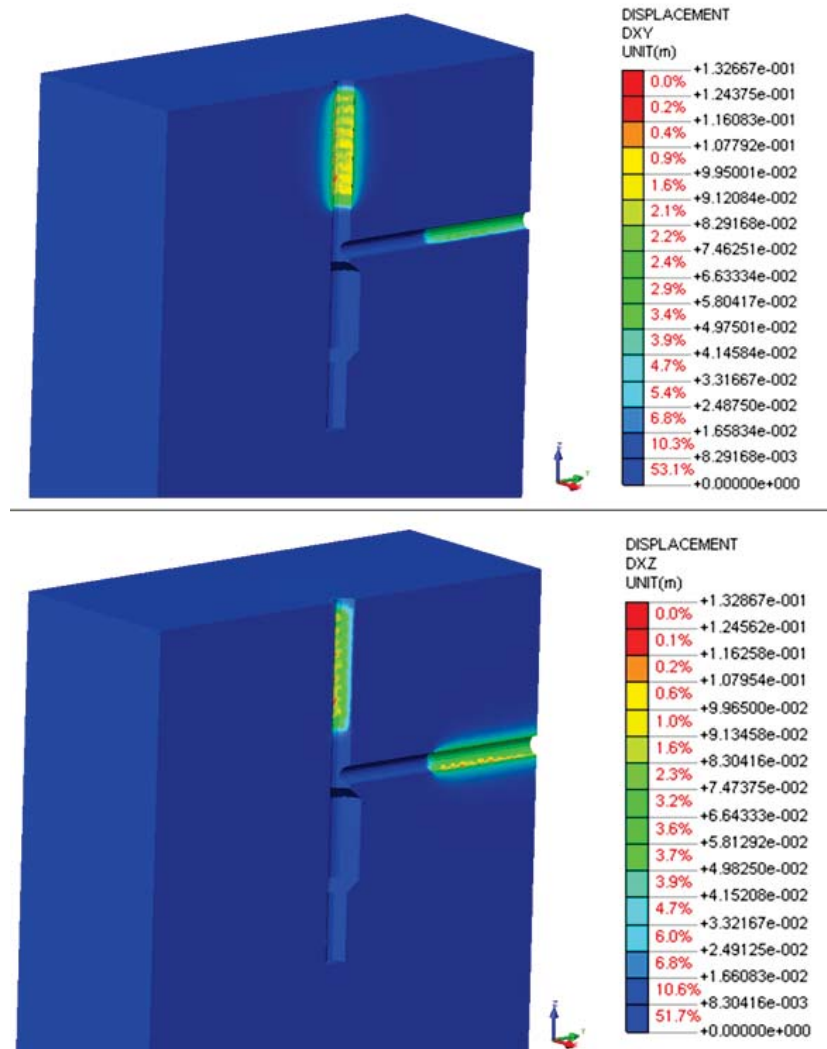


Figure 7. The displacement investigation at the periphery of the openings at stage 10 for the shaft and mine roadway, respectively.

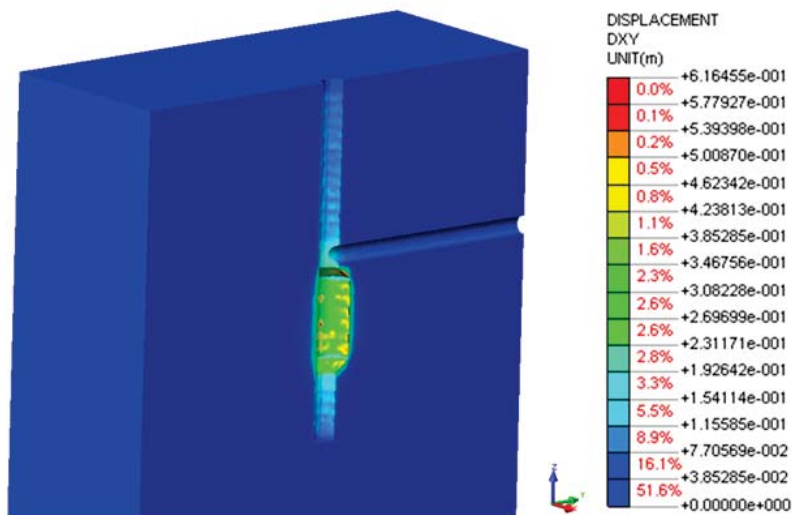


Figure 8. The displacement investigation at the periphery of the shaft and silo at stage 34.

The obtained evidence proved that there is no doubt we are dealing with a high squeezing ground condition.

Therefore, the three-dimensional, static numerical model could be completed for a prediction of the squeezing problem's evaluation. The obtained results show that the underground structure is positioned in high squeezing ground. For this reason, appropriate support measures must be ensured.

4 A SOLUTION FOR THE SUPPORTING PROBLEMS IN HIGH SQUEEZING GROUND

4.1 Yielding elements

In this study the shotcrete lining is accommodated with yielding elements because the shotcrete lining is one of

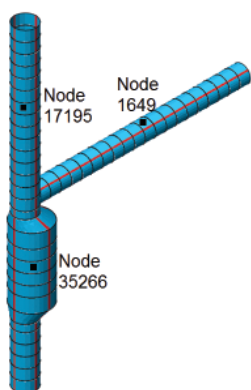


Figure 9. Model with yielding support system and incorporated yielding elements (red color) and shotcrete (blue color).

the most commonly used support elements. The thickness of the shotcrete lining is 250 mm. In addition, the shotcrete shell is improved by using yielding elements that are incorporated into the shotcrete lining (Figure 9), thus allowing a controlled transfer of the stress across the longitudinal gaps. Their construction is relatively simple, and the structure consisted of four sets provided by Midas GTS.

The numerical modeling is undertaken to predict the deformability in the desired manner. The suitable yielding element in these circumstances is designed for a

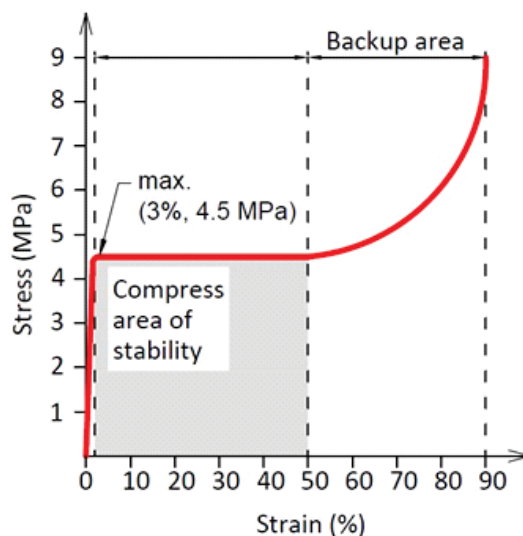


Figure 10. Stress vs. strain of yielding element.

load level of 4.5 MPa, which is reached at a strain of 3% (Figure 10). The compressed area of stability is from 3% to 59% strain, which represents the ideal energy absorption. Above a 59% strain the backup zone is reached, which represents the energy-absorption reserve, although the shotcrete lining is expected to take over the entire load. The tests concerning the ductile behavior of the yielding elements made clear the required deformability for the purposes of the construction.

4.2 Stresses and forces

The maximum and minimum tangential stresses appear in the Y direction for the shaft and in the X direction for the mine roadway. This is significant because the maximum and minimum radial stresses appear in the Y direction for the shaft and in the Z direction for the mine roadway in the global coordinate system. The gravitational stress, which is essential for the shaft and the silo, is considered along the Z direction. A detailed analysis is made for the nodes on the shotcrete lining in the model with the incorporated yielding elements, an approximated position of the nodes is presented in Figure 9, and the results of the analysis are presented in Figure 11. The yielding elements used in this analysis are suitable. The tangential forces increased in the yielding elements and the compressive strength is not exceeded at any stage of the construction. This is logical and the main goal of controlled deformation is achieved.

Figure 11 shows the calculated values of the normal stresses S_{XX} , S_{YY} , and S_{ZZ} depending on the simulated stage of the construction of the analyzed mine roadway, shaft, and silo. The main difference between the calculated stresses in the early simulation stages of excavation – shaft sinking and installation of primary support system – is seen in the stress magnitudes at the periphery of the silo, with half value stresses at the periphery of the mine roadway, and at the upper part of

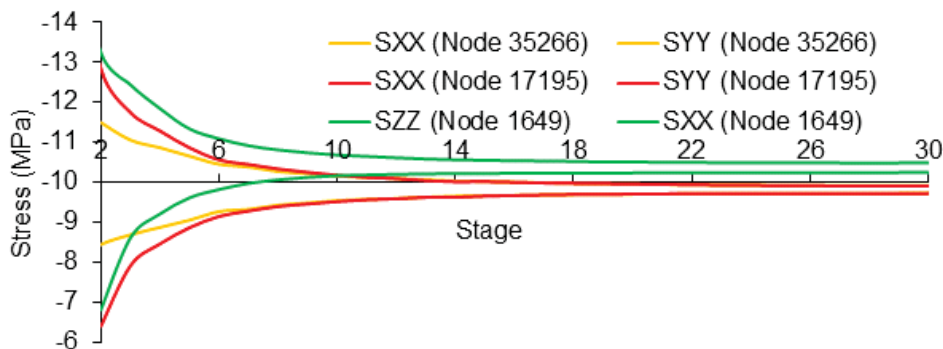


Figure 11. Tangential and radial stresses for mine roadway, shaft and silo.

the shaft that is analyzed. The main reason for this stress redistribution is in the chronological simulation of the construction of these underground facilities, which in practice represents a complex system of underground structures for the purposes of the shaft's operation. In addition, the element coordinate system for a detailed analysis is used. Generally, the force distribution of the shaft and the silo lining in the X direction (Figure 12) of the local coordinate system is taken into consideration. The maximum part of the shaft area is under 2.9 MN/m, and the maximum part of the silo area is under 6.8 MN/m. The critical area of the forces is located in the infinitesimal part of the silo and it is proposed that it could be stabilized by a thicker shotcrete lining or by a shotcrete with a higher compressive strength class. If the critical forces would be spread over the larger part of the structure it could be stabilized with the numerous deformable elements in the lining. This is a reasonable option with respect to a symmetric distribution of them, where the large strains are expected. It can be concluded that the size of the forces depends on the dimensions of the underground structures [10].

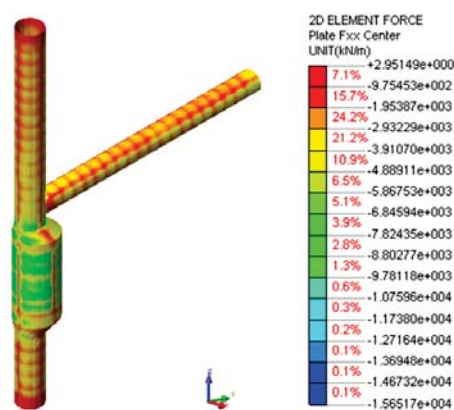


Figure 12. Tangential forces of underground structures in the element coordinate system.

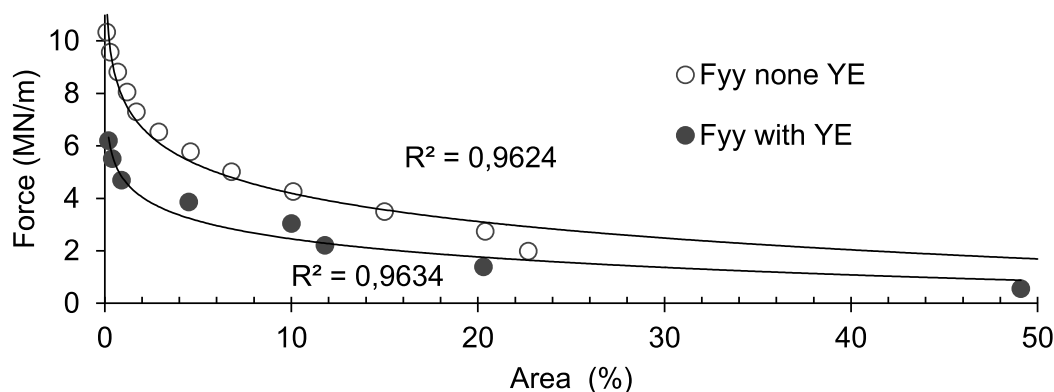


Figure 13. Tangential forces of the mine roadway with and without the incorporated yielding elements.

Moreover, a study with and without the incorporated yielding elements is made for the mine roadway, which is analysed in the Y direction in the local coordinate system. The force distributions are more favourable and generally are 40 % lower with the incorporated yielding elements. This means that almost half of the area is under the lowest force value and the compressive strength of the shotcrete is not exceeded at any force level if support measures with incorporated yielding elements (Figure 13) are applied.

5 DISCUSSION

Critical strain plays an important role in the determination of squeezing problems [17]. In this study the critical strain is obtained from numerical modelling, otherwise it could also be obtained from actual monitoring from the field, as in the Saint Martin La Porte access tunnel [10]. The magnitude of the tunnel's convergence, which is obtained by numerical modelling, ensures a prediction of the allowable space that is needed to accommodate the ground deformation. With this procedure the re-profiling is avoided in the construction stage as it was needed in Yacambú–Quibor Tunnel [13]. With numerical modeling, the additional costs could be avoided during the design stage. The full-face excavation method has been proved to be appropriate in case studies of the Saint Martin La Porte access tunnel and the Lyon-Torino Base Tunnel [18]. There, also, the recently established yielding elements were used. For that reason the full excavation method is used in this study. This method provides a large working space and there large equipment can be effectively used for the installation of the appropriate support measures. The procedure of the evaluation of the degree of squeezing is described

from laboratory tests and data obtained from numerical modelling. It is supposed that the squeezing level cannot be precisely predicted from samples, but it is obvious that the dimensions of the underground structure have a major influence on the developed displacements and the stress changes.

6 CONCLUSION

This study's main focus was on high squeezing ground behaviour, as it is not commonly investigated separately from other squeezing degrees, but often appears in underground excavations. The results of the explained analysis provide a solution for supporting a complex underground structure in high squeezing ground at great depths. The main aim of the present analysis is to find the proper yielding element, which has the proper rigidity, and helps reduce the stresses in the shotcrete lining. It could be concluded that the yielding elements incorporated into the shotcrete lining play an important role in the support measures in high squeezing ground to guarantee the stability of the support systems in all the stages of the construction, and the operation of the shaft.

Acknowledgements

The authors would like to express their sincere gratitude to Innovative Scheme for Co-Financing Doctoral Studies.

REFERENCES

- [1] Aydan, O., Akagi, T., Kawamoto, T. 1996. The squeezing potential of rock around tunnels, theory

- and prediction with examples taken from Japan. *Rock mechanics and rock engineering* 29, 125-143.
- [2] Barla, G. 1995. Squeezing rocks in tunnels. *ISRM News J* 3(4), 44-49.
- [3] Aydan, O., Akagi, T., & Kawanoto, T. 1993. The squeezing potential of rocks around tunnels. *Rock Mechanics and Rock Engineering* 26(2), 137-163.
- [4] Barton, N. 2002. Some New Q Value Correlations to Assist in Site Characterisation and Tunnel Design. *International Journal of Rock Mechanics and Mining Sciences* 39, 185-216.
- [5] Goel, R., Jethwa, J., Paithankar, G. 1995. Tunnelling through the young Himalayas — A Case History of Maneri-Uttarkashi Power Tunnel. *Engineering Geology* 39, 31-44.
- [6] Jethwa, J., Singh, B. 1984. Estimation of Ultimate Rock Pressure for Tunnel Linings under Squeezing Rock Conditions—A New Approach. In *Proceedings of ISRM Symposium on Design and Performance of Underground Excavations*, pp. 231-238. Cambridge: Brown, E.T., Hudson, J.A.
- [7] Hoek, E. 2001. Big Tunnels in Bad Rock. *Journal of Geotechnical and Geoenvironmental Engineering* 127, 726-740.
- [8] Singh, B., Jethwa, J., Dube, A. 1992. Correlation between observed support pressure and Rock Mass Quality. *Tunnelling and Underground Space Technology* 7, 59-74.
- [9] Schubert, W. 1996. Dealing with squeezing conditions in Alpine tunnels. *Rock Mechanics and Rock Engineering* 29(3), 145-153.
- [10] Barla, G., Bonini, M., Semeraro, M. 2011. Analysis of the Behaviour of a Yield-Control Support System in Squeezing Rock. *Tunnelling and Underground Space Technology* 26, 146-154.
- [11] Singh, B., & Goel, R. K. 1999. *Rock Mass Classification*. Elsevier.
- [12] Goel, R., Jethwa, J., Dhar, B. 1996. Effect of Tunnel Size on Support Pressure. *International Journal of Rock Mechanics and Mining Sciences* 33(7), 749-755.
- [13] Hoek, E., Guevara, R. 2009. Overcoming Squeezing in the Yacambú-Quibor Tunnel, Venezuela. *Rock Mechanics and Rock Engineering* 42, 389-418.
- [14] Hoek, E., & Marinos, P. 2000. Predicting Tunnel Squeezing Problems in Weak Heterogeneous Rock Masses. *Tunnels & Tunnelling International* 45-51 (part 1), 33-36.
- [15] MIDAS IT Co. Ltd. 2002. *Basic & Advanced Tutorials*. Beijing.
- [16] Kovári, K. 2003. History of the Sprayed Concrete Lining Method – Part I. *Tunnelling and Underground Space Technology* 18, 57-69.
- [17] Singh, M., Singh, B., Choudhari, J. 2007. Critical Strain and Squeezing of Rock Mass in Tunnels. *Tunnelling and Underground Space Technology* 22, 343-350.
- [18] Barla, G. 2009. Innovative tunnelling construction method to cope with squeezing at Saint Martin La Porte access adit (Lyon-Torino Base tunnel). Dubrovnik, Croatia: *Rock Engineering in Difficult Conditions in Soft Rocks and Karst*. Proceedings of Eurock. ISRM Regional Symposium.

VPLIV VIRTUALNE STOPNJE SPECIFIČNE DEFORMACIJE NEKOHEZIVNEGA ZRNATEGA MEDIJA NA METODO DISKRETNIH ELEMENTOV

Kiichi Suzuki

Saitama University,
Department of Civil and Environmental Engineering
Saitama 338-8570, Japonska
E-pošta: ksuzuki@mail.saitama-u.ac.jp

Ključne besede

metoda diskretnih elementov (DEM), povzročena anizotropija, kvazi-statično stabilno stanje, stopnja specifične deformacije, edinstvenost

Izvleček

Metoda diskretnih elementov (DEM) je alternativno računalniško orodje za povečanje laboratorijskih eksperimentov, ki ima prednosti v detajliranju makro- in mikro-mehanskih informacij. Vendar pa je treba poudariti, da DEM po navadi ne upošteva konvergence za vsak časovni korak, ker je za izračun potreben ogromen čas. V tem primeru to pomeni, da edinstvenost rešitve ni zagotovljena, razen v primeru zelo majhne stopnje specifičnih deformacij, čeprav obnašanje zgleđa kakovostno smiselno. Najprej je bil preiskan vpliv stopnje specifičnih deformacij med številčnimi imaginarnimi vhodnimi parametri za nekohezivni material na monotonih, dvoosnih strižnih preizkusih. Nato so bile iz DEM simulacij pridobljene nove ugotovitve. Stopnja specifične deformacije ima pomemben vpliv na strižno obnašanje, še posebej po doseženi vrhnji rednosti vzorcev gostega gostotnega stanja. Ne obstaja statično stabilno stanje, ampak kvazi-statično stabilno stanje. "Močno" razmerje strukture je tesno povezano z napetostnim razmerjem. Največje število uskladtve zdrsa se pojavi okrog razmerja fazne transformacije, strižni pas se pojavi okoli vrhnje trdnosti.

INFLUENCE OF THE VIRTUAL STRAIN RATE OF NON-COHESIVE GRANULAR MEDIA ON THE DISCRETE ELEMENT METHOD

Kiichi Suzuki

Saitama University,
Department of Civil and Environmental Engineering
Saitama 338-8570, Japan
E-mail: ksuzuki@mail.saitama-u.ac.jp

Keywords

discrete element method (DEM), induced anisotropy, quasi-static steady state, strain rate, uniqueness

Abstract

The discrete element method (DEM) is an alternative computational tool for augmenting laboratory experiments because of its advantages in detailing macro- and micro-mechanical information. However, it should be noted that the DEM does not usually consider the convergence for each time step, because of the necessity for a huge calculation time. In that case, it indicates that the uniqueness of the solution is not guaranteed, except in the case of a very small strain rate, even though the behavior looks qualitatively reasonable. At first, the influence of strain rate among numerically imaginary input parameters for a non-cohesive material was investigated for monotonic, biaxial shear tests. Then, new findings were obtained from the DEM simulations. Strain rate has a significant influence on the shear behavior, especially after the peak strength of dense specimens. A quasi-static steady state exists, not a static steady state. The “strong” fabric ratio is closely related to the stress ratio. The maximum slip coordination number occurs around the phase-transformation ratio and the shear band appears around the peak strength.

1 INTRODUCTION

The discrete element method (DEM) is a numerical analysis tool originally developed by Cundall and Strack [1] for simulating blocky and granular materials. Various studies on the shear behavior in element tests have been conducted, e.g., confining the pressure and the initial void ratio (2, 3); the stress chain [1]; the fabric tensor [4, 5]; and the critical state condition [3, 6-8]. On the other hand, there are very few studies about the validation and verification of the DEM [9, 10]. The uniqueness of a DEM solution and the effects of modeling details (e.g., the strain rate, the damping constant and the time step) have not been investigated sufficiently for a non-cohesive material. Moreover, it might be very difficult to study these effects for a cohesive material [11]. Suzuki and Kuhn [12] have shown that the strain rate among numerically imaginary input parameters for a non-cohesive material has a greater influence on the behavior after the peak strength, using different strain rates of 4.0 s^{-1} to 0.0008 s^{-1} . Here, it should be noted that the DEM does not usually consider the convergence for each time step because of the necessity for a huge calculation time. In this case it indicates that the uniqueness of the solution is not guaranteed, except for the case of a very small strain rate, even though the behavior looks qualitatively reasonable.

In this paper the behaviors of two kinds of specimens (i.e., loose and dense samples) in biaxial compression tests were studied qualitatively and quantitatively, considering the influence of the virtual strain rate, not the real

strain rate, especially in order to clarify the relevance between the macro- and micro-mechanical behaviors.

2 NUMERICAL EXPERIMENTAL METHOD

2.1 Sample preparation

DEM simulations were run with the Oval code, developed by Kuhn [13] and based upon the principles in Cundall and Strack [1]. The contact forces were modeled with linear springs, with tangential forces limited by the friction coefficient. Two-dimensional assemblies were created with 8,192 egg-shaped, oval particles, a smooth non-circular shape that is composed of four arcs, joined to an approximate ellipse. To prepare the virtual specimens, oval particles of nine different sizes (2–10 mm), having the same aspect ratio of 0.60, were loosely arranged on a rectangular grid. The assemblies were isotropically compacted until a pressure of 100 kN/m² was attained, followed by a quiescent period of constant isotropic stress that allowed any unbalanced contact forces to dissolve. Two specimens were created using inter-particle friction coefficients of 0.0 and 0.6 during the compaction stage, producing dense and very loose samples, having void ratios of 0.112 and 0.246, respectively.

The assemblies were loaded in monotonic, drained, biaxial compression with vertical loading until they attained an equivalent deviatoric strain of 0.8 (i.e., 80 %) that might be in the steady state at the large strain. The simulation conditions are given in Table 1. During monotonic loading in the vertical direction, a constant confining stress of 100 kN/m² was maintained by continually adjusting the horizontal width of the assembly (i.e., the horizontal strain). Periodic boundaries were used to avoid the non-homogeneity at the corners, which would otherwise occur if rigid boundaries were used [14].

Table 1. Calculation conditions for the biaxial compression loading.

Parameter	Type or value
Shape	Oval
Number n	8,192
Diameter d	2.0–10.0×10 ⁻³ m
Density ρ_s	2.65×10 ³ kg/m ³
Initial void ratio e_0	0.112, 0.246
Spring constant k_n, k_s	5.0×10 ⁷ N/m
Coefficient of friction between particles μ_p	0.6
Damping constant h	0.08
Time step Δt	1.0×10 ⁻⁵ s
Vertical axial strain rate $\dot{\epsilon}_v$	0.004 s ⁻¹

Global damping [1] is used to give a more stable solution, compared with the contact damping [15]. During monotonic loading, an inter-particle friction coefficient of 0.60 was used with the assemblies.

2.2 Convergence condition

A solution convergence condition was checked at each time step to monitor the unbalanced resultant force index I_{uf} [13, 16]:

$$I_{uf} = \sqrt{\frac{\frac{1}{N_p} \sum_{p=1}^{N_p} (f_{res}^p)^2}{\frac{1}{N_c} \sum_{c=1}^{N_c} (f^c)^2}} \quad (1)$$

where N_p, N_c = the numbers of particles and contacts, respectively; f_{res}^p = the unbalanced particle force; and f^c the contact force. The low values of I_{uf} indicate nearly quasi-static conditions and the minimal effect of numerical damping.

2.3 Scalar quantities of stress and strain

The following scalar quantities of stress are used to present the results of the biaxial loading conditions:

$$p = \frac{1}{2} \sigma_{ii} = \frac{\sigma_v + \sigma_h}{2} \quad (2a)$$

$$q = \sigma_v - \sigma_h \quad (2b)$$

where p, q = the mean and equivalent deviatoric stresses for the two-dimensional problem, and v, h = the subscripts for the vertical and horizontal directions (i.e., the directions of loading and confinement, respectively). The strain quantities are as follows:

$$\epsilon_{vol} = \frac{-\Delta e}{1 + e_0} \quad (3a)$$

$$\bar{\epsilon} = \frac{1}{2} (\epsilon_v - \epsilon_h) \quad (3b)$$

where $\epsilon_{vol}, \bar{\epsilon}$ = the compressive volumetric and equivalent deviatoric strains for the two-dimensional problem, and $\Delta e, e_0$ = the incremental and initial void ratios. The incremental strains, $d\epsilon_{vol}$ and $d\bar{\epsilon}$, complement the stresses, p and q , such that the incremental work is the simple sum $p d\epsilon_{vol} + q d\bar{\epsilon} = \sigma_{ij} d\epsilon_{ij}$. The stress is computed from contact quantities using the Cauchy equation,

$$\sigma_{ij} = \frac{1}{A} \sum_{c=1}^{N_c} l_i^c f_j^c \quad (4)$$

where f_j^c = the components of the contact force, l_i^c = the corresponding branch vector connecting the centers of two particles, and A = the full area of the two-dimensional assembly.

3 SHEAR BEHAVIOR UNTIL THE QUASI-STATIC STATE

The vertical strain of 0.004 s^{-1} , as shown in Table 1, is used as the reference standard for comparing the other rate, i.e., 4.0 s^{-1} . The monotonic, bi-axial, shear compression tests were traced until an equivalent deviatoric strain of 0.8 for loose and dense specimens.

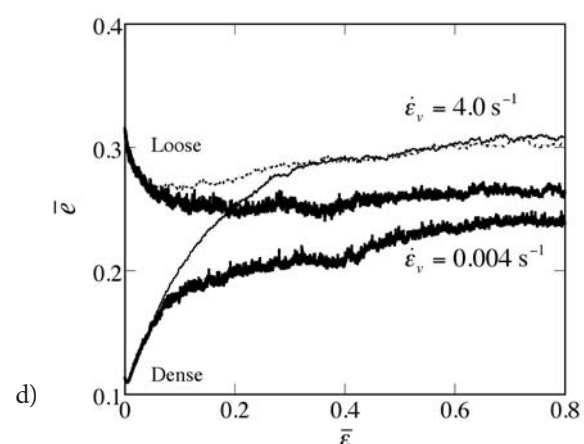
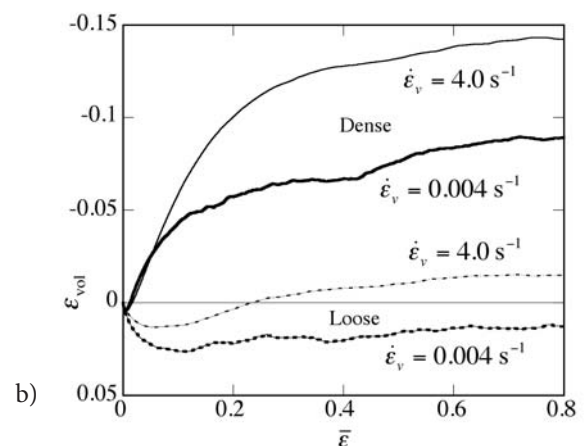
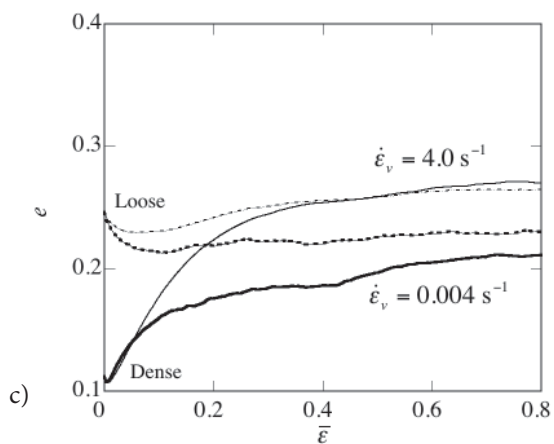
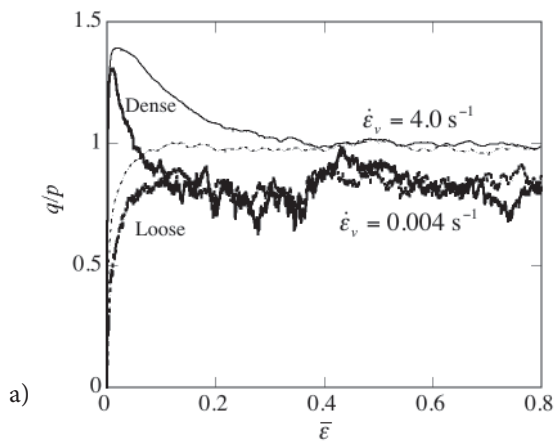
3.1 Stress-strain-dilatancy

Figs. 1(a) and (b) show the stress ratio q/p and the volumetric strain ε_{vol} as functions of the equivalent deviatoric strain $\bar{\varepsilon}$. In the case of $\dot{\varepsilon}_v = 4.0 \text{ s}^{-1}$, the stress ratios for the dense and loose specimens reach a nearly constant value at around the equivalent deviatoric

strain of about 0.4 (i.e., 40 %), which is considered to be the steady state. On the other hand, in the case of $\dot{\varepsilon}_v = 0.004 \text{ s}^{-1}$ the stress ratios approach a smaller value, compared with the case of $\dot{\varepsilon}_v = 4.0 \text{ s}^{-1}$ at around an equivalent deviatoric strain of 0.1, and then these harden and have the second peak stress ratio. It should be referred to as a quasi-static steady state, not a static steady state, because the large fluctuation continues, although these curves are relatively similar. It is obvious from Fig. 1(b) that these volumetric strains for dense and loose specimens are quantitatively quite different, depending on the strain rate. It is also clear that the results with larger strain rates do not satisfy the equilibrium due to the unbalanced force if the convergence was not attained.

3.2 Void ratio and effective void ratio

Figs. 1(c) and (d) show the variation of the two-dimensional void ratio e and the effective void ratio \bar{e} until an equivalent deviatoric strain of 0.8 is reached at a constant confining stress of 100 kN/m^2 , respectively. The



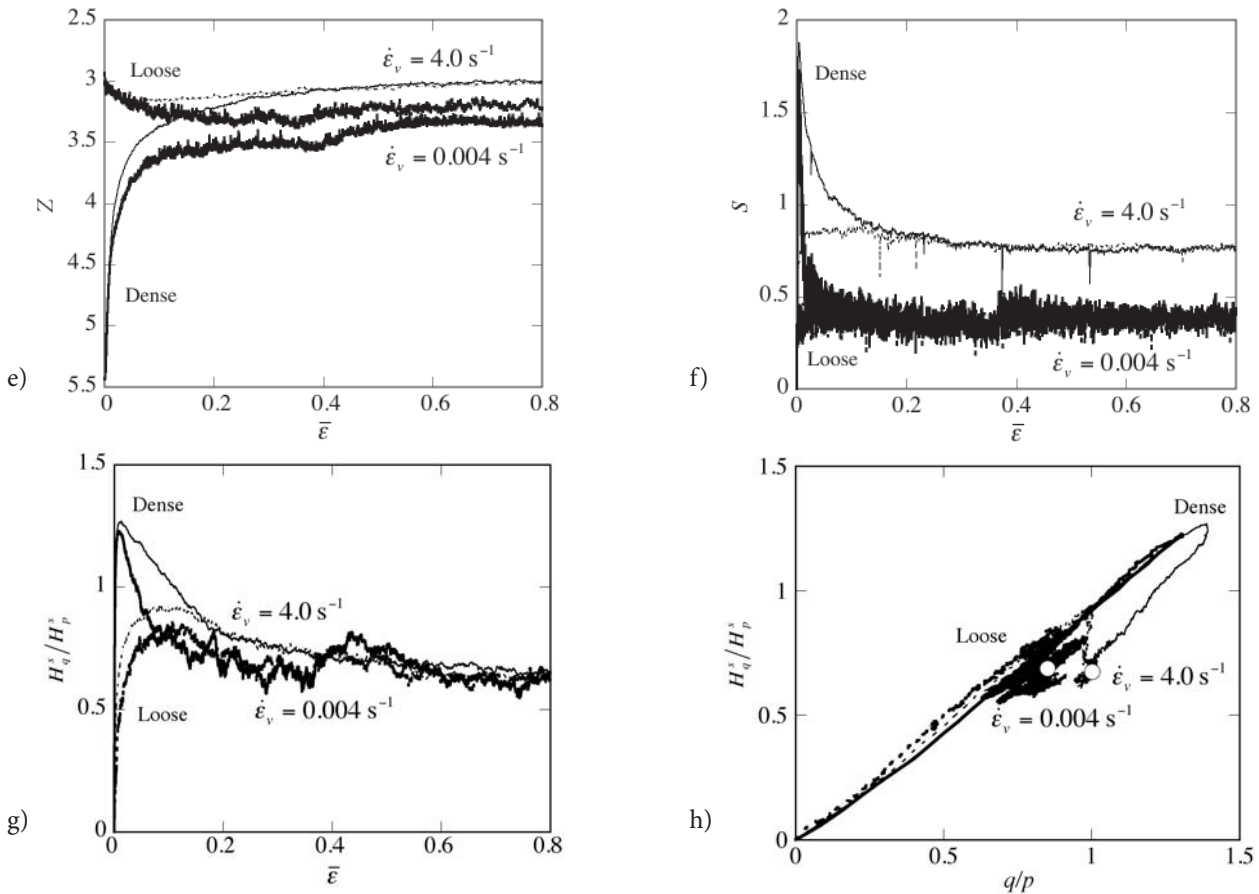


Figure 1. Various responses until an equivalent deviatoric strain of 0.8: (a) Stress ratio-equivalent deviatoric strain, (b) Volumetric strain-equivalent deviatoric strain, (c) Void ratio-equivalent deviatoric strain, (d) Effective void ratio-equivalent deviatoric strain, (e) Coordination number-equivalent deviatoric strain, (f) Slip coordination number-equivalent deviatoric strain, (g) “Strong” fabric ratio-equivalent deviatoric strain, (h) Relationship between “strong” fabric ratio and stress ratio.

effective void ratio proposed by Kuhn [17] assigns the non-load-bearing particles as part of the void volume rather than as part of the solid volume. In its initial state, the void ratio and the effective void ratio are about equal for the dense specimen, as nearly all the particles participate in supporting the initial isotropic stress, but a large difference is present with the loose sample. The difference is equivalent to the non-uniform contact-force distribution or stress chain [15] (also refer to Figs. 2(a) and (c) below). In the small strain rate to guarantee the solution, the effective void ratio, as well as the void ratio for dense and loose specimens, does not reach some constant at an equivalent deviatoric strain of 0.8.

3.3 Coordination number and slip coordination number

Figs. 1(e) and (f) show the variation of the coordination number and the slip coordination number until an equivalent deviatoric strain of 0.8 is reached. The coordination

number Z is the average number of contacts per particle, whereas the slip coordination number S is defined as the average number of sliding contacts per particle:

$$Z = 2 \frac{N_c}{N_p} \quad (6a)$$

$$S = 2 \frac{N_s}{N_p} \quad (6b)$$

where N_c , N_s = the numbers of contacts and sliding contacts, respectively, and N_p = the total number of particles. The direction of the vertical axis in Fig. 1(e) is reversed to allow a comparison with the effective void ratio in Fig. 1(d). The two figures show an inverse correlation between the coordination number and the effective void ratio [18]. The coordination number does not reach a constant value at an equivalent deviatoric strain of 0.8, as with the effective void ratio. On the other hand, it is clear from Fig. 1(f) that the slip coordination number significantly decreases and oscillates in the case of a small strain rate.

3.4 Fabric tensor ratio

Although a granular fabric can connote several meanings, a simple measure is the average of the orientations of the contact normal vectors n_i^c [19].

$$H_{ij} = \frac{1}{N_c} \sum_{c=1}^{N_c} n_i^c n_j^c \quad (7)$$

The following fabric tensor is used for oval particles using the branch vector l_i^c [13].

$$H_{ij} = \frac{1}{N_c} \sum_{c=1}^{N_c} l_i^c l_j^c \quad (8)$$

The scalar quantities of the fabric tensor are conveniently defined in a manner similar to those of the stress tensor [18]:

$$H_p = \frac{1}{2} H_{ii} = \frac{H_v + H_h}{2} \quad (9a)$$

$$H_q = H_v - H_h \quad (9b)$$

Fig. 1(g) shows the variation of the “strong” fabric ratio, in which the superscript “S” indicates “strong”. The strong fabric ratio is computed as in Eq. (9), but only includes the subset of contacts having a contact force that is greater than the following average contact force \bar{f} :

$$\bar{f} = \frac{1}{N_c} \sum_{c=1}^{N_c} (f^c)^2 \quad (10)$$

The concept of a strong fabric is based on the observation that the probability distributions of the contact force among the strong contacts differs significantly from the corresponding distribution among the “weak” contacts (i.e., those contacts with a contact force that is less than the mean force) [20, 21]. In comparison with Fig. 1(a), the “strong” fabric ratio becomes relatively unique and independent of the strain rate. Fig. 1(h) shows the “strong” fabric ratio versus the stress ratio in the case of a small strain rate. It indicates that the “strong” fabric ratio is closely related to the stress ratio.

3.5 Contact forces

Figs. 2(a) and (b) and Figs. 2(c) and (d) show the contact-force distributions before the shear loading and after the shear loading until an equivalent deviatoric strain of 0.8, for dense and loose specimens, respectively. The shape of the deformed specimens is squat rectangular due to the restriction of a periodic cell, although the laboratory experimental results show a barrel-shaped failure for a loose specimen with rough platens. It is clear from Figs. 4 and 6 that there is a large evolution of the contact-force distribution or shear bands for a dense specimen around the first and second peak-stress ratios.

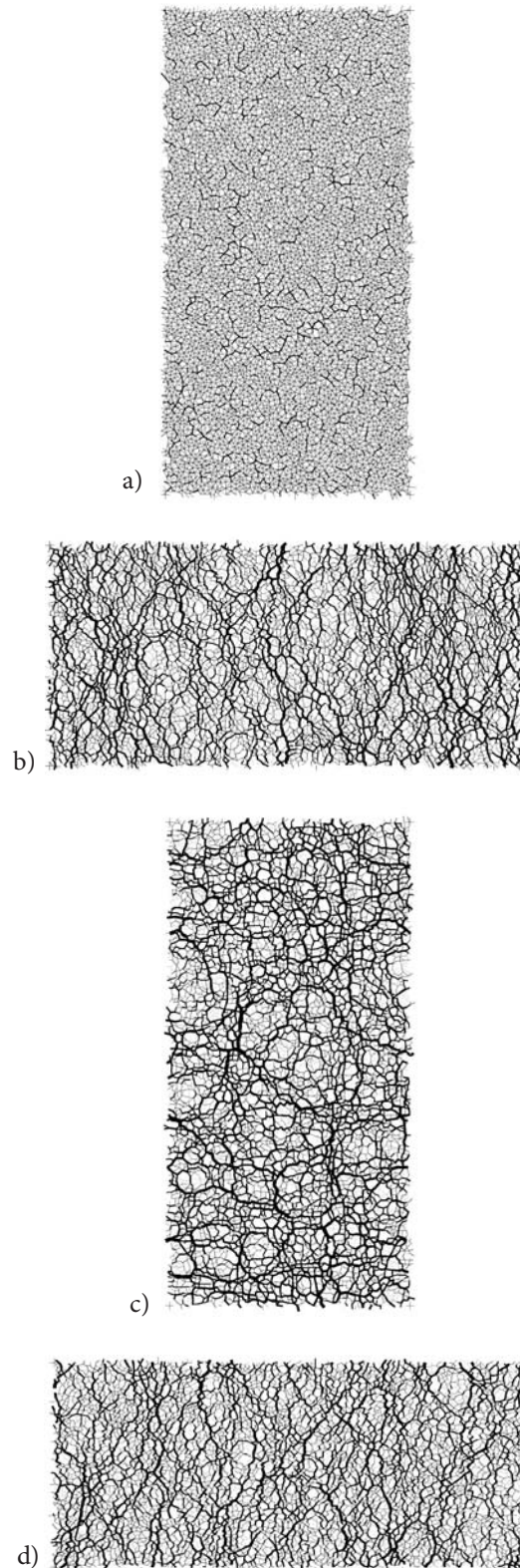


Figure 2. Contact-force distribution before/after shear loading: (a) Before shear loading (dense specimen), (b) After shear loading (dense specimen), (c) Before shear loading (loose specimen), (d) After shear loading (loose specimen).

4 EVOLUTION OF THE FABRIC AROUND THE PEAK-STRESS RATIOS

4.1 First peak-stress ratio

The shear behavior around the first peak-stress ratio as shown in Fig. 1(a) is further investigated here. Figs. 3(a), (b) and (c) show the stress ratio, the volumetric strain and the slip coordination number until an equivalent deviatoric strain of 0.02 (i.e., 2%). In the case with a

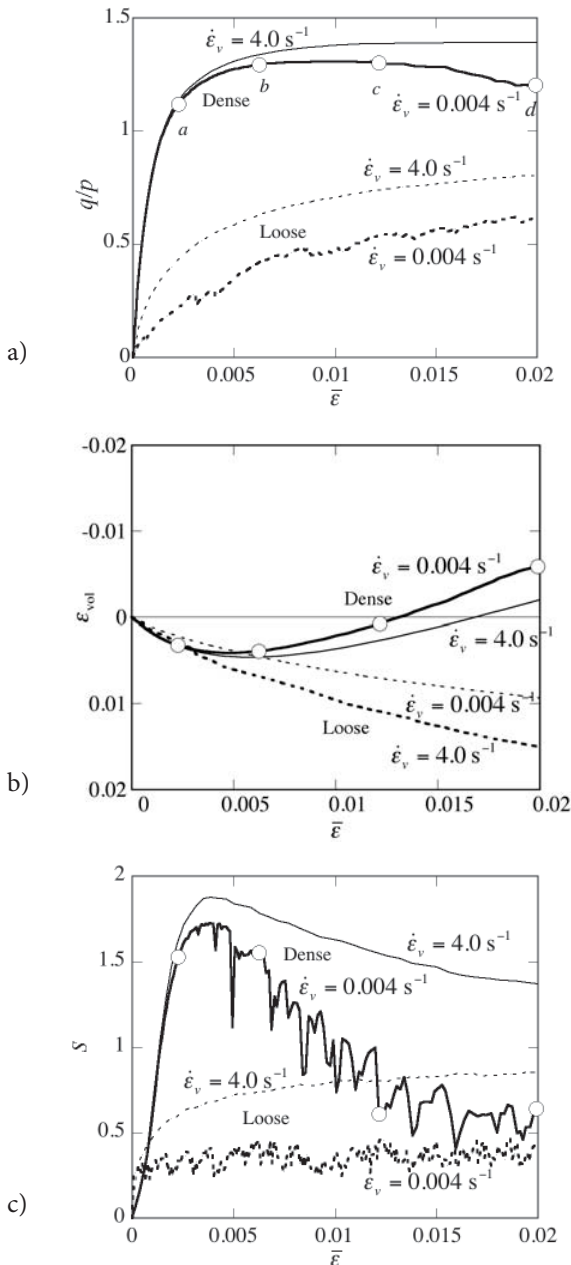


Figure 3. Responses to an equivalent deviatoric strain of 0.02: (a) Stress ratio, (b) Volumetric strain, (c) Slip coordination number.

small strain rate, the first peak-stress ratio for the dense specimen occurs around an equivalent deviatoric strain of 0.01, while the slip coordination number has its maximum value around an equivalent deviatoric strain of 0.004 (i.e., 0.4%) and then it reduces with oscillations due to slipping and sticking at the contacts. It is clear that the occurrence of the maximum slip coordination number corresponds to the transition from a contractive increment to a dilative increment for the volumetric strain (i.e., referred to as the phase-transformation point).

Figs. 4(a)–(d) show the contact-force distributions of four strains, “a”-“d” that are indicated in Fig. 3. It is clear that the strain localization gradually develops at various locations of the specimen at strains in “a” and “b”, and that there is one clear shear band and other possible shear bands developed at the strain in “c”, although two shear bands clearly exist in “d”. Yoshida [22] also presented image-analysis data from the plane strain

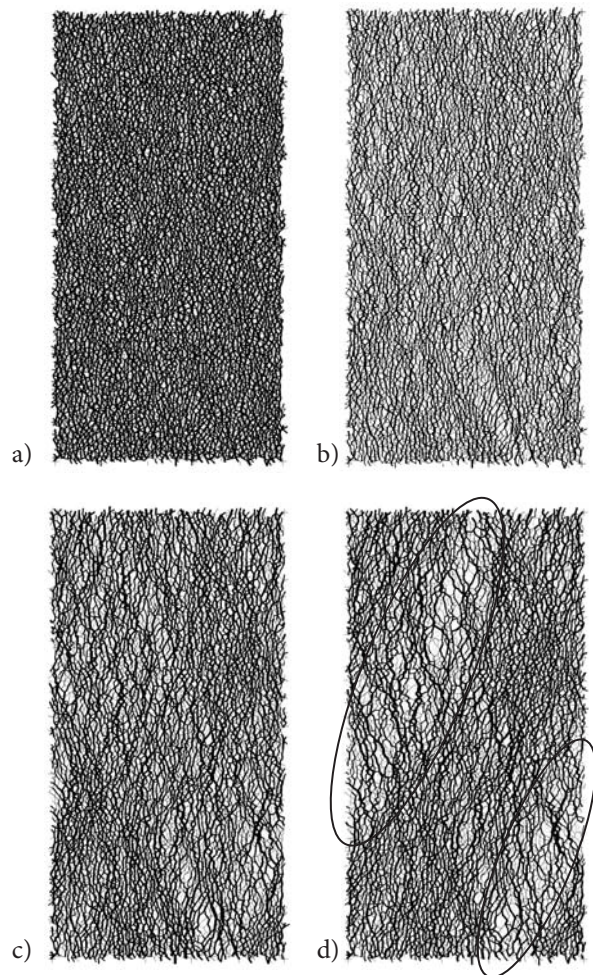


Figure 4. Variations of the contact-force distribution to an equivalent deviatoric strain of 0.02: (a) a, (b) b, (c) c, (d) d.

compression test that some strain localization regions can appear before the peak stress, and one of them rapidly develops into the dominant shear band.

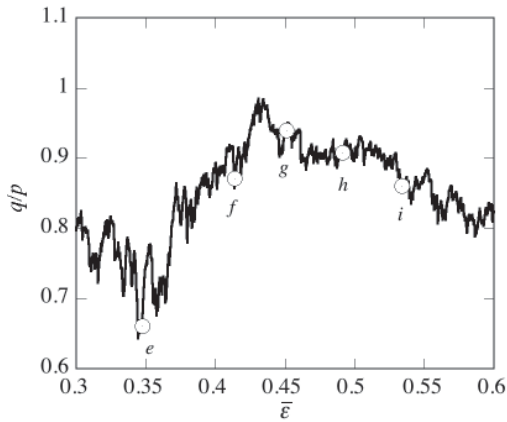


Figure 5. Stress ratio-equivalent deviatoric strain around the second peak-stress ratio.

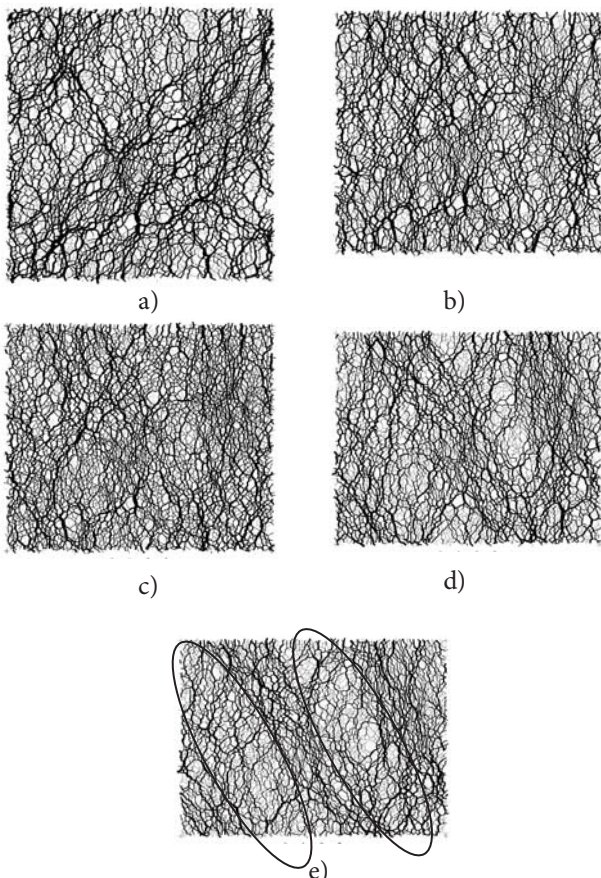


Figure 6. Variations of the contact-force distribution around the second peak-stress ratio: (a) *e*, (b) *f*, (c) *g*, (d) *h*, (e) *i*.

4.2 Second peak-stress ratio

The second peak-stress ratio has been recognized as a double strain-softening curve in the laboratory experimental results [23]. Fig. 5 shows the stress ratio-equivalent deviatoric strain curve around the second peak-stress ratio for the dense specimen. Figs. 6(a)–(e) show the spatial contact-force distributions at five strains “e”–“i” that are indicated in Fig. 5. It is clear that a dominant shear band inclined to the right exists in “e” before the second peak, and the fabric gradually changes, then two shear bands inclined to the left appear clearly in “i” after the second peak. This indicates that the equilibrium obtained after the first strain softening varies toward another equilibrium, together with the subsequent strain.

5 CONCLUSIONS

The behaviors up to the point of a large strain of 0.8 is reached with both dense and loose specimens were investigated in order to clarify the importance of a sufficiently small strain rate that guarantees the uniqueness of the solution, compared with a relatively large strain rate. There is a large difference qualitatively, as well as quantitatively, between the shear behaviors at a small strain rate with that at a relatively large strain rate. It should be noted that a small strain rate should be used, otherwise a unique solution cannot be guaranteed [11]. The following new conclusions can be made.

1. When the strain rate is large, it seems that a static steady state exists for the stress ratio, the coordination number, the slip coordination number and the “strong” fabric ratio. On the other hand, when the strain rate is sufficiently small, it seems to be a quasi-static steady state, although these observed results for dense and loose specimens approach each other.
2. It is shown by the unique solution that the “strong” fabric ratio is closely related to (and is almost equal to) the stress ratio.
3. For a dense specimen, the slip coordination number gradually increases and then becomes a maximum at the point that the volumetric strain changes from a contractive increment to a dilative increment, i.e., the phase-transformation ratio, and gradually decreases while fluctuating. It can be said that strain localization starts around the phase transformation point and the shear band appears around the peak strength.
4. For a dense specimen, the second peak strength appears after the first peak strength as a double strain-softening curve. The equilibrium after the first strain softening varies toward another equilibrium together with the subsequent strain.

Acknowledgements

The writer thanks M. R. Kuhn, Professor, University of Portland and M. Zaman, Professor, University of Oklahoma for their insightful comments on this paper.

REFERENCES

- [1] Cundall, P.A., Strack, O.D.L. 1979. A discrete numerical model for granular assemblies. *Geotechnique* 29, 1, 47-65.
- [2] Sitharam, T.G. 1999. Micromechanical modelling of granular media: The power of discrete element modelling, in: Sharma V.M., Saxena K.R., Woods R.D. (Eds.), *Distinct element modelling in geomechanics*. Oxford/IBH Publishing, New Delhi, India, pp. 47-88.
- [3] Thornton, C. 2000. Numerical simulations of deviatoric shear deformation of granular media. *Geotechnique* 50, 1, 43-53.
- [4] Rothenburg, L., Bathurst, R. 1989. Analytical study of induced anisotropy in idealized granular materials. *Geotechnique* 39, 4, 601-614.
- [5] Sazzad, M.M., Suzuki, K., Modaresi-Farahmand-Razavi, A. 2012. Macro-micro responses of granular materials under different b values using DEM. *Int. J. Geomech.* 9, 4, 220-228.
- [6] Chen, Y-C., Ishibashi, I. 1990. Dynamic shear modulus and evolution of fabric of granular materials. *Soils Found.* 30, 3, 1-10.
- [7] Rothenburg, L., Kruyt, N.P. 2004. Critical state and evolution of coordination number in simulated granular materials. *Int. J. Solids Struct.* 41, 5763-5774.
- [8] Nouguier-Lehon, C., Cambou, B., Vincens, E. 2003. Influence of particle shape and angularity on the behaviour of granular materials: a numerical analysis. *Int. J. Numer. Analyt. Meth. Geomech.* 27, 1207-1226.
- [9] Cui, L., O'Sullivan, C. 2005. Development of a mixed boundary environment for axi-symmetric DEM analyses. *Proc., 5th Int. Conf. on Micromechanics of Granular Media*, Stuttgart, Germany, pp. 301-305.
- [10] O'Sullivan, C., Cui, L., O'Neill, S.C. 2008. Discrete element analysis of the response of granular materials during cyclic loading. *Soils Found.* 48, 4, 511-530.
- [11] Luding, S. 2004. Micro-macro models for anisotropic granular media. *Proc., 2nd Int. Symp. on Continuous and Discontinuous Modelling of Cohesive-Frictional Materials*, Stuttgart, Germany, pp. 195-206.
- [12] Suzuki, K., Kuhn, M.R. 2014. Uniqueness of discrete element simulations in monotonic biaxial shear tests. *Int. J. Geomech.* 14, 5, 06014010.
- [13] Kuhn, M.R. 2002. Oval and OvalPlot: Programs for analyzing dense particle assemblies with the Discrete Element Method. <<http://faculty.up.edu/kuhn/oval/oval.html>>.
- [14] Cundall, P.A., Strack, O.D.L. 1983. Modeling of microscopic mechanisms in granular. *Proc., U.S./Japan Seminar on New Models and Constitutive Relations in the Material Mechanics of Granular Materials*, Ithaca, U.S.A., pp. 137-149.
- [15] Suzuki, K., Iwashita, K. 2010. A consideration on quantitative evaluation under biaxial isotropic compression using DEM. *J. Geotech. Eng. JSCE* 66, 2, 289-298 (in Japanese).
- [16] Ng T-T. 2006. Input parameters of discrete element methods. *J. Eng. Mech.* 132, 7, 723-729.
- [17] Kuhn, M.R. 1999. Structured deformation in granular materials. *Mech. Mater.* 31, 407-429.
- [18] Suzuki, K., Kuhn, M.R. 2014. Discrete element simulations of cyclic biaxial shear granular material with oval particles. *Int. J. Geomech.* 14, 3, 06014005.
- [19] Satake, M. 1982. Fabric tensor in granular materials. *Proc., IUTAM Symp. on Deformation and Failure of Granular Materials*, Rotterdam, The Netherlands, pp. 63-68.
- [20] Antony, S.J., Momoh, R.O., Kuhn, M.R. 2004. Micromechanical modelling of oval particulates subjected to bi-axial compression. *Comput. Mater. Sci.* 29, 4, 494-498.
- [21] Radjai, F., Jean, M., Moreau, J-J., Roux, S. 1996. Force distributions in dense two-dimensional granular systems. *Phys. Rev. Lett.* 77, 274-277.
- [22] Yoshida, T. 1995. Strain localization and shear banding during failure of sand. *D. Eng. Thesis*, Univ. Tokyo, Tokyo, Japan (in Japanese).
- [23] Suzuki, K., Yamada, T. 2006. Double strain softening and diagonally crossing shear bands of sand in drained triaxial tests. *Int. J. Geomech.* 6, 6, 440-446.

IMPLEMENTACIJA IN VERIFIKACIJA KONSTITUTIVNEGA MODELA VMESNE PLOSKVE GEOSINTETIK-ZEMLJINA V ELEMENTU GEOGRID PROGRAMA FLAC^{3D}

Wu Haimin (vodilni avtor)

Hohai University,
College of Water Conservancy and Hydropower Engineering
Nanjing 210098, Kitajska
E-pošta: wuhaimin@hhu.edu.cn

Shu Yiming

Hohai University,
College of Water Conservancy and Hydropower Engineering
Nanjing 210098, Kitajska

Dai Linjun

Hohai University,
College of Water Conservancy and Hydropower Engineering
Nanjing 210098, Kitajska

Teng Zhaoming

Hohai University,
College of Water Conservancy and Hydropower Engineering
Nanjing 210098, Kitajska

Izvleček

Zaradi zapletenosti interakcije med geosintetikom in zemljino, enostavni konstitutivni modeli za vmesne ploskve, ki so vgrajeni v geosintetične elemente splošnih računalniških programov, ne zadovoljujejo zahtev za numerično simulacijo različnih odzivov na vmesni ploskvi med geosintetikom in zemljino. Na osnovi rezultatov direktnega strižnega preizkusa kompozitne vmesne ploskve iz geomembrane (CGM) in poliuretana (PUR) zmešanega z drobljenim kamenjem, je bil za opis obnašanja vmesne ploskve uporabljen nelinearno elastičen idealno plastičen model. S pomočjo uporabniško definirane programa v okolju FISH je detajlno predstavljena metoda vključitve konstitutivnega modela vmesne ploskve v element Geogrid postopka hitre Lagrangeeve tridimenzionalne analize kontinua. Nato je bil konstitutivni model elementa Geogrid uporabljen za simulacijo direktnega strižnega preizkusa vmesne ploskve CGM-PUR zmešanima z drobljenim kamenjem. Rezultati numeričnih preizkusov so potrdili veljavnost in zanesljivost vključenega modela. Predstavljena metoda in diagram poteka za implementacijo nelinearno elastičnega idealno plastičnega konstitutivnega modela vmesne ploskve v element Geogrid podajata napotek uporabnikom, ki želijo simulirati drugačna obnašanja vmesne ploskve med geosintetikom in zemljine s pomočjo FLAC^{3D}.

Ključne besede

vmesna ploskev geosintetik-zemljina, konstitutivni model, numerično modeliranje, FLAC^{3D}, element Geogrid

IMPLEMENTATION AND VERIFICATION OF A GEOSYNTHETIC-SOIL INTERFACE CONSTITUTIVE MODEL IN THE GEOGRID ELEMENT OF FLAC^{3D}

Wu Haimin (corresponding author)

Hohai University,
College of Water Conservancy and Hydropower Engineering
Nanjing 210098, China
E-mail: wuhaimin@hhu.edu.cn

Shu Yiming

Hohai University,
College of Water Conservancy and Hydropower Engineering
Nanjing 210098, China

Dai Linjun

Hohai University,
College of Water Conservancy and Hydropower Engineering
Nanjing 210098, China

Teng Zhaoming

Hohai University,
College of Water Conservancy and Hydropower Engineering
Nanjing 210098, China

Keywords

geosynthetic-soil interface, constitutive model, numerical modelling, FLAC^{3D}, geogrid element

Abstract

Due to the complexity of geosynthetic-soil interactions, the simple interface constitutive models embedded in the geosynthetic elements of general computing software cannot satisfy the requirements for a numerical simulation of different geosynthetic-soil interface behaviours. Based on the direct shear test results of a composite geomembrane (CGM) and polyurethane (PUR) mixed crushed stones interface, a nonlinear elastic, perfectly plastic model was used to describe the interface behaviours. The method of incorporating an interface constitutive model into the Geogrid element of a fast Lagrange analysis of continua in three dimensions (FLAC^{3D}) procedure was presented in detail through a user-defined program in the FISH environment. Then the incorporated model of the Geogrid element was used to simulate the direct tests of the CGM-PUR mixed crushed stones interface. The results of the numerical tests confirmed the validity and reliability of the incorporated model. The method and program flowchart for implementing the nonlinear elastic, perfectly plastic interface constitutive model into the Geogrid element can provide a reference for users who want to simulate other geosynthetic-soil interface behaviours with FLAC^{3D}.

1 INTRODUCTION

Geosynthetics are increasingly used with soils as a composite structure due to their numerous advantages. This is relevant to many geotechnical engineering situations, such as the geomembrane barrier of an earth-rock-fill dam and waste landfills, geotextile- or geogrid-reinforced structures. A deeper understanding of the geosynthetics-soil interaction is of paramount importance for a stability assessment and deformation analysis of composite structures. The key point of solving the geosynthetic-soil interaction problem is to accurately describe the shear stress-displacement relationship of the interface. Several researchers, such as Byrne [1]; Jenevein et al. [2]; Esterhuizen et al. [3]; Kim [4]; Zhang et al. [5]; and Bacas et al. [6] have proposed different constitutive models to describe the geosynthetic-soil interface behaviours based on the results of laboratory tests and field investigations. The interface constitutive models were also incorporated into numerical programs to simulate the geosynthetics-soil interactions involved in the different structures [7, 8, 9, 10]. Several numerical computing software packages, such as PLAXIS, ABAQUS and FLAC/FLAC^{3D}, can provide structural elements to simulate the mechanical behaviours of flexible geosynthetics. But these structural elements only provide a single and simple generalized interface

model for users to simulate the different geosynthetic-soil interactions. This seriously limits the application of the software in solving problems that contain different geosynthetic-soil interfaces.

Due to its distinct advantage of solving the large strain problems of rock and soil structures, the finite-difference code FLAC/FLAC^{3D} has been used to solve geotechnical engineering problems containing geosynthetics by many researchers, such as Jones and Dixon [11]; Fowmes et al. [12,13,14]; Wu. et al. [15]; and Wu and Shu. [16]. The Geogrid element in FLAC and FLAC^{3D} can only simulate the shear stress vs. shear displacement relationship of a geosynthetic-soil interface according to the linear elastic, perfectly plastic model. But it is not able to simulate the geosynthetic-soil interfaces characterized by nonlinear or strain-softening behaviours.

Studies on the improvement and further development of Geogrid elements in the FLAC and FLAC^{3D} software have rarely been reported. Jones and Dixon [7]; Fowmes et al. [9]; Wu et al. [17] have incorporated the results of interface direct tests into the FLAC and FLAC^{3D} program to simulate the strain-softening behaviours of a geosynthetic-soil interface using the embedded FISH language, respectively. Their simulations were achieved by incorporating the geosynthetic-soil interface constitutive model into the Interface element, but not the Geogrid element of the FLAC or FLAC^{3D}. Although the interface element can simulate the geosynthetic-soil interface behaviours, it cannot simulate the mechanical behaviour of the geosynthetics itself. Only the shear stress distribution at the interface can be solved using their incorporated models. And they cannot be used to calculate the stress and strain of the geosynthetics when considering the geosynthetic-soil interaction. So a further improvement needs to be performed to accomplish a numerical simulation of the geosynthetic-soil interaction using the Geogrid element in FLAC^{3D}.

In this paper, the implementation of the direct shear testing results of the CGM-PUR mixed crushed stones interface was taken as an example to present the method of incorporating a new geosynthetic-soil interface constitutive model into the Geogrid element of the FLAC^{3D}. Firstly, a nonlinear elastic, perfectly plastic model for the interface was used to describe the direct shear test results for the CGM-PUR mixed crushed stones interface. Then the interface model was incorporated into the Geogrid elements of the FLAC^{3D} through a user-defined program in the FISH environment. Finally, the direct shear tests on the CGM-PUR mixed crushed stones interface were simulated by an improved Geogrid element to verify the incorporated geosynthetic-soil interface model.

2 ORIGINAL INTERFACE CONSTITUTIVE MODEL OF THE GEOGRID ELEMENT IN FLAC^{3D}

The Geogrid element in FLAC^{3D} is a type of plane-stress element that can resist a membrane load but not a bending load [18]. The Geogrid elements can be used to model the flexible geosynthetics whose shear interactions with the soil are important, such as the geomembrane, the geotextiles and the geogrids.

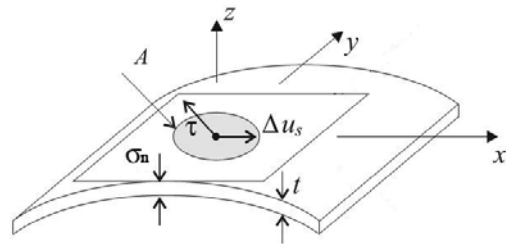


Figure 1. Mechanical behaviour in the shear direction of the Geogrid-soil interface.

The Geogrid element is embedded in the interior of the grid zones (soil) in FLAC^{3D}. As shown in Fig. 1, the interaction between Geogrid and the zone element is defined by the mechanical behaviours of the Geogrid-soil interface. The interface behaviour is represented numerically at each Geogrid node by a rigid attachment in the normal direction and a spring-slider in the tangent plane to the Geogrid surface.

In the normal direction the Geogrid element is slaved to the soil-grid motion. In order to be different from the common soil-structure interface, the normal discontinuous deformation such as penetration or separation on the geosynthetic-soil interface is not considered. And the effective normal stress is assumed to be acting equally on both sides of the Geogrid surface. The velocity and displacement normal to the Geogrid surface are transferred directly to the nodes of the soil zone. The node exerts no normal force on the soil-grid if all the Geogrids that share the node are co-planar; however, if they are not co-planar, then a proportion of their membrane force will act in the normal direction [18].

In the tangent plane of the Geogrid surface, a shear-directed frictional interaction occurs between the Geogrid and the soil grid. The relative displacement between the Geogrid and the soil grid is the source of the frictional shear stress on the interface. In computing the relative displacement at the Geogrid-soil interface, an interpolation scheme is used that is based on the displacement field in the zone to which the node is linked. The interpolation

scheme uses weighting factors that are determined by the distance to each of the zone grid points [18].

The shear stress that is exerted on the node of the Geogrid during the calculation time step $t + \Delta t$ can be expressed as follows:

$$\tau^{(t+\Delta t)} = \tau^{(t)} + \Delta\tau \quad (1)$$

where $\tau^{(t+\Delta t)}$ is the shear stress exerted on the node of the Geogrid during the calculation time step $t + \Delta t$; $\tau^{(t)}$ is the shear stress exerted on the node of the Geogrid during the calculation time step t , and $\Delta\tau$ is the incremental shear stress between t and $t + \Delta t$.

The incremental shear stress $\Delta\tau$ is determined by the Geogrid-soil interface constitutive model, i.e., the shear stress-shear displacement relationship:

$$\tau = f(u) \quad (2)$$

where τ is the shear stress of the Geogrid-soil interface, and u is the shear displacement of Geogrid-soil interface.

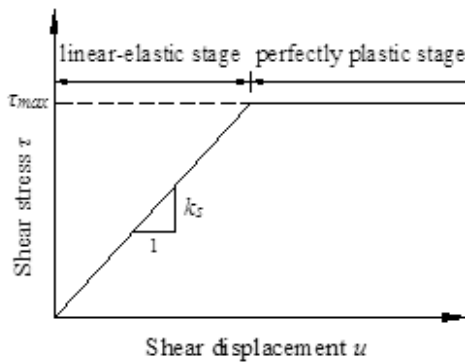


Figure 2. Elastic, perfectly plastic model of the Geogrid-soil interface.

The original interface constitutive model of the Geogrid element in FLAC^{3D} is shown in Fig.2. The relationship between the shear stress and the shear displacement is defined by the linear elastic, perfectly plastic model. In the linear elastic stage, the shear stress and shear displacement relationship can be expressed as:

$$\tau = f(u) = k_s u \quad (3)$$

where k_s is the shear stiffness (constant) of the Geogrid-soil interface.

After the shear stress reaches a peak shear strength of the interface, plastic failure occurs with an increase of the shear displacement. The interface shear strength of the Geogrid element in FLAC^{3D} is defined by the Mohr-Coulomb failure criterion:

$$\tau = \tau_{\max} = c + \sigma_n \tan \phi \quad (4)$$

where τ_{\max} is the shear strength of the Geogrid-soil interface; c is the cohesion of the Geogrid-soil interface; ϕ is the friction angle of the Geogrid-soil interface, and σ_n is the normal stress of the Geogrid-soil interface.

3 DIRECT SHEAR TEST OF THE CGM-PUR MIXED CRUSHED STONES INTERFACE

The direct shear test results of the CGM- PUR mixed crushed stones interface will be taken as an example to illustrate the method of incorporating a new geosynthetic-soil interface constitutive model into the Geogrid elements of FLAC^{3D}. And the direct shear tests of the CGM-PUR mixed crushed stones interface will be introduced in a simple way.

3.1 Test materials

The CGM commonly used as a surface barrier for rock-fill dams in China was chosen for the tests. A photograph of a CGM is shown in Fig. 3. It consists of a 0.8-mm-thick HDPE geomembrane laminated to 400 g/m² PET needle punched nonwoven geotextile on both sides. Its ultimate tensile strength (ASTM D4595, 2005) in the machine direction and the cross-machine direction are 75.9kN/m and 58.3kN/m, respectively.

As shown in Fig. 4, the PUR mixed crushed stones is a new elastic porous material that is casted using polyure-



Figure 3. Composite geomembrane.



Figure 4. PUR mixed crushed stones.

thane adhesive mixed crushed stones. Due to its higher bending strength, excellent resilience and permeability, it can be used as the cushion layer of CGM in the surface barrier of a high rockfill dam on a thick riverbed alluvial deposit [19]. The basic properties of the crushed stones are given in Table 1.

Table 1. Basic properties of the crushed stones for the tests.

Size range (mm)	d ₅₀ (mm)	C _u	C _c	ρ _d (g/cm ³)	Φ (°)
5-20	10	4.2	2.4	1.725	48

3.2 Test apparatus and procedure

A large-scale direct shear apparatus was used for the tests. The device comprises a 300-mm square-top box and a 300 mm × 350 mm lower box. The maximum shear displacement can reach 50 mm with no loss in the area of the shear plane. A rigid iron block was filled in the lower box. The tests were performed according to the procedure in ASTM D5321-08 [20]. The CGM specimen was glued to the rough top face of the lower block with adhesive. The left end of the CGM was fixed on the side of the lower box with a steel bar and screws. Then the 300 mm × 300 mm pre-casted PUR mixed crushed stones specimen was placed in the top box. The tests were carried out in dry conditions. And the bottom surface of the PUR mixed crushed stones keeps a good contact state with the top surface of the CGM. The tests were performed on each interface at constant normal stresses of 25, 50, 75 and 100kPa, respectively. The rate of shearing was kept at 1.0 mm/s. Each test was conducted until the shear displacement reached 20 mm.

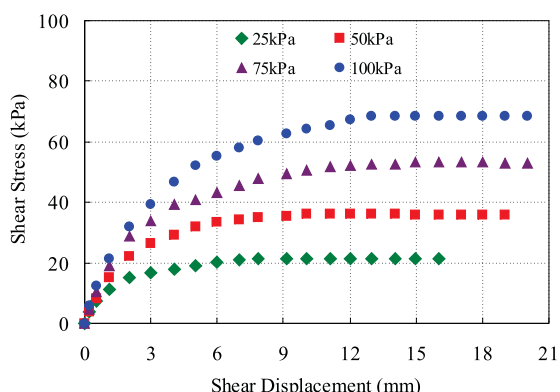


Figure 5. Shear stress vs. shear displacement of the CGM-PUR mixed crushed stones interface.

3.3 Test results

The shear behaviours of the CGM-PUR mixed crushed stones interface are shown in Fig. 5. The interface shear stress vs. shear displacement curves under different normal stresses show obviously nonlinear characteristics at the beginning of the shearing. When the shear stress reaches the peak strength, plastic failure occurs with an increase of the shear displacement. The CGM-PUR mixed crushed stones interface shows the failure mode of the elastic, perfectly plastic and sliding along the interface.

The peak shear stress versus normal stress for the CGM-PUR mixed crushed stones interface is shown in Fig. 6.

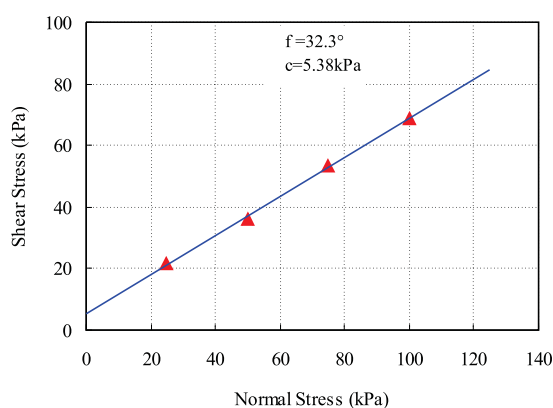


Figure 6. Shear stress vs. normal stress of the CGM-PUR mixed crushed stones interface.

It is clear that the peak shear stresses increase with the increasing of the normal stress. The shear strength of the interface can be expressed as a function of the normal stress using the Mohr-Coulomb criterion. The interface shear strength parameters ϕ and c obtained by fitting a straight line through the plots of the peak shear stress vs. the normal stress are 32.3° and 5.38kPa, respectively.

4 CONSTITUTIVE MODEL OF THE CGM-PUR MIXED CRUSHED STONES INTERFACE

4.1 Nonlinear elastic, perfectly plastic interface model

Based on the results of the direct shear tests, a nonlinear elastic, perfectly plastic interface constitutive model (Fig. 7) that combines the nonlinear hyperbolic model

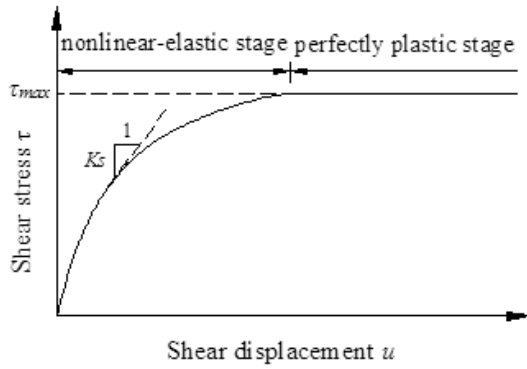


Figure 7. Nonlinear elastic, perfectly plastic model of the interface.

[21] with the Mohr-Coulomb plastic failure envelope can be used to describe the mechanical behaviour of the CGM-PUR mixed crushed stones interface. As shown in Fig.7, the complete shear stress, shear displacement response of the nonlinear elastic, perfectly plastic interface constitutive model can be divided into two sections: the pre-peak nonlinear elastic stage and the post-peak perfectly plastic failure stage.

4.1.1 Nonlinear-elastic stage

Before the shear stress reaches the peak strength, the relationship between the interface shear stress and the shear displacement can typically be modelled by a hyperbolic equation proposed by Kondner [22]:

$$\tau = \frac{u}{a + bu} \quad (5)$$

The parameters a and b can be expressed as:

$$a = \frac{1}{k_1 \gamma_w \left(\frac{\sigma_n}{Pa}\right)^n} \quad (6)$$

$$b = \frac{R_f}{\sigma_n \tan \phi + c} \quad (7)$$

where γ_w is the unit weight of water, σ_n is the normal effective stress of the interface; Pa is the atmospheric pressure; τ is the shear stress; c is the cohesion of the interface; ϕ is the friction angle of the interface; k_1 , n and R_f are nonlinear parameters that can be derived from the interface direct shear tests.

The shear stiffness of the interface k_s can be represented by a tangent modulus of the shear stress vs. shear displacement curve[23]:

$$k_s = \frac{\partial \tau}{\partial u} \quad (8)$$

By combining the four equations above, the shear stiffness of the interface k_s can be expressed as follows:

$$k_s = K_1 \gamma_w \left(\frac{\sigma_n}{Pa}\right)^n \left[1 - R_f \frac{\tau}{c + \sigma_n \tan \phi}\right]^2 \quad (9)$$

4.1.2 Perfectly plastic failure stage

When the shear stress reaches the peak shear strength of the CGM-PUR mixed crushed stones interface, plastic failure occurs with a further increase of the shear displacement. The shear-strength envelope in the post-peak stage is the same as that of the original interface's shear-strength failure criterion (Eq. (4)) of the Geogrid element in FLAC^{3D}.

4.2 Parameters of the CGM-PUR mixed crushed stones interface model

The fitting curves of the interface shear stress vs. the shear displacement from the test results using the nonlinear elastic, perfectly plastic interface model are shown in Fig. 8. The fitting parameters for the interface model are given in Table 2. It is clear that the fitting curves using the model show good agreement with the test results under different normal loads.

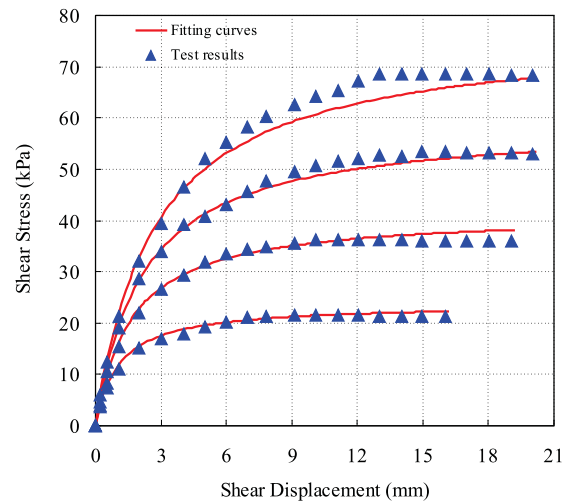


Figure 8. Fitted curves of shear stress vs. shear displacement for the CGM-PUR mixed crushed stones interface.

Table 2. Fitting parameters of the interface model.

K	n	R_f	$c(\text{Pa})$	ϕ (°)
2871	0.185	0.893	5380	32.3

5 IMPLEMENTATION OF THE CGM-PUR MIXED CRUSHED STONES INTERFACE MODEL

In order to simulate the mechanical behaviours of the CGM-PUR mixed crushed stones interface, the nonlinear elastic, perfectly plastic interface model was incorporated into the Geogrid element of FLAC^{3D} by applying the user-defined FISH program.

By comparing the original interface constitutive model of the Geogrid element in FLAC^{3D} (Fig. 2) with the nonlinear elastic, perfectly plastic model for the CGM-PUR mixed crushed stones interface (Fig. 7). It is clear that the main difference is the pre-peak stage of the two models. So the implementation works mainly focus on

replacing the linear-elastic stage (Eq. (3)) of the shear stress vs. displacement curve by the nonlinear-elastic stage (Eq. (8) and Eq. (9)) with the user-defined FISH program. The general method and detailed procedure for incorporating the interface model into the Geogrid element of FLAC^{3D} are described in this section.

5.1 Procedure for incorporating the program

A detailed program flowchart for the implementation of the CGM-PUR mixed crushed stones interface model is shown in Fig. 9.

Firstly, a loop-control function is used to define the total number of calculation steps at the beginning of the main program of FLAC^{3D}.

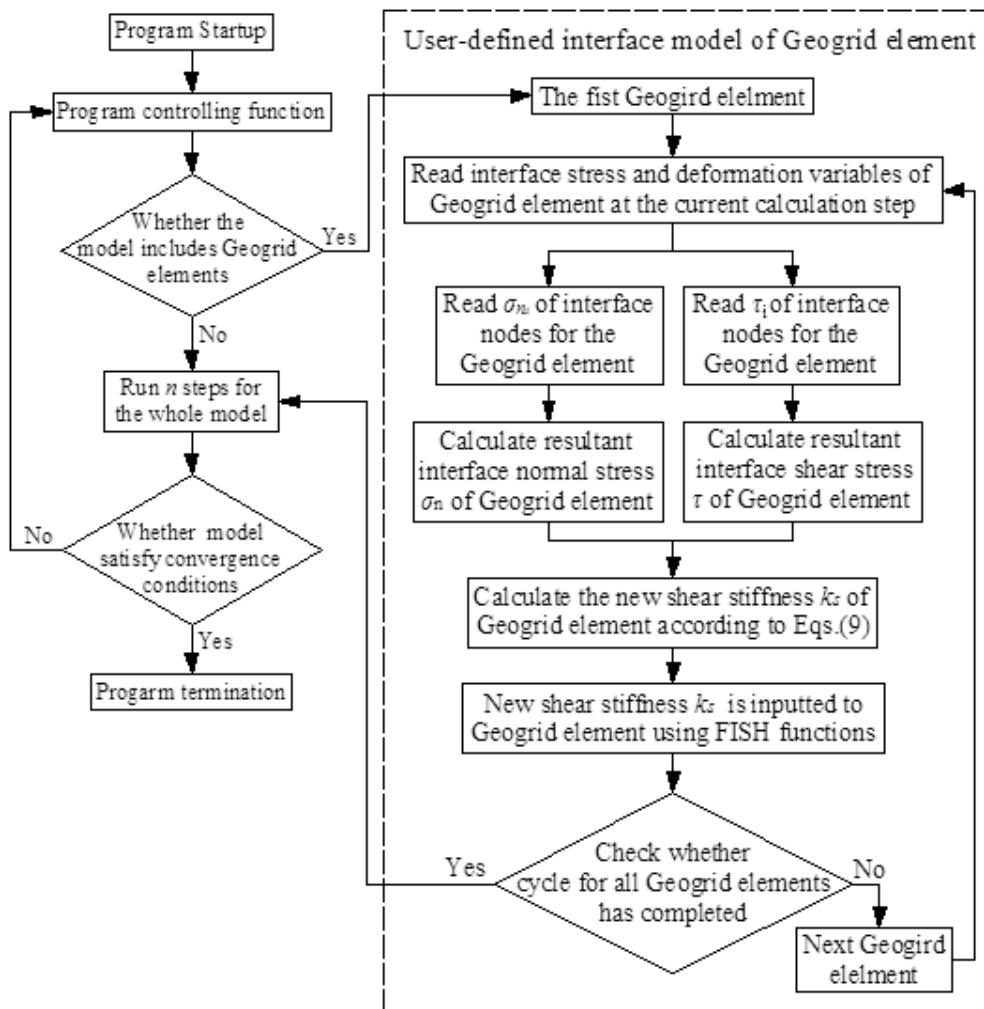


Figure 9. Program flowchart for the implementation of the nonlinear elastic, perfectly plastic interface model in the Geogrid element of FLAC^{3D}.

Secondly, a case statement of Fish is used to check whether the numerical model contains the Geogrid element. If there are Geogrid elements included in the model, the program module that defines the user-defined interface model will be called. Through the running of the user-defined interface model, the parameters and the theoretical formulae of the shear stress vs. shear displacement relationship of all the Geogrid elements will be updated. Then, the main program will be activated to run n steps. In the event that there is no Geogrid element that can be detected by the case statement, the main program will be directly activated to run n steps without calling the program module of the user-defined interface model.

Thirdly, the main program of FLAC^{3D} will check whether all the elements in the model satisfy the convergence conditions. If the convergence conditions are satisfied, the main program runs to completion. In the case that the convergence conditions are not satisfied, the main program will return to the loop-control function and a new cycle will be carried out by repeating the steps above until all the elements reach an equilibrium state.

The detailed program for the user-defined interface model of the Geogrid element (right part of Fig. 9) is described as follows.

At every calculation step, the program first reads the normal effective stress and the shear stress of the three interface nodes for every Geogrid element. The resultant interface normal stress and shear stress of the Geogrid element are calculated according to the node variables. Then the stiffness of the interface is calculated according to the resultant Geogrid element variables by Eq. (9). And the shear stiffness is inputted into the Geogrid element using Fish functions. Then the case statement of the Fish is used to check whether the cycle of all the Geogrid elements has completed. If it has been completed, the main program returns to the step of running n steps. In the other case the cycle will be carried out for the next Geogrid element. In this way, the user-defined interface model is continuously carried out until the cycle for all the Geogrid elements has completed.

5.2 Several points need attention

Several key points needed attention during the programming of the implementation of the CGM-PUR mixed crushed stones interface model and are presented here:

(1) When defining the total number of calculation steps, a large enough but appropriate integer should be set to ensure that all the elements can reach an equilibrium state within the number of steps.

- (2) At every calculation step, it should be checked to see whether the interface normal effective stress σ_n read from the last step of every Geogrid element is positive. At the beginning of every cycle, the stress and displacement of the elements are still in an unbalanced state and the normal effective stress read from the last step may be a negative number or zero. This may result in an error of the main program. In this case, a small positive number should be inputted as the initial value of σ_n .
- (3) The interface shear stress and the shear displacement are not variables of the Geogrid element, but variables of the nodes of the Geogrid element. Since the parameters updating and inputting for the Geogrid element is based on the shear stress and shear displacement of the element, the nodal shear stress and shear displacement obtained from the last step must be transformed into element variables to calculate the new interface parameters.
- (4) In the perfectly plastic stage of the interface model, some plastic sliding along the interface occurs. Then the interface elements begin to yield, and the shear stress will be corrected according to the original yield criterion (Eq. (4)) of FLAC^{3D}. So the updating of the shear stiffness and the shear strength parameters in plastic stage is not required in the program module of the user-defined interface model.
- (5) When the parameters of all the Geogrid elements have been updated through the program module of the user-defined interface model, the main program will be activated to run n steps. An integer that is equal to or larger than 1 should be set to n . If n is too large, a shorter calculation time and a lower calculation accuracy of the model may be the result. So the users should adjust n according to the limitation of the calculation time and the requirement of the calculation accuracy.

6 VERIFICATION OF THE INCORPORATED INTERFACE MODEL

In order to verify the correctness of the incorporated interface model of the Geogrid element, a numerical example is used to model the interface direct shear tests between the CGM and the cushion material casted by the PUR mixed crushed stones. As shown in Fig. 10, the numerical model of the test is composed of two parts. The upper part is a shear box with a cushion material in it; the lower is a rigid block where the geomembrane is glued to the top surface. In order to keep a constant contacting area during shearing, the area of the lower box is larger than that of the upper. The incorporated nonlinear elastic, perfectly plastic interface model of the

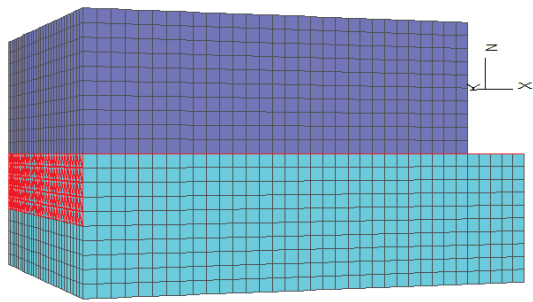


Figure 10. Numerical model of direct shear test for the CGM-PUR mixed crushed stones interface.

Geogrid element in last section is used to simulate the CGM-PUR mixed crushed stones interface behaviours.

In order to compare the numerical results with the results of the theoretical model and the test results, a linear elastic model was employed for the cushion material in the upper box as well as the rigid block in the lower box. Gravitational forces were not considered during the numerical experiments. The parameters in Table 2 resulting from the direct shear tests were used for the imbedded interface model. According to the typical procedures for the direct shear test, a constant normal pressure was applied on the top surface of the cushion material. Then, the displacements and velocities of all elements were reset to zero. A fixed shear velocity of 1×10^{-5} m/s was applied to all the elements of the lower part to simulate the actual shearing rate of 1 mm/min. This led to a displacement on the interface between the upper cushion

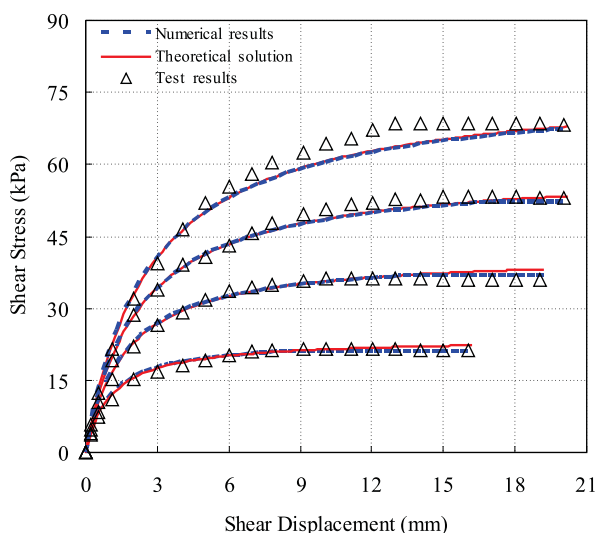


Figure 11. Relationship for shear stress vs. shear displacement of the Geogrid-Zone interface.

and the lower CGM. Four numerical direct-shear tests were simulated with constant normal pressures of 25kPa, 50kPa, 75kPa, and 100kPa, respectively.

The numerical results of the average interface shear stress vs. the shear displacement curves and the comparison with the test results and the theoretical solution are shown in Fig. 11. It is obvious that the numerical results are very close to the theoretical solutions calculated by Eq. (5)-(7) using the same parameters. And both the numerical and theoretical solutions also show good agreements with the shear direct test results. Fig. 11 illustrates that the incorporated interface model in the Geogrid element of the FLAC^{3D} procedure is capable of modelling the nonlinear elastic, perfectly plastic behaviour of the interface between the CGM and the PUR mixed crushed stones.

7 CONCLUSIONS

- (1) The Geogrid element in FLAC^{3D} can only model geosynthetic-soil interactions that accord with the linear elastic, perfectly plastic model. That restricts the application range of FLAC^{3D} in solving problems involving different geosynthetic-soil interfaces. The implementation of the direct shear testing results on the CGM-PUR mixed crushed stones interface was taken as an example to present the method of incorporating a new geosynthetic-soil interface constitutive model into the Geogrid elements of FLAC^{3D}.
- (2) By fitting the direct shear test data, the nonlinear elastic, perfectly plastic interface model can be used to describe the mechanical behaviours of the CGM-PUR mixed crushed stones interface. The constitutive model of the CGM-PUR mixed crushed stones interface was incorporated into the Geogrid element of the FLAC^{3D} procedure by the user-defined FISH program. The method and program flowchart of the implementation of geosynthetic-soil interface model into the Geogrid element of FLAC^{3D} was presented in detail.
- (3) A numerical simulation of the direct shear test of a CGM-PUR mixed crushed stones interface was performed to verify the correctness of the incorporated interface model. The numerical results represent good agreement with the theoretical solution and the test results. The improved Geogrid element FLAC^{3D} can be used for the nonlinear and plastic characteristics of the geosynthetic-soil interface behaviour.
- (4) The method and basic procedures of the implementation of a geosynthetic-soil interface constitutive model into the Geogrid element in FLAC^{3D} described in this paper can offer a reference for the

incorporation of other geosynthetic-soil interface constitutive models into FLAC^{3D} using the FISH programming platform.

- (5) It must be emphasized that the incorporated interface model in the Geogrid elements of FLAC^{3D} of this paper is mainly used to simulate the monotonical shear behaviours in the tangential direction of the geosynthetic-soil interface. The simulation of the cyclic shear and normal dilatant behaviours of the geosynthetic-soil interface may be a future study on the basis of this work.

Acknowledgements

The research is supported by National Natural Science Foundation of China (Nos. 51409083 and 51379069), Jiangsu Planned Projects for Postdoctoral Research Funds (No. 1302010A). Authors would like to thank the anonymous referees whose comments helped us improve the presentation of this paper.

REFERENCES

- [1] Byrne, J.R. 1994. Design issues with displacement-softening interfaces in landfill liners. *Proc., Waste Tech*, 1-26, Charleston, S.C.
- [2] Jenevein, D. R., Deschamps, R. J., Leonards, G. A., Byrne, R.J. 1996. The stability of landfills with strain softening liner interfaces. *Proc., 2nd Int. Congr. on Envir. Geotechnics*, Osaka, Japan, 1, 229-232.
- [3] Esterhuizen, J.J.B., Filz, G.M., Duncan, J.M. 2001. Constitutive behavior of geosynthetic interfaces [J]. *Geotech. and Geoenviron. Eng.* 127(10), 834-840.
- [4] Kim, D. 2007. Multi-Scale Assessment of Geotextile-Geomembrane Interaction. Ph. D. Dissertation. Atlanta: Georgia Institute of Technology.
- [5] Zhang, G., Wang, L.P., Zhang, J.M. 2010. Monotonic and cyclic modeling of interface between geotextile and gravelly soil. *International Journal for Numerical and Analytical Methods in Geomechanics* 34, 1346-1361.
- [6] Bacas, B. M., Konietzky, H., Berini, J. C., Sagaseta, C. 2011. A new constitutive model for textured geomembrane/geotextile interfaces. *Geotextiles and Geomembranes* 29(2), 137-148.
- [7] Murugesan, S., Rajagopal, K. 2006. Geosynthetics-encased stone columns: numerical evaluation. *Geotextiles and Geomembranes* 24, 349-358.
- [8] Li, A.L., Rowe, R.K. 2008. Effects of viscous behavior of geosynthetic reinforcement and foundation soils on the performance of reinforced embankments. *Geotextiles and Geomembranes* 26, 317-334.
- [9] Palmeira, E.M., 2009. Soil-geosynthetic interaction: modelling and analysis. *Geotextiles and Geomembranes* 27, 368-390.
- [10] Anubhav, S., Basudhar, P.K. 2010. Modeling of soil-woven geotextile interface behavior from direct shear test results. *Geotextiles and Geomembranes* 28, 403-408.
- [11] Jones, D.R.V., Dixon, N. 2005. Landfill lining stability and integrity-the role of waste settlement. *Geotextiles and Geomembranes* 23, 27-53.
- [12] Fowmes, G.J., Dixon, N., Jones, D.R.V. 2008. Validation of a numerical modelling technique for multilayered geosynthetic landfill lining systems. *Geotextiles and Geomembranes* 26, 109-121.
- [13] Fowmes, G.J., Jones, D.R.V., Dixon, N., 2005. Analysis of a landfill directive compliant steep wall lining system. *Proceedings of the 10th International Waste Management and Landfill Symposium*, Sardinia.
- [14] Fowmes, G.J., Dixon, N., Jones, D.R.V., Cowland, J., 2006. Modelling of lining system integrity. *Proceedings of the 8th International Conference on Geosynthetics*, Yokohama, Japan, p. 207.
- [15] Wu, W., Wang, X.T., Aschauer, F. 2008. Investigation on failure of a geosynthetic lined reservoir. *Geotextiles and Geomembranes* 26, 363-370.
- [16] Wu Hai-min, Shu Yi-ming 2012. Stability of geomembrane surface barrier of earth dam considering strain-softening characteristic of geosynthetic interface. *KSCE Journal of Civil Engineering* 16(7), 1123-1131.
- [17] Wu Haimin, Shu Yiming, Zhu Jungao 2011. Implementation and verification of interface constitutive model in FLAC^{3D}. *Water Science and Engineering* 4 (3): 305-316.
- [18] Itasca Consulting Group, Inc. 2005. Fast Lagrangian analysis of continua in three dimensions, version 3.0, and user's manual[R]. Minneapolis.
- [19] Wu, H. M. 2013. Research on Key Problems in Geomembrane Surface Barrier of Rock-fill Dam on Thick Riverbed Alluvial Deposit, Ph. D. Dissertation, Hohai University, Nanjing, China. (in Chinese)
- [20] ASTM 2008. Standard test method for determining the coefficient of soil and geosynthetic or geosynthetic and geosynthetic friction by direct shear method. D5321, ASTM, Philadelphia.
- [21] Clough G.W., Duncan J. M. 1971. Finite Element Analysis of Retaining Wall Behavior, *Journ. Soil Mech. & Found. Div.* 97, 12, 1657-1674.
- [22] Kondner, R.L. 1963. Hyperbolic stress-strain response: cohesive soils. *Journal of Soil Mechanics and Foundations Division* 89 (1), 289-324.
- [23] Duncan, J.M., Chan, C.Y. 1970. Nonlinear analysis of stress and strain in soils. *Journal of Soil Mechanics and Foundations Division* 96 (5), 1629-1653.

ANALIZA PREISKAVE Z DILATOMETROM V PREKONSOLIDIRANIH SEDIMENTIH, KOTLINA REKE DUERO V ŠPANIJU

F. Escolano Sánchez

University Polytechnic of Madrid,
Civil Engineering Department
Alfonso XII, 3 y 5 - 28014 Madrid, Španija
E-pošta: felix.escolano@upm.es

M. Bueno Aguado

Euroconsult SA
28700. S.S. Reyes. Madrid, Španija

Izvleček

Preizkus z dilatometrom je uporaben za terenske geotehnične raziskave. Njegove rezultate lahko primerjamo z rezultati dobljeni z uporabo matematičnih modelov. V članku prikazani matematični model koncentričnih obrojev uporablja konstitutivne enačbe iz modela "Hardening Soil Model". Veliko število preizkusov izvedenih na Dueñas geoloških faciesih, s konsistencami v rangu med trdimi glinami in mehкими kamninami, je bilo primerjanih z rezultati modela. S tem so bili parametri modela "Hardening Soil Model" prilagojeni materialom na Dueñas faciesih.

Ključne besede

Dueñas, geotehnični parametri, Hardening soil Model, mehke kamnine in glinene deformacije

ANALYSIS OF A DILATOMETER TEST IN OVER-CONSOLIDATED SEDIMENTS, BASIN OF THE DUERO RIVER, SPAIN

F. Escolano Sánchez

University Polytechnic of Madrid,
Civil Engineering Department
Alfonso XII, 3 y 5 - 28014 Madrid, Spain
E-mail: felix.escolano@upm.es

M. Bueno Aguado

Euroconsult SA
28700. S.S. Reyes. Madrid, Spain

Keywords

Dueñas, geotechnical parameters, hardening soil model, soft rocks and clays deformation

Abstract

A dilatometer test is a useful method for in-situ geotechnical surveys. It can be compared with the results obtained using a mathematical model. The mathematical model of concentric rings shown in this article is governed by the constitutive equation of the "Hardening Soil Model". A large number of tests made on the Dueñas Geological Facies, with a consistency ranging from firm clays to soft rocks, are compared to the model results. In this way, the "Hardening Soil Model" parameters are adjusted to the Dueñas Facies materials.

1 INTRODUCTION

The pressuremeter test is very useful for determining the geotechnical feature parameters of original soils and for reducing the most common changes in the mechanical characteristics caused by sampling. It also allows us to test the original soil in its natural state of effective and pore-water pressure [1,2] Another advantage of this test is that a greater volume of material is tested in situ than would be tested in the laboratory, thus being closer to the real loading state encountered afterwards in engineering works.

A pressuremeter test is an *in-situ* stress-strain test performed on the wall of a borehole using a cylindrical probe that is expanded radially. To obtain viable test results, any disturbance to the borehole wall must be minimized.

The equipment used is called a PBP (pre-bored pressuremeter), because it is best suited to the type of substrate studied (over-consolidated clays and soft rocks) and the standard applied is the ASTM D 4719-87 [3]. Table 1 shows the applicability of different types of pressuremeters [4].

In lightly over-consolidated clays, in a lot of consolidated ones as well as in a wide range of soft rocks, the volume

Table 1. Applicability.

SUBSTRATE	PROBE PBP	PROBE SBP	PROBE PIP
Soft Clays	A	A	A
Hard Clays	A	A	A
Sparse Sands	B ¹	A	A
Dense Sands	B ¹	B	C
Gravels	C	N	N
Soft rocks	A	B	N
Hard rocks	A	N	N

A = High; B = Medium; C = Low; N = None (1) Using fluted sleeve (Clarke 1996).

of soil examined by the pressuremeter test reaches states of tension that exceed the elastic levels.

The interpretation and study of the strain and deformation states, produced in these cases, requires the use of soil constitutive models that allow this simulation.

The current wide variety of computing programs includes soil advanced constitutive equations that simulate plastic states. Although these models should be implemented according to some initial parameters, these are usually far from those obtained in geotechnical tests. In the case of the over-consolidated clays and soft rocks, the constitutive model known as the “Hardening Soil Model” reliably reproduces the different stages of strain and deformation observed in field and laboratory tests. This effect on the constitutive model has been studied [1-2]. Thanks to the interpretation of the pressuremeter test using this constitutive model, a sound comprehension of the soil tensional processes, as well as a suitable adjustment of the tested model parameters, are achieved. During the geotechnical studies carried out for the high-speed train line between Valladolid and Burgos, several

dilatometer tests were carried out in Dueñas Geological Facies. The geotechnical knowledge of Dueñas and the dilatometer test have been thoroughly studied with the support of the constitutive equation.

A specific programme has been developed to define the pressuremeter tests that are also appropriate for other geotechnical units and used in the mentioned unit. This article explains the most relevant features of the method and compares its results with those obtained in the tests’ campaign. Finally, this study brings forward the geotechnical parameters of Dueñas Facies according to the “Hardening Soil Model” constitutive equation.

2. GEOGRAPHICAL AND GEOLOGICAL FRAME OF THE SURVEY AREA

The survey area is located in the Arlanzón river valley, between the Burgos and Palencia provinces, in the Iberian Peninsula NW quadrant. From the geological point of view, it is located inside the sedimentary basin of the Duero river, which spreads along approximately 50,000 km² (Figure 1).

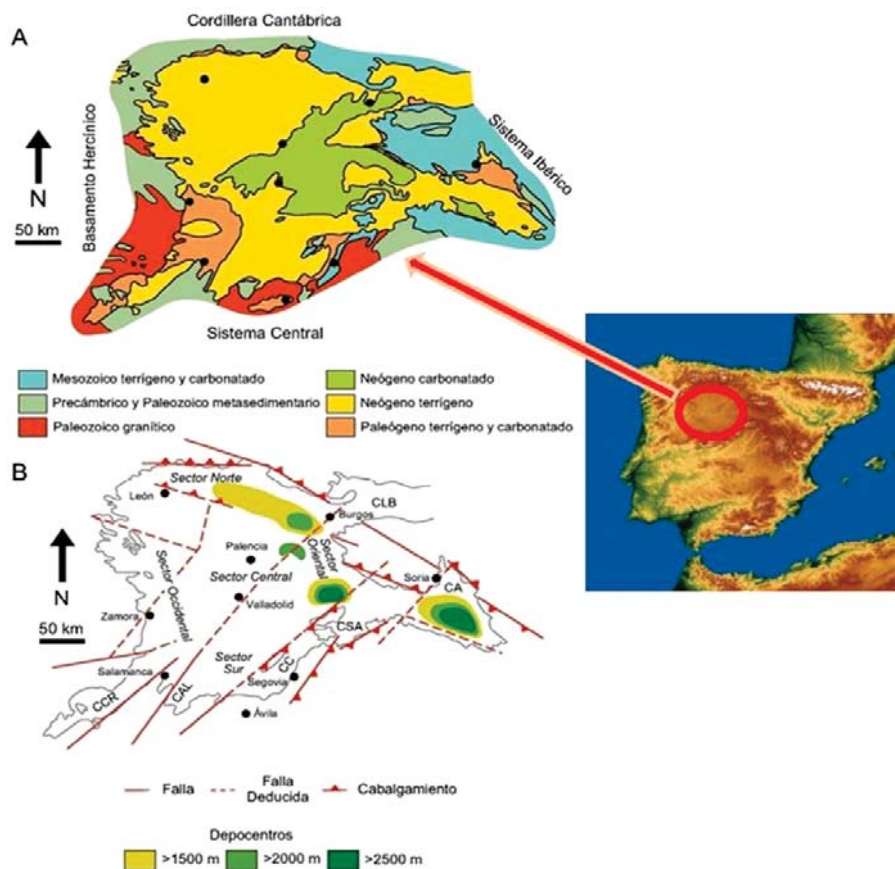


Figure 1. Geological and geographical location of the study area and the thickness of the sediments.

The sedimentary basin of the Duero river is an intra-plate depression that began to form at the end of the Cretaceous Period due to the Alpine movement of old basement fractures, produced during the Hercynian orogeny [5].

The sediments that filled this depression are organized according to a centripetal model in such a way that the terrigenous materials are disposed along the external edge of the basin and the chemical facies (carbonate) can only be found in the centre.

It should be pointed out that there is a noticeable asymmetry of the basin so that the chemical central facies are displaced towards the oriental edge. The thickness of the sediments that filled the depression is uneven, reaching a thickness of over 2500 m in some areas [5].

The thickest areas are located on a WSW-ESE oriented surface that impacts the cities of León, Palencia, Aranda de Duero and Soria (Figure 1). This pattern shows the behavior of the bedrock fractures during the basin sedimentation following the hors-graben general model.

The colmatation of this basin was not constantly and continuously carried out, it was achieved by “impulses” of maximum subsidence combined with periods of calm and even others of no sedimentation.

It was a continental sedimentation corresponding with a perimetral system of coalescent alluvial fans, which drain into a central saline endorheic lacustral basin. The climatic conditions were typical of an arid or semi-arid climate with a variable seasonal rainfall.

These general climatic conditions were almost constant during the whole Neogene Period. In the Quaternary geological period the basin fill is eroded, becoming in that way an exorheric basin and the fluvial net fits in. This process arranges along the time and is showed in the sedimentation of many terrace levels.

2.1. Stratigraphy of the survey area

All the exposed materials of the area are sedimentary and they can be gathered into four major soil groups:

- “Dueñas” formation. This is the most representative. It comprises an alternation of thin layers of clays, marlstones, marly limestones and gypsumy marlstones. This lithologic group has a colour that goes from light-green to whitish, its aspect is massive and its thickness is uniform.
- “Tierra de Campos” formation. This is a lithologic group composed by clays, whose colour goes from pink to reddish, mixed with sandstones, gravels and conglomerates, whose colour goes from yellowish to reddish.
- “Cuestas” formation. This comprises an alternation of limestones, marly clays and marlstones. Its general coloration is whitish or cream and it forms a uniform level of soil, whose thickness goes from 45 to 50 m, approximately.
- “Páramo” limestone formation. This is composed of a group of thick limestone layers whose grain is fine, its structure massive and its colour from whitish to cream. Its widest thickness is from 5 to 10 m approximately.

As was mentioned above, the importance and representativeness of the “Dueñas” formation, from a geological point of view, is the subject of this article.

3 DUEÑAS FACIES GEOTECHNICAL FEATURES

Dueñas Facies is part of the tertiary sediments in the Duero depression. The basin sediments have been eroded by the fluvial net and have formed wide valleys. In the hillsides and fields of these valleys, there are horizons of clays, marlstones and limestones corresponding to the units called “Cuestas Facies”, “Tierra de Campos and Dueñas Facies”.

The Dueñas Facies, chronologically older than the previous ones, comprises an alternation of 0.20–0.60 m, layers of clays, marlstones, marly limestones and gypsumy marlstones. Its colour goes from light-green to whitish and its general aspect is massive and uniform. The diffraction analyses with oriented aggregates carried out on samples from both layers give the mineralogical composition, as stated below in Table 2.

Table 2. Mineralogical composition of Dueñas Facies.

		MINERALS				
Unity	Quartz	Dolomite	Micas + kaolinites	Calcite	Gypsum	Motmorillonite
TD/y	<7%	30 s 50%	10 a 30%	<5%	30 a 55%	<10%
TD/m	<10%	20 a 50%	20 a 55%	10 a 15%	<0.5%	<10%

The superior layer, named TD/m, comprises clays and dolomites in similar levels. The inferior layer, named TD/y, has a gypsum mineral in almost a 50% proportion. This mineralogical composition reflects in its plastic features. The values obtained in the tested samples are shown in the plasticity chart below, Figure 2. In the case of gypsum marlstones (TD/y), as well as in the clays (TD/m), the samples have a wide level of liquid limits with values from 20 to 90. In both cases the points are mainly on line A. In addition, at the same liquid limit the clayey unit (TD/m) usually has a lower plasticity rate.

In a natural state, the density and humidity in both units are placed in rates of different values. The results from the different tests are depicted in Figure 3. A higher density and a lower humidity are observed in the samples of gypsum marlstones unit (TD/y). The quali-

ties of the resistance and the deformation in both units are also different from those obtained in the dilatometer tests. These results will be discussed afterwards.

4 HARDENING SOIL MODEL

The constitutive equation called the “Hardening Soil Model (HS-model)” has been developed [6]. It is a model formulated inside the framework of elastoplastic theory, which explains the behaviour of a simulated soil by pseudo-elastic models, and among them the hyperbolic model stands out as being the best known.

In this section only the most relevant features that allowed an explanation of the pressuremeter test are mentioned. As in any elastoplastic model, the HS-model comprises:

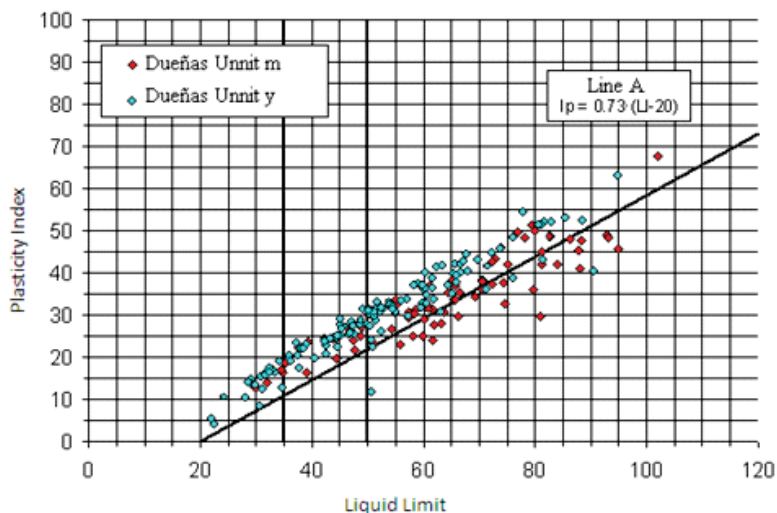


Figure 2. Graph of plasticity.

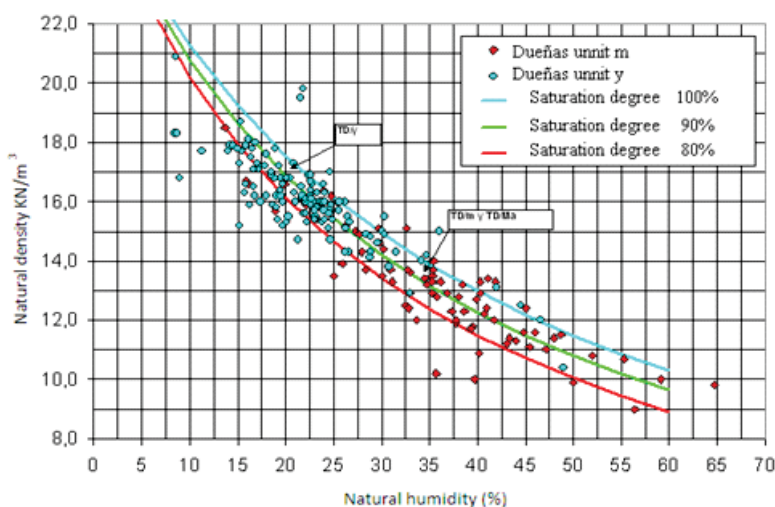


Figure 3. Dueñas Facies natural density and humidity.

- A defined failure criterion for effective pressures.
- An elastic behaviour for strain states under the failure level.
- A plastic power function that determines the direction of plastic deformations.
- A hardening law that modifies the failure criterion according to the previously achieved strain states and deformation tests.

A typical feature of an HS model is that the hardening law is defined by the plastic deformation through the previous shear. The HS model's failure criterion is depicted in the equation:

$$f = q_a/E_{50} q/(q_a - q) - 2q/E_{ur} - \gamma_p \quad (1)$$

where:

q : stress deviator ($q = \sigma_1 - \sigma_3$)

q_a : failure deviator asymptote obtained by the equation:

$$q_a = q_f/R_f \quad (2)$$

q_f : failure deviator for an average effective pressure p , from:

$$q_f = 6 \sin(\phi)/(3 - \sin(\phi)) (p + c \cotan(\phi)) \quad (3)$$

where:

- c and ϕ are the Mohr Coulomb's failure criterion parameters.
- The E_{50} and E_{ur} load module and download module obtained by the expressions:

$$E_{50} = E_{50}^{ref} (\sigma_3 + c \cotan(\phi))/(\sigma_{ref} + c \cotan(\phi))^m \quad (4)$$

$$E_{ur} = E_{ur}^{ref} (\sigma_3 + c \cotan(\phi))/(\sigma_{ref} + c \cotan(\phi))^m \quad (5)$$

where:

- E_{50}^{ref} and E_{ur}^{ref} are the reference modules for the confining pressure σ_{ref} .
- m is the influence exponent of the confining pressure in the deformation module.
- γ_p is the value of plastic shearing deformation obtained by the expression:

$$\gamma_p = \varepsilon_1^p - \varepsilon_2^p - \varepsilon_3^p \quad (6)$$

The elastic behaviour below the failure level is an elastic equation with a deformation module E_{ur} and a Poisson's coefficient ν .

Finally, the plastic deformations are defined by the plastic potential function " g " with the expression:

$$g_{13} = (\sigma_1 - \sigma_3)/2 - ((\sigma_1 + \sigma_3)/2) \sin(\psi) \quad (7)$$

$$g_{12} = (\sigma_1 - \sigma_2)/2 - ((\sigma_1 + \sigma_2)/2) \sin(\psi) \quad (8)$$

where:

ψ is the dilatancy angle.

The second surface simulates the plastic deformation direction when two main strains match up (compression and traction biaxial states). To sum up, there are seven essential geotechnical parameters to define the constitutive equation:

c : the effective cohesion

ϕ : the effective friction angle

E_{50}^{ref} : the load module for a reference pressure

E_{ur}^{ref} : the reload module for a reference pressure

R_f : the failure relation

m : the influence exponent of the confining pressure in deformation module

ν : the Poisson's coefficient

ψ : the dilatancy angle.

5 THE INTERPRETATION MODEL OF THE PRESSUREMETER TEST

The interpretations of the pressuremeter tests were performed according to a concentric-rings model [7]. Figure 4 shows a schematic representation of the used model.

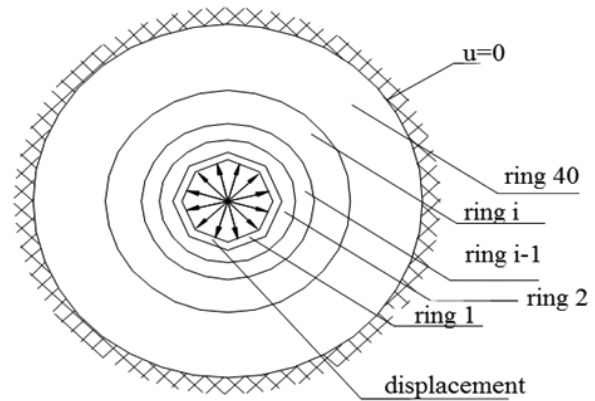


Figure 4. Rings model.

It is an axisymmetric model made of forty concentric cylindrical rings of variable thickness. This thickness grows with its radius so that the narrowest ring is close to the bore hole. The external radius of the model is approximately 10 metres. The internal one is the borehole radius, which is usually 5 cm in size. Initially, the internal radius of each ring is determined by the expression:

$$r_i = r_{i-1} + i^2/2000 \quad (9)$$

where:

r_i is the internal radius of the “ i ” ring in the meter.

An outline condition of no radial deformation is established on the external edge of the 40th ring of the model. On the internal edge of the first ring a “ u ” displacement takes place. In order to use the small deformation hypothesis, the magnitude of the “ u ” displacement is limited, so the variation in the radial deformation in any ring must be under 0.5%

For small deformations, each ring responds to the displacement according to an elastic and linear behavior. The used parameters are the unload deformation module E_{ur} and the Poisson’s ratio ν of the element when the displacement takes place. As a result, a “ u ” displacement is obtained in each ring in its internal outline.

According to the displacement of each ring, the average deformation ring is determined by the expressions:

$$\varepsilon_{ri} = (u_{i+1} - u_i)/(r_{i+1} - r_i) \quad (10)$$

$$\varepsilon_{ti} = (u_i + u_{i+1})/(r_i + r_{i+1}) \quad (11)$$

where:

ε_{ri} and ε_{ti} are the radial and circumferential deformations, respectively.

The vertical deformation is obtained by considering the total vertical pressure constant. Taking these deformations as a starting point and using a numerical integration procedure, the effective strains compatible with the constitutive equation are determined.

After each deformation increment, the ring model is updated with the new radii dimensions.

In the case of the undrained test, the deformation module is a transformation of the previous one, obtained by the condition of a constant shear modulus G .

$$G_u = G$$

$$E_u/(1 + \nu_u) = E_{ur}/(1 + \nu) \quad (12)$$

The adopted undrained Poisson’s module is 0.495.

The generated pore-water pressure in each element is a function of the volumetric deformation (ε_v) and the water-compression module. It is supposed to have a superior magnitude than the soil magnitude. The generated pore-water pressure in each interval and ring (v_i) is determined using the expression [8].

$$v_i = 300 E_{ur} (v_u - \nu) / \{3 (1 + \nu) (1 - 2 * \nu)\} \varepsilon_v \quad (13)$$

With these effective pressures and the pore-water pressure, the total pressures are determined as:

$$\sigma = \sigma' + \nu \quad (14)$$

The total radial pressure of the first ring corresponds to the one applied inside the borehole.

Additionally, the traction states are limited so that no negative effective stress could appear. No negative values are allowed for the interstitial pressure either. The model requires the definition of an initial state pressure, which must be similar to the corresponding geostatic one. The initial pore-water pressure will be a function of the phreatic level measured in the borehole.

6 MODEL CHARACTERISTIC RESULTS

The application of successive displacements inside the first ring of the model implies a relation between the internal pressure and the deformation of the borehole wall with a relatively hyperbolic shape [9]. Figure 5a shows the evolution of the total pressure on the borehole wall. The total radial pressure has two stages.

The first one with mainly elastic deformation is characterized by large increments of pressure for small deformations. The second one, in which the plastic deformation is increasingly more relevant and, the deformation grows quickly in increments of pressure similar to those found in the first phase. The radial pressure extends constantly versus the deformation, so that the shape of the curve is an inclined asymptote.

The circumferential pressure also has two stages, although in this case the pressure has lower values than the initial one. On the other hand, the total vertical pressure remains constant and close to the initial value.

Figure 5b depicts the same representation as the previous one with the three effective pressures close to the interstitial pressure. There is also an elastic initial stage followed by a plastic one for the radial and circular pressures. However, in the latter, the circumferential pressure reached a horizontal asymptotic value. This value reflects the total plastification of the internal rings.

The HS model is a constitutive equation whose function of breakage and plastification criterion can be represented in the plan p - q :

$$p = (\sigma_1 + \sigma_2 + \sigma_3)/3 \quad (15)$$

$$q = \sigma_1 - \sigma_3 \quad (16)$$

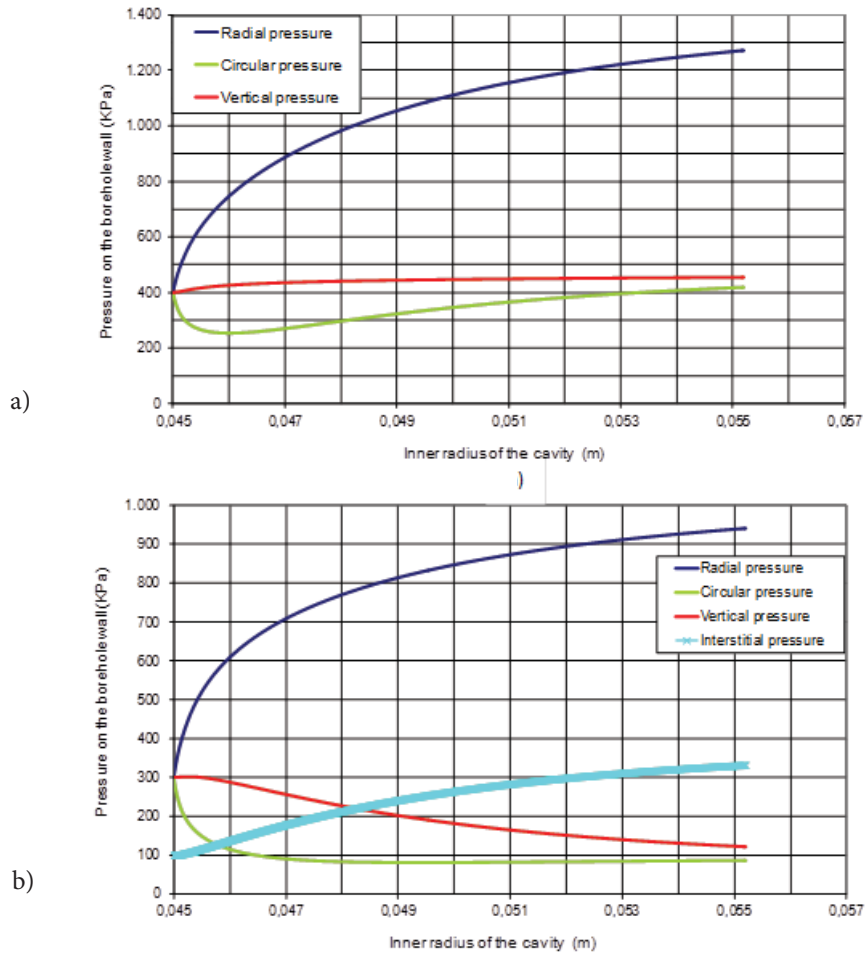


Figure 5. Pressures on the borehole drilling. Total pressures (a) and effective and interstitial pressures (b).

As the function that defines the breakage criterion depends on the previous shear plastic deformation, its representation is a group of curves, the superior limit of

which is the q_a value. Figure 6 shows the p and q evolution in the test, together with the q_a limit.

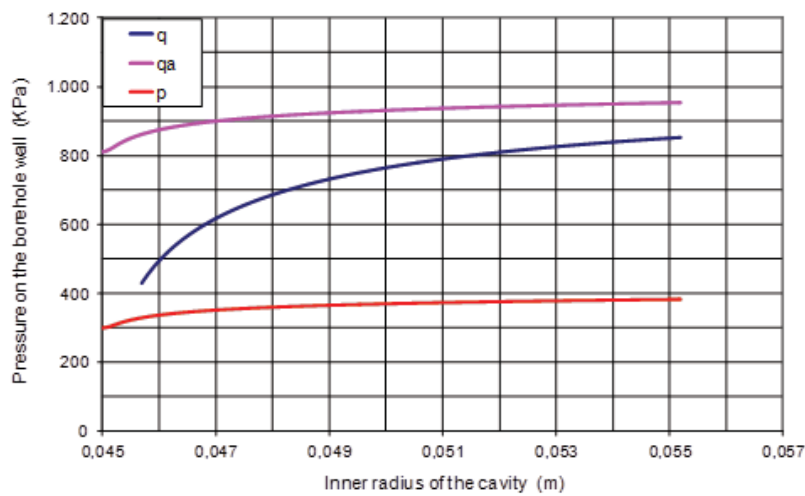


Figure 6. Test p - q graph.

The graph shows how the strain deviator q grows until it becomes asymptotic with the line defined by q_a . The plastic deformations take place along the whole loading process. It must be made clear that the dilatometer test is basically a test of $p=\text{constant}$.

This model allows a study of the evolution of pressures inside the soil. Figure 7 shows this evolution. It is clear that the volume of soil affected by the test does not expand by more than 2.0 m around the borehole. The strain variations between 2.0 m and 10 m of the model are almost null.

The circumferential effective pressure decreases quickly close to the borehole wall. As it moves away from the borehole wall, the circumferential pressure decreases slowly, until it reaches an asymptotic value corresponding to its initial value.

A similar behaviour is observed in the circular and vertical pressure. In the same way, the farther we are from the borehole, the lower the pore-water pressure becomes as it reaches its initial value.

7 COMPARISON BETWEEN THE TEST RESULTS AND THE MODEL

The results of the model have been compared with in-situ tests in the Dueñas unit. Among the thirty-five pressuremeter tests carried out, three have been distinguished. In the first group gypsum marlstones (TD/y) are tested, in the second one there are clays from hard to very hard from Dueñas clayey layers (TD/m) and, finally, in the third group there are clays of high consistency, also from Dueñas clayey layers (TD/m).

The graphs in Figure 8a and 8b below show the four main tests from those carried out with gypsum marlstones (TD/y). This material is classified as soft rock. This graph depicts the adjustment with the rings model.

Three of the tests were adapted to the radial total pressures curve and the fourth one is adjusted to the radial effective pressures curve, both in the same calculation. The parameters used in this calculation are presented in the chart below (Table 3).

Table 3. Parameters used in this calculation are gathered in the chart below to a depth of 20 m.

HS-Model Parameters for gypsum marlstones in Dueñas unit	
Effective cohesion	0.5 MPa
Internal friction angle	45°
Dilatancy angle	3°
Loading reference module E_{50}^{ref}	400 MPa
Downloading reference module E_{ur}^{ref}	600 MPa
m	0.8
R_f	0.7

Initial state equal to 20 m deep. (*) reference pressure 100 KPa

The test results are analogous to those of the proposed model. Nevertheless, two different behaviours are observed. In the three tests of Figure 10 the radial pressure grows to an inclined asymptotic straight line. This behaviour should belong to a model where the pore-water pressure does not disappear, but it is added to the effective pressure to support the pressure on borehole walls. The adjustment of these experimental curves takes place with the total pressure of the model.

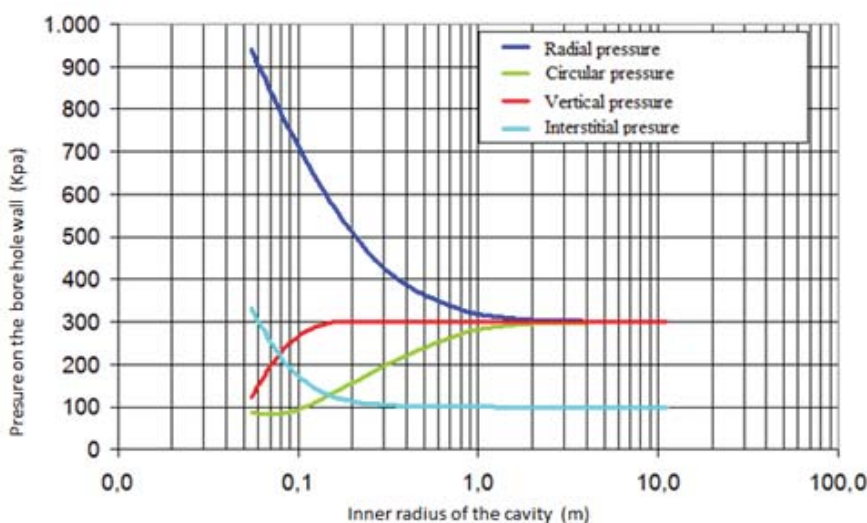


Figure 7. Evolution of pressures inside the soil.

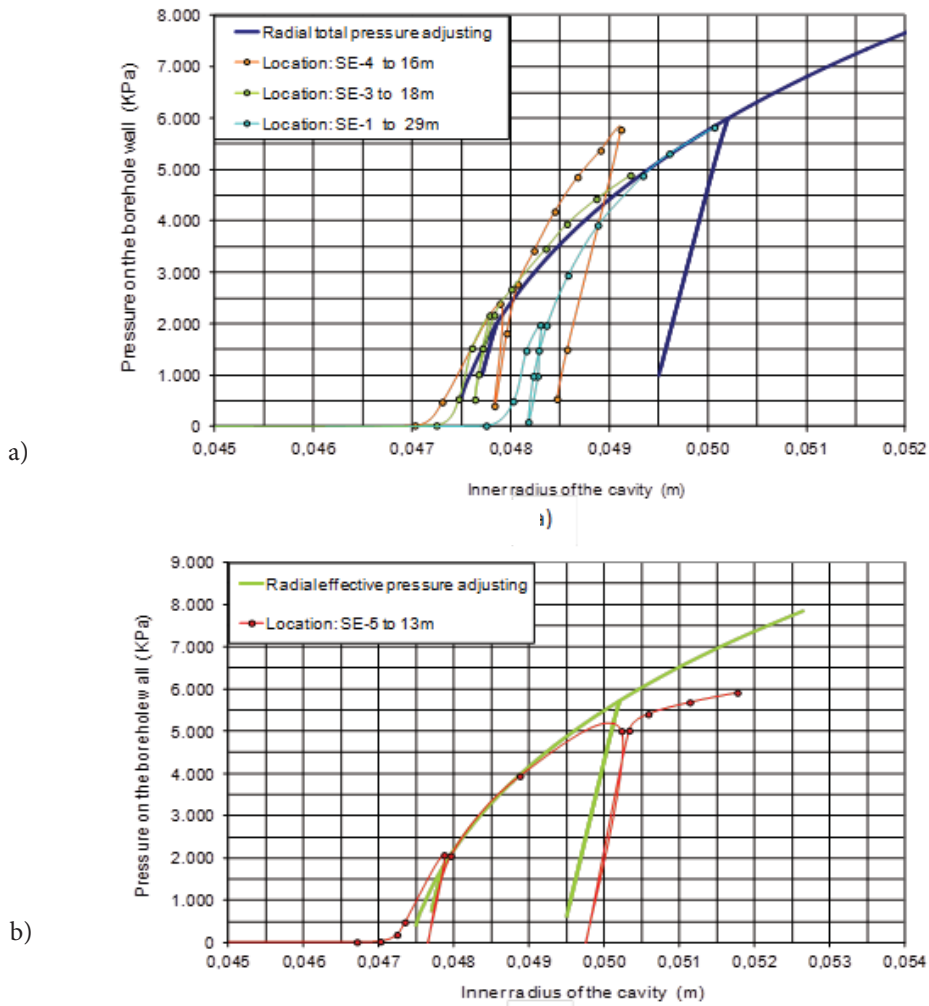


Figure 8. Pressuremeter tests with gypsum marlstones. Total pressures (a) and effective pressures (b).

The test in Figure 8b shows how for pressures over 6 MPa the curve begins to bend to a horizontal straight line. In this case, the test has a drained behavior. The drainage can occur along the loading of the rifting of the rock or a limit to the generated interstitial pressure

due to the exhaustion of the confining vertical pressure.

Figure 9 also shows a sequence of pressure pressuremeter tests, which represents those carried out in soil from a

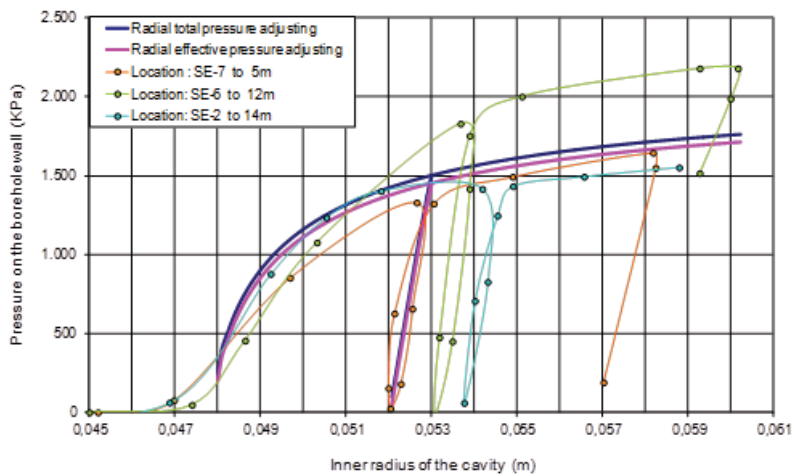


Figure 9. Pressuremeter tests with clays from hard to very hard consistency.

hard to a very hard consistency of the clayey unit (TD/m). Their results are compared to the model adjustment.

The parameters used in this analysis are gathered in the chart below (Table 4).

Table 4. Parameters used in this calculation are gathered in the chart below to a depth of 10 m.

HS-Model Parameters for hard to very hard clays in Dueñas Facies	
Effective cohesion	0.25 Mpa
Internal friction angle	30°
Dilatancy angle	3°
Loading reference module E_{50}^{ref}	60 MPa
Downloading reference module E_{ur}^{ref}	90 MPa
m	0.8
R_f	0.7

Initial state equal to 10 m deep. (*) reference pressure 100 KPa

Finally, Figure 10 depicts the tests with soil of firm consistency of the clayey unit (TD/m). Their results are compared to the model adjustment. The parameters used in this analysis are gathered in the chart in next column (Table 5).

8 DISCUSSION

The pressuremeter is a test of horizontal load, which allows us to obtain a detailed account of the main geotechnical parameters of the soil behavior [9]. To obtain these parameters, however, it is advisable to define a soil constitutive equation and a mathematical model

Table 5. Parameters used in this calculation are gathered in the chart below to a depth of 10 m.

HS-Model Parameters for hard to very hard clays in Dueñas Facies	
Effective cohesion	30 Kpa
Internal friction angle	28°
Dilatancy angle	3°
Loading reference module E_{50}^{ref}	8 MPa
Downloading reference module E_{ur}^{ref}	15 MPa
m	0.8
R_f	0.7

Initial state equal to 10 m deep. (*) reference pressure 100 KPa

able to carry out the test. The mathematical model was realized with the commercial program Plaxis 8.1 [10].

The natural soil is heterogeneous enough so that the tests done with similar materials are not identical, but they vary within a range of values. In this way the adjustments made with the rings model aim to simulate the average behaviour of the tests carried out with the same material. The *in-situ* tests reflect that the response of the natural soil goes from a drained behaviour without generated interstitial pressures to an undrained one [11]. The adjustment is achieved by choosing a set of parameters that leads to an analytical curve. The set of parameters is modified until the analytical curve matches with the experimental one. Each parameter accounts for a part of the curve. At the same time, typical values of the main parameter for this kind of soil, cohesion and friction internal angles are used.

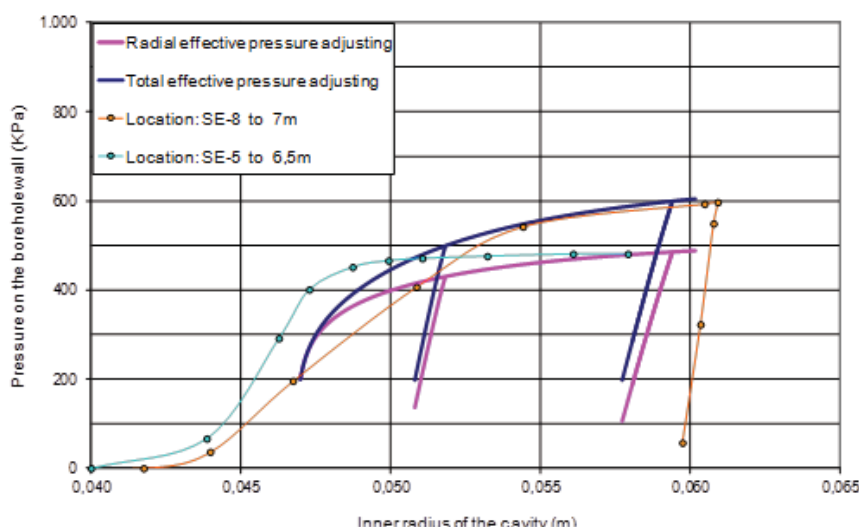


Figure 10. Pressuremeter tests with clays of firm consistency.

The vertical deformation was determined by the hypothesis of constant vertical pressure, which seems to be more appropriate for tests near to the surface. Other hypotheses may be used, such as the null vertical deformation. This model could achieve a better adjustment to the experimental curve.

All these considerations mean that the use of parameters obtained by the test should not be unique, but it should be considered as a range of values for each parameter. The range depends on both the experimental curves and the set of parameters. Small variations of a parameter could also achieve a valid adjustment. Each soil requires a sensitivity analysis of the parameter.

The test must be complemented with other mechanical tests as well as a certain caution in their expected magnitude. This means that the engineer has to use a certain geotechnical common sense when choosing the parameters.

The pressuremeter test develops large deformations close to the borehole wall. The used model must employ a definition of deformation according to its magnitude. The use of the hypothesis for a small deformation requires the modification of the model's geometry as the deformation advances. Because the strain is greater than 1%, and the inner ring deforms a lot, the model has to be modified with the ring mesh at each step.

The tests carried out in Dueñas Facies have allowed us to test a variety of clayey materials with a variable consistency from firm to very hard. The materials classified as soft rocks have also been tested. This range of materials allows us to quantify the geotechnical parameters of the hardening soil model.

The main parameters in the adjustment are the cohesion, the friction angle and the modules of deformation in load and download. The other three parameters, i.e., exponent, dilatancy angle and R_f value, permit a small adjustment in the curve shape defined by the previous parameters.

9 CONCLUSIONS

The pressuremeter test has proven to be a useful tool that completes the geotechnical survey of the soil [10, 11]. As a result of it the geotechnical parameters applied to advanced constitutive equations are also possible. This article shows an application that adjusts the test results with those obtained by the model ruled by the "Hardening Soil Model" constitutive equation. This model was studied [12]. The model adjusts to the *in-situ* tests so it is possible to find geotechnical parameters for the different levels of soil that form Dueñas Facies.

In this way the parameters obtained can be applied to computer programmes that develop these kinds of constitutive equations, as it is an advanced model of soil behaviour designed for foundations and structures developed in Dueñas Facies.

REFERENCES

- [1] Bryson, L.S., Salehian, A. 2011. Performance of constitutive models in predicting behavior of remolded clay. *Acta Geotechnica* 6, 143-154. doi: 10.1007/s11440-011-0144-5.
- [2] Sfriso, A., Weber, G. 2010. Formulation and validation of a constitutive model for sands in monotonic shear. *Acta Geotechnica* 5, 257-272. doi: 10.1007/s11440-010-0127-y.
- [3] ASSTM 2007. Active Standard ASTM D4719. Developed by Subcommittee: D18.02. Book of Standards Volume: 04.08
- [4] Clarke, B.G. 1996. Pressuremeter testing in ground investigation. Part 1- site operations. *Geotechnical Engineering* 119, 96-108. doi: 10.1680/igeng.1996.28169.
- [5] Alonso-Gavilan, G. 1981. Estratigrafía y sedimentología del Paleógeno del borde de la cuenca del Duero. Th. D. Universidad de Salamanca.
- [6] Schanz, T., Vermeer, P.A. 2000. The Hardening soil model: formulation and verification. *Computational Geotechnics*.
- [7] EUROCODE 7 1999. Geotechnical design. Par 3: Design assisted by fieldtesting. Madrid.
- [8] Escolano, F., Bueno, M., Sanchez, R. 2014. Interpretation of the pressuremeter test using numerical models based on deformation tensor equations. *Bulletin of Engineering Geology and the Environment*, 73, 141-146. doi: 10.1007/s10064-013-0528-x.
- [9] Aubeny, CP, Whittle, AJ., Ladd, C.C. 2000. Effects of disturbance on undrained strengths interpreted from pressuremeter tests. *Journal of geotechnical and geoenvironmental engineering*, 126, 12, 1133-1144.
- [10] PLAXIS Manuals version 8.1. Balkema. Rotterdam.
- [11] Clough, G.W. 1990. The development of pressuremeter testing. In *Pressuremeters: Proceedings of the Third International Symposium on Pressuremeters*, Organised by the British Geotechnical Society and Held at Oxford University, 2-6 April 1990 (p. 25). Amercam Society of Civil Engineers.
- [12] Liu, El., Xing, H.L. 2009. A double hardening thermo-mechanical constitutive model for overconsolidated clays. *Acta Geotechnica* 4, 1-6. doi:10.1007/s11440-008-0053-4.

POVEZAVA MED TLAČNO IN NATEZNO TRDNOSTJO Z APNOM OBDELANIH GLIN, KI VSEBUJEJO KOKOSOVA VLAKNA

Vivi Anggraini (vodilni avtor)

Universiti Putra Malaysia,
Faculty of Engineering, Department of Civil Engineering
43400 Serdang, Selangor Darul Ehsan, Malezija
E-pošta: vianggraini@gmail.com

Bujang B.K. Huat

Universiti Putra Malaysia,
Faculty of Engineering, Department of Civil Engineering
43400 Serdang, Selangor Darul Ehsan, Malezija
E-pošta: bujang@eng.upm.edu.my

Afshin Asadi

Universiti Putra Malaysia,
Faculty of Engineering, Housing Research Centre
43400 Serdang, Selangor Darul Ehsan, Malezija
E-pošta: afshin.asadi@yahoo.com

Haslinda Nahazanan

Universiti Putra Malaysia,
Faculty of Engineering, Department of Civil Engineering
43400 Serdang, Selangor Darul Ehsan, Malezija
E-pošta: n_haslinda@upm.edu.my

Izvlecek

V članku so predstavljeni izsledki študije vplivov kokosovih vlaken na mehanske karakteristike z apnom obdelanih glin. Z apnom obdelani vzorci gline so bili pripravljene z različnimi vsebnostmi kokosovih vlaken, in sicer z 0.5%, 1%, 1.5% in 2% teže glede na suho težo zemljine. Časovni razvoj mehanskega odpora utrjenih vzorcev je bil opazovan tako, da so bili preizkušeni po 7, 28 in 90 dneh od dneva obdelave z apnom. Rezultati preizkusa enoosne tlačne trdnosti so bili uporabljeni za določitev odnosa med tlačno trdnostjo in indirektno natezno trdnostjo z apnom utrjene zemljine. Nadalje je bilo ugotovljeno, da je optimalni delež kokosovih vlaken zmešanih v zmesih zemljina-apno enak 1% suhe mase ter, da je takšna ojačitev v 90 dneh zvišala najvišjo tlačno trdnost in indirektno natezno trdnost. Dodajanje kokosovih vlaken spremeni krhki odziv z apnom obdelane gline v bolj duktilnega.

Ključne besede

kokosova vlakna, apno, tlačna trdnost, posredna natezna trdnost, glinena zemljina, karakteristike porušitve

RELATIONSHIP BETWEEN THE COMPRESSIVE AND TENSILE STRENGTHS OF LIME-TREATED CLAY CONTAINING COCONUT FIBRES

Vivi Anggraini (*corresponding author*)

Universiti Putra Malaysia,
Faculty of Engineering, Department of Civil Engineering
43400 Serdang, Selangor Darul Ehsan, Malaysia
E-mail: vianggraini@gmail.com

Bujang B.K. Huat

Universiti Putra Malaysia,
Faculty of Engineering, Department of Civil Engineering
43400 Serdang, Selangor Darul Ehsan, Malaysia
E-mail: bujang@eng.upm.edu.my

Afshin Asadi

Universiti Putra Malaysia,
Faculty of Engineering, Housing Research Centre
43400 Serdang, Selangor Darul Ehsan, Malaysia
E-mail: afshin.asadi@yahoo.com

Haslinda Nahazanan

Universiti Putra Malaysia,
Faculty of Engineering, Department of Civil Engineering
43400 Serdang, Selangor Darul Ehsan, Malaysia
E-mail: n_haslinda@upm.edu.my

Keywords

coconut fibre, lime, compressive strength, indirect tensile strength, clay soil, failure characteristics

Abstract

The effects of coconut fibre on the mechanical characteristics of lime-treated clay are investigated in this study. The lime-treated clay specimens were prepared with a variety of coconut-fibre contents, i.e., 0.5%, 1%, 1.5% and 2%, in terms of the weight of dry soil. The stabilized specimens were tested at 7, 28 and 90 days after the treatment in order to observe the evolution of the mechanical resistance with time. The results of the unconfined compressive strength tests were used to determine the relationships between the compressive strengths and the indirect tensile strengths of the stabilized soil. Furthermore, the optimum percentage of coconut fibre mixed in the soil/lime mixtures was 1% of the dry mass and reinforcement at 90 days increases the peak compressive strength and the indirect tensile strength. Coconut-fibre inclusion changes the brittle behaviour of the lime-treated clay soil to give it a more ductile character.

1 INTRODUCTION

The construction of a building on top of weak or soft soil is extremely risky because such soil has a tendency to swell and crack due to its low shear strength, uneven moisture distribution, high compressibility and low tensile strength. The interest with respect to the tensile strength of the soil is associated with the different tensile cracks that can develop in earth structures, such as dams, slopes, retaining structures, or with capping-clay sealing-system sanitary landfills [1].

Chemical stabilization using lime and cement is a proven technique for improving the performance strength and stabilization of clay soil in order to immobilize the water in the clay based on chemical reactions and to reduce the plasticity index of the clay. This reduction in the plasticity is usually accompanied by a reduction in the potential for swelling. Rajasekaran and Rao [2] reported that lime is commonly used to change the properties of soils because of its more stable performance, lower price, and greater abundance. Lime is most effective for treating soils that are capable of holding large amounts of water [3].

Another possible solution involves the inclusion of randomly distributed, tensile-reinforcement elements in clay soil. Fibres have been mixed with soils to improve the strength and the mechanical behaviour of soils [4; 5; 6; 7; 8]. Maher and Ho [5] and Cai et al. [9] found that with the inclusion of discrete polypropylene fibres, the tensile strength of clays tended to increase and induce more ductile failures. Generally, the high tensile strength and extendibility of the added fibres help to effectively reduce the compressibility and brittleness of the host

soil, which is generally superior to traditional soil-improvement approaches, such as using cement and/or lime [7; 9; 10; 11; 12; 13].

The effectiveness of the fibres depends upon the strength of the fibres as well as on how they interact with the soil under normal stresses through adhesion. When a tensile force needs to mobilize in the fibres, as in drying shrinkage and desiccation cracks, adhesion restrains the fibres from pull out and thus allows its tensile resistance to develop. The objective of this paper is to determine the relationship between the unconfined compressive strength and the indirect tensile strength of a soil treated with lime and coconut fibre.

2 MATERIALS AND METHODS

2.1 Materials

The soil samples were taken from Klang, Selangor Malaysia. Table 1 presents the properties of the soil samples. The soil has the symbol CH, in accordance with BS 1377-2, and can be classified as inorganic clay with a high plasticity.

Table 1. Basic properties of the soil that is used for this study.

Parameters	Values
Natural Moisture Content (%)	103
Unit Weight (kN/m^3)	16
Specific Gravity	2.67
Grain Size Analysis	
Sand (%)	20
Silt (%)	35
Clay (%)	60
Consistency Limit	
Plastic Limit (%)	49
Liquid Limit (%)	80
Plasticity Index	26
Salinity	1.7
Organic Content (%)	6
Activity	1.25
BS Classification	CH

A powder-hydrated lime was used as the stabilizing material for this study. Table 2 presents the oxide elements of the lime.

Coconut fibre was used as the fibrous reinforcement. The fibres were obtained from a factory in Batu Pahat,

Table 2. Chemical composition of the lime.

Constituents	(%)
Ca(OH)_2	92 %
CaCO_3	1.5 %
MgO	0.4 %
SiO_2	1.4 %
Al_2O_3	0.3 %
Fe_2O_3	0.2 %
SO_3	0.5 %
H_2O	0.3 %

South Malaysia. Coconut fibre is abundantly available in southern and coastal India, Indonesia, Malaysia, Philippine, Brazil and other countries. The discrete fibres were obtained by cutting the coconut fibre to a length of 1 cm. The diameter of the coconut fibre was approximately 0.1–0.3mm (Fig. 1)



Figure 1. Short coconut fibres.

2.2 Methods

2.2.1 Sample Preparation

Two series of soil mixtures, with and without the additives, were thoroughly mixed with various moisture contents. The soft clay and coconut fibres were initially mixed thoroughly, with the water being added, and then the moist mixture was mixed with lime.

All of the mixing was carried out manually and proper care was taken to prepare homogeneous mixtures at each stage of the mixing. Table 3 gives the details of the maximum dry density and optimum water content for

Table 3. Mix Design.

Mixture number	Description	Maximum dry density (g cm ⁻³)	Optimum water content (%)
S	Unstabilized soil, e.g., with neither lime, nor fibre	1.35	25
SL	Soil + 8% lime	1.3	26
SLCF1	Soil + 8% lime + 0.5% fibres	1.28	26.8
SLCF2	Soil + 8% lime + 1.0% fibres	1.27	27.3
SLCF3	Soil + 8% lime + 1.5% fibres	1.26	28
SLCF4	Soil + 8% lime + 2.0% fibres	1.25	28.2



Figure 2. Instron 3366 universal testing machine.

various fibre and lime contents as well as the notation used for them in this paper.

The soil samples were compacted at the maximum dry density and optimum water content using the static compaction method, as specified in the standard Disturbed Sample Preparation Static Compaction (Resilient Modulus of Soil) AASHTO Designation: T 307-99 (2003). The specimens were prepared using an Instron 3366 model universal testing machine with a load capacity of 5 kN (Fig 2).

The static compaction pressure was adjusted in order to reach the same dry density as a standard Proctor for the optimum water contents given in Table 5. The compaction was carried out using a hydraulic pressure at a fixed displacement rate of 1 mm/min and a downward static compaction pressure of 1.7 MPa. This pressure was used to prepare all the tested samples. A three-layered compaction was adopted to keep the uniformity of specimens.

Table 4 shows the size of the specimens for each test carried out in this investigation.

Table 4. Size of specimens for different tests.

Test	Size	
	Diameter (mm)	Height (mm)
Indirect tensile strength test (Brazilian test)	50	50
Unconfined compressive test	50	100

2.3 Testing Programme

2.3.1 Tensile test for a single fibre

The tab shape was cut at the mid-gauge length (cutting line) after being gripped in a test machine before the fibre is tested (Fig. 3). The specimen was tested with a crosshead speed of 1 mm/min using a total of 25 specimens [14]. These specimens were tested at a room temperature of 23° C with a relative humidity of 65 %. Individual fibre-breaking loads were recorded and their diameters were measured using an optical microscope of the Leica MS 5 type.

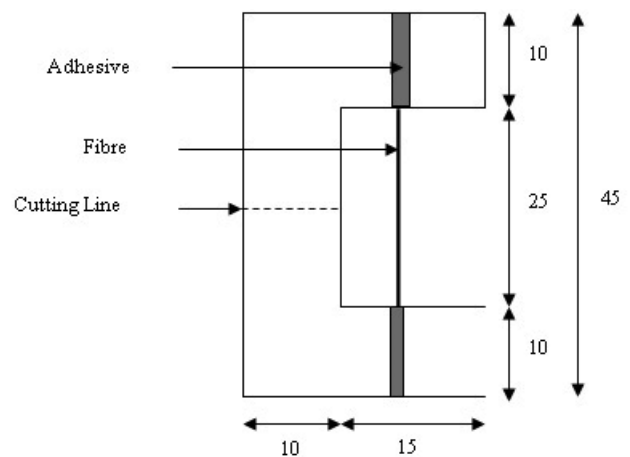


Figure 3. The fiber was attached and glued to the tab shape which was designed with gauge length of 10 mm.

$$TS = \frac{F}{A} \quad (1)$$

where TS = tensile strength, F = maximum force at the break, and A = average fibre area.

2.3.2 Mechanical Properties of the fibres and their composites

The experimental program was designed to determine the effect of the lime and the coconut fibres on the mechanical properties of the soil (Table 5).

Table 5. Experimental program.

Test Type (1)	Testing Procedure (2)	Loading Rate (3)	Curing Age (Days) (4)
Indirect tensile strength	Brazilian tension test	1 mm/min	7, 28 and 90
Unconfined compressive strength	ASTM (D2166)	1 mm/min	7, 28 and 90

2.3.3 Unconfined compressive strength (UCS)

The unconfined compression test was used to quickly obtain the approximate strength of the soil samples. The unconfined compressive strength (UCS) was taken as the peak stress, with the corresponding axial strain at failure (ϵ_f) in the stress-strain curve.

2.3.4 Indirect tensile strength (ITS)

In order to observe the behaviour of the soil-fibre mixtures on the tensile force due to desiccation during the drying stage, a tensile test was performed. The ITS test was conducted by applying the load along the cores in between two flat, parallel plates according to the indirect Brazilian test, as described by Dexter and Kroesbergen [15].

The ITS value is determined by using the modified equation proposed by Muntohar et al. [16]

$$ITS = \frac{2P_{\max}}{\pi \cdot L \cdot D} \quad (2)$$

where ITS = indirect tensile strength, P_{\max} = maximum applied load, and L and D = length and diameter of the specimen, respectively.

Table 6. Coconut-fibre tensile strength.

Diameter (mm)	Length (mm)	Tensile Strength (TS) (MPa)	Elongation at break (%)
0.23	5	102	34.0
0.25	9	98	32.7
0.23	10	90	30.0
0.24	11	92	30.7
0.22	10	83	27.7
0.23	10	85	28.3
0.21	11	78	26.0
0.23	12	98	32.7
0.24	13	82	27.3
0.24	14	89	29.7
0.24	15	93	31.0
0.23	14	80	26.7
0.23	13	99	33.0
0.23	12	97	32.3
0.23	11	98	32.7
0.24	13	102	34.0
0.24	10	94	31.3
0.23	12	89	29.7
0.23	11	79	26.3
0.23	12	76	25.3
0.23	12	102	34.0
0.24	12	70	23.3
0.24	10	78	26.0
0.20	13	98	32.7
0.23	11	101	33.7

3 RESULTS AND DISCUSSION

3.1 Tensile test of a single coconut fibre

The tensile strength of the coconut fibres is listed in Table 6. Because of the remarkable fluctuation in the fineness of the fibres, the tensile strength of the fibre usually varies a great deal. To lessen the influence of the coconut-fibre variation, 25 samples were selected and used for the calculation. The differences of the tensile strengths among the results were not significant, nor were the elongations at the break. The average tensile strength was 90 MPa, representing the tensile value of the proposed material. The tensile strength of a single coconut fibre will be mobilized and works together with the soil particles under certain loads. The reinforcement function of the coconut fibre will improve the strength

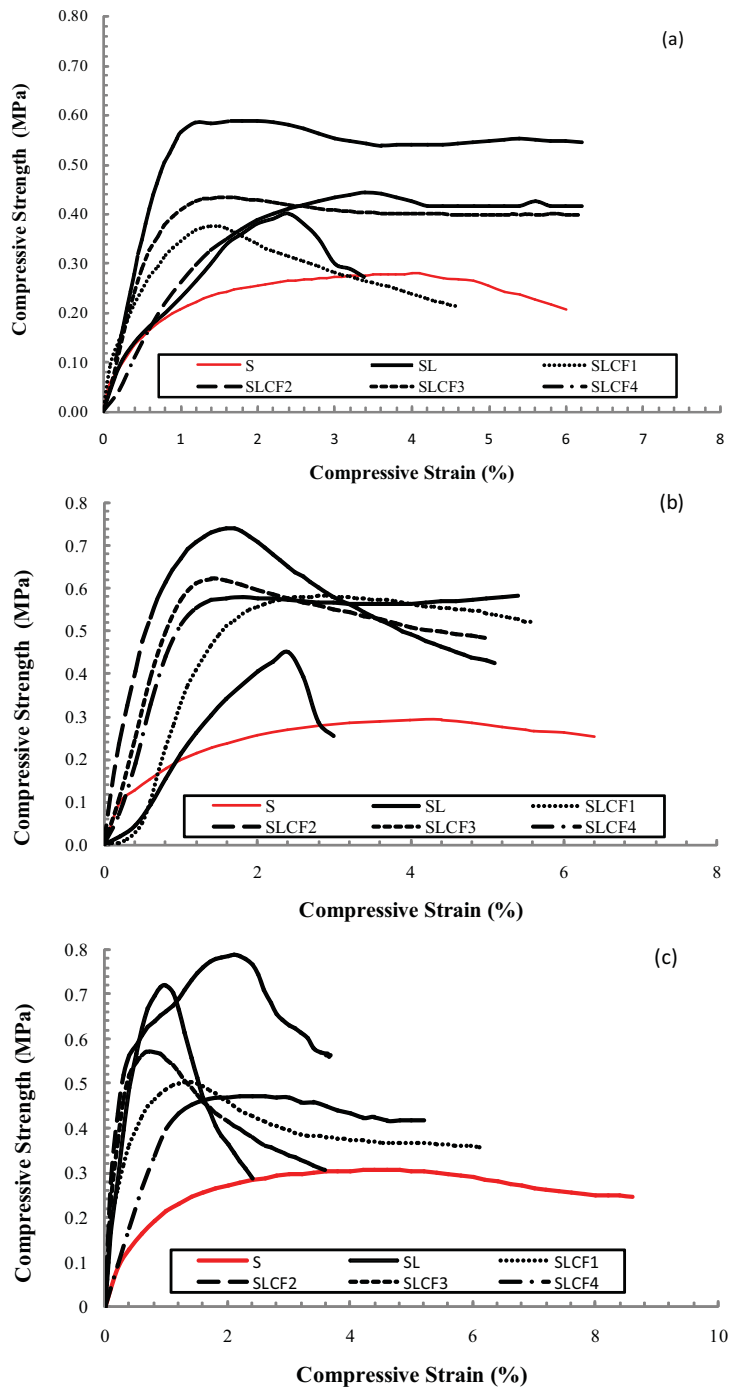


Figure 4. Compression strength-strain relationship at various fibre contents at (a) 7 days, (b) 28 days and (c) 90 day-curing.

of the soil in the early stage and be good for the soil's stability as its high initial strength [17; 18].

3.2 Unconfined Compression Strength (UCS)

Figure 4 shows a selection of stress-strain curves from the unconfined compression tests. As is clear from the figure, the overall behaviour of the lime-treated clay was

significantly influenced by the fibre content. The peak strength, stiffness and brittleness are changed at any stage of the curing period. The untreated soil (S) showed ductile behaviour at a failure strain of 4%; however, the inclusion of lime in the soil changed the behaviour of the samples from ductile to brittle, which may correspond to the formation of calcium hydroxide when the lime reacts with the water [2; 9]. The general pattern that can be

observed is that the inclusion of the fibres increases the compression strength and changes the brittle behaviour of the lime-treated clay, leading to more ductile behaviour. The introduction of 1% coconut fibre significantly increases the compressive strength and the initial Young's modulus of the lime-treated clay, whereas the addition of coconut fibres to a level of more than 1% reduces it.

When the specimens were subjected to a load, the interaction between the soil particles and the fibre provided the linkage effect in the soil-fibre mixtures. However, too much fibre added could reduce the effectiveness of the improvement in the strength, in as much as the fibres adhere to each other to form lumps and could not make full contact with the soil particles [8; 9; 18].

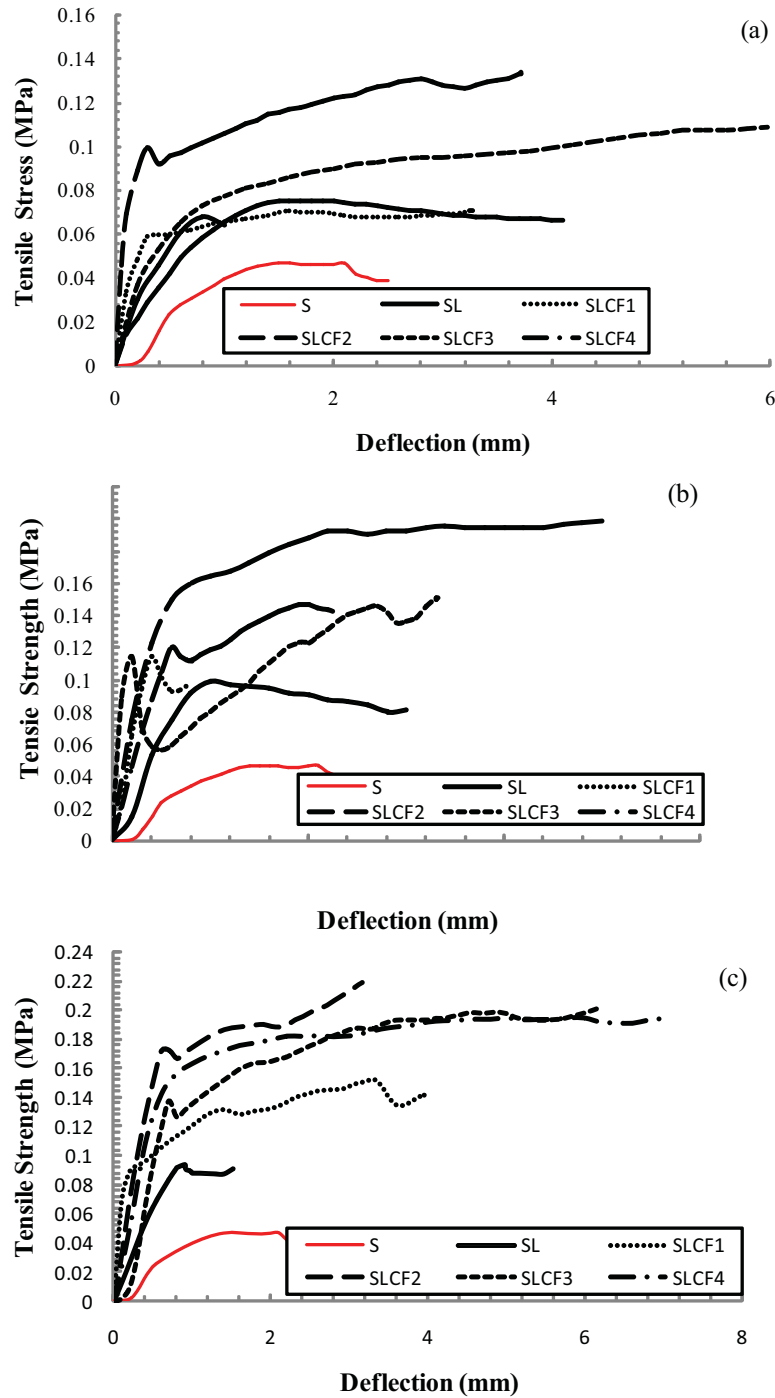


Figure 5. Tensile strength-deflection relationships at various fibre contents at (a) 7 days, (b) 28 days (c) 90 day-curing.

3.3 Indirect Tensile Strength (ITS)

The results from the Brazilian indirect tensile tests performed on the soft clay treated lime and coconut-fibre inclusion composite are presented in Fig 5. As is clear from the figure, the treated soil showed a reinforcing effect, which is well illustrated by the failure mode at different times. It is clear that the samples with fibres continued to carry loads after the samples experienced the ultimate failure load. In contrast, SL had a more brittle behaviour, which may correspond to the brittle behaviour of the hardened lime. Furthermore, the fibre-reinforced soil became fully activated and the load continued to increase for large deflections up to 1 mm, without any indications of failure. The interfacial friction and the bonding between the contact area of the soil particles and the fibres may help in the load transfer and contribute to an increase in the tensile resistance of the fibre-reinforced soil.

Table 7 presents the effect of curing on the UCS and ITS of the selected samples, showing that the strength increased as the curing time increased. Because of the time-dependent pozzolanic reactions, the stabilization of the lime soil is a long-term process [2]. Thus, the strength of the stabilized soil increases and the curing time increases. Generally, the compressive strength increased with time, together with the tensile strength. The highest values were observed for SLCF2 after 90 days of curing for both the unconfined compressive strength and the indirect tensile strength. The enhancement of the SLCF2 compared with the SL was 41%, 64% and 13% for the unconfined compressive strength at 7, 28 and 90 days of curing, respectively. The enhancement of the SLCF2 compared with the SL was from 43%, 77% and 80% for the indirect tensile strength at 7, 28 and 90 days of curing, respectively. This finding may be attributable to the cementitious product of the lime/coconut fibre, which binds the soil particles together and imparts a more compact matrix structure, and thus greatly restricts the arrangement of particles on the interface and increases the interfacial effective contact area. The hydrated cement-like products of the lime/coconut fibre that cover the fibre surface might improve the interfacial

Table 7. Values of UCS and ITS at various curing times.

Mix. Number	UCS (MPa)			ITS (MPa)		
	7 days	28 days	90 days	7 days	28 days	90 days
S	0.27	0.29	0.31	0.05	0.06	0.07
SL	0.41	0.45	0.71	0.07	0.09	0.10
SLCF1	0.37	0.51	0.57	0.08	0.12	0.13
SLCF2	0.58	0.74	0.80	0.10	0.16	0.18
SLCF3	0.43	0.57	0.63	0.09	0.11	0.16
SLCF4	0.44	0.47	0.57	0.08	0.12	0.14

bond characteristics and increase the interlock force and friction coefficient between the fibre and the soil. The cement-like product from lime and waste fibre was also reported by Cai et al. [9] and Muntohar et al. [16].

The initial values of the Young's modulus obtained from the unconfined compressive strength tests are in accordance with values of the Young's modulus from the indirect tensile-strength test (Table 8). The initial Young's modulus of the naturally compacted clay soil is 50 MPa for both tests. When lime is present in the treatment, the Young's modulus continues to increase with time. The Young's modulus rapidly increases during the first 28 days. The highest Young's modulus was obtained for the treatment SLCF2 was 69 MPa, 73 MPa and 85 MPa at 7, 28 and 90 days of curing for the unconfined compressive strength and 70 MPa, 74 MPa and 79 MPa at 7, 28 and 90 days of curing for indirect tensile strength. However, as the quantity of coconut fibre increases, the Young's modulus reduces. The enhancement for the treatment SLCF2 compared with the SL shows 35%, 33% and 16% at 7, 28 and 90 days, respectively, for the unconfined compressive strength. Furthermore, for the indirect tensile strength, the enhancement of the treatment SLCF2 with SL was 27%, 25% and 25% at 7, 28 and 90 days, respectively. SLCF2 is a sufficient treatment to improve the stiffness of the soil specimens, but it reduces and changes to more ductile as the quantity of coconut fibre increases.

3.4 Relationship between Unconfined Compressive Strength (UCS) and Indirect Tensile Strength (ITS)

Fig. 6 shows the ratio of the unconfined compressive strength to the indirect tensile strength (UCS/ITS). Four different coconut-fibre contents were applied to the lime-treated soil. The ratio varies between 3.6 and 5.8 for the lime-treated clay reinforced with coconut fibre. As can be seen from the figure, the highest value was associated with a coconut-fibre content of 1%. However, the ratio of unconfined compressive strength reduces

Table 8. Values of Young's modulus (E) from UCS and ITS for various curing times.

Mix. Number	Young's modulus (MPa)-UCS			Young's modulus (MPa)-ITS		
	7 days	28 days	90 days	7 days	28 days	90 days
S	50	50	50	50	50	50
SL	51	55	73	55	59	63
SLCF1	51	68	68	68	73	78
SLCF2	69	73	85	70	74	79
SLCF3	59	68	73	68	79	84
SLCF4	45	68	68	45	68	73

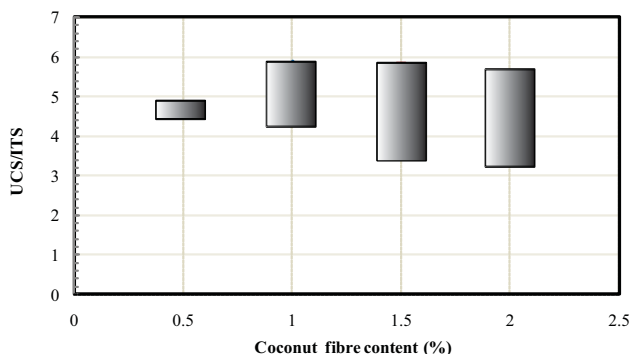


Figure 6. Variation of UCS/ITS of clay-lime mixture with coconut fibre.

with an increase in the fibre content, which shows that the coconut fibres were not efficient when the soil is subjected to compression rather than to tension.

Fatahi et al. [19] reported that there is no particular pattern detected in the variation of UCS/ITS with the cement or fibre content. The ratio varies between 6.3 and 9.8, 5.7 and 7.9, and 4.4 and 7.1, for cement-treated kaolinite reinforced with polypropylene, carpet and steel fibres, respectively.

Fig. 7 shows the relationship between the initial Young's modulus (E) of the compressive strength test and the indirect tensile strength test for various fibre contents. The initial Young's modulus is calculated as the slope of the initial section of the stress-strain curve. As can be seen from the figure, the stiffness of the lime-treated soil increases with the fibre content. The improvement is more remarkable when the amount of coconut fibre is 1 %. However, the stiffness of the lime-treated clay reinforced with coconut fibre decreases with the amount of coconut fibre by more than 1%. This is probably due to the lower friction in the interfacial zone of the fibre and the lime in the treated soil. This indicates that the

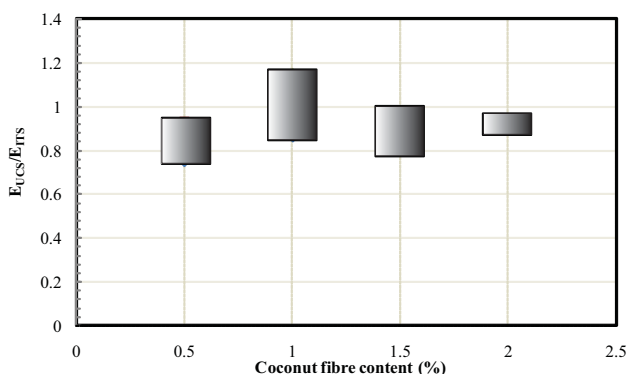


Figure 7. Variation of Eucs/EITS of clay-lime mixture with coconut fibre.

higher contents of coconut fibres increase the ductility of the material. However, as can be seen from the figure, Eucs/EITS decreases with increasing coconut-fibre content. It was observed that the ratio ranges between 0.75 and 1.2.

3.5 Effect of fibre content on the tensile failure of the fibre-lime-reinforced soil.

Fig. 8 shows a typical failure pattern for the samples after an indirect tensile strength test for all the samples. As is clear from the figure, the tension failure was caused by the tensile stress acting perpendicular to the loaded diameter. The cracking pattern of the specimens without a fibre inclusion was wide and microcracks with higher density were located in the soil specimens. However, with inclusion of the fibre-reinforced lime-treated soil, the width of the central crack decreased and the density of the microcracks reduced. It was observed that as soon as the tension cracks, caused by the loading, began to perform, the coconut fibres that were attended as connections, efficiently obstructed the further opening and accordingly prevented the samples from being subject to complete failure.

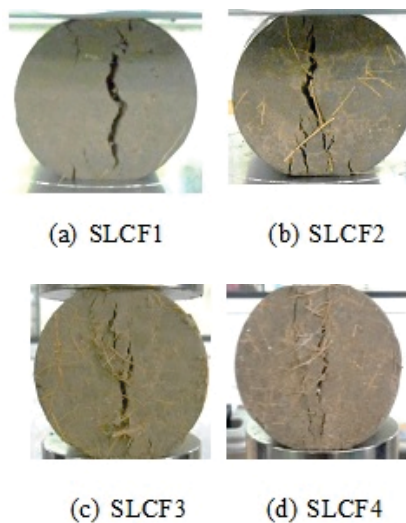


Figure 8. Typical tensile failure characteristics of fibre and lime treated soil of indirect tensile strength test: (a) SLCF1; (b) SLCF2; (c) SLCF3; (d) SLCF4.

4 CONCLUSIONS

In this study the effects of various coconut-fibre contents on the unconfined compressive strength and indirect tensile strength of lime-treated clay were investigated. The unconfined compression test results indicate that the strength increases with the addition of fibres and that

the brittle lime-treated clay is changed to a more ductile material. It was revealed that 1% of coconut fibres and 90 days of curing time were the most effective in terms of compressive strength and indirect tensile-strength enhancement, which may correspond to a more effective interaction of the fibres as lime hardened further.

As expected, both the unconfined compressive and the tensile strengths and the stiffness and brittleness of the treated clay increase with the addition of the lime. Furthermore, regardless of the lime content, the addition of coconut fibres increases the initial Young's modulus. However, the stiffness and strength of the coconut-fibre-reinforced limed clay decreases with a fibre content of more than 1 %. This is also true for the ratio of the UCS and ITS as well as the strength and the Young's modulus. The tensile-strength tests and the obtained results are very useful tools for recognizing the probability of tensile-crack development.

Acknowledgements

The financial support of the Research Management Center (RMC) of the Universiti Putra, Malaysia, under RUGS No. 9346000 is gratefully acknowledged.

REFERENCES

- [1] Vaniček I. 2011. Present day position of geotechnical engineering. ECSMGE Athens, 12, 2011.
- [2] Rajasekaran G., Narasimha Rao S. 1997. Lime stabilization technique for the improvement of marine clay. *Soils and foundations* 37(2), 97-104.
- [3] KAMAL UDDIN M., Buensuceso B. 2002. Lime treated clay: Salient engineering properties and a conceptual model. *Soils and foundations* 42(5), 79-89.
- [4] Consoli N.C., Prietto P.D., Ulbrich L.A. 1998. Influence of fiber and cement addition on behavior of sandy soil. *Journal of Geotechnical and Geoenvironmental Engineering* 124(12), 1211-1214.
- [5] Maher M., Ho Y. 1994. Mechanical properties of kaolinite/fiber soil composite. *Journal of Geotechnical Engineering* 120(8), 1381-1393.
- [6] Mandal J., Murthi M. 1989. Potential use of natural fibres in geotechnical engineering. Paper presented at the Proceedings of the International Workshops on Geo-Textiles, Bangalore, November.
- [7] Park S.S. 2011. Unconfined compressive strength and ductility of fiber-reinforced cemented sand. *Construction and Building Materials* 25(2), 1134-1138.
- [8] Prabakar J., Sridhar R. 2002. Effect of random inclusion of sisal fibre on strength behaviour of soil. *Construction and Building Materials* 16(2), 123-131.
- [9] Cai Y., Shi B., Ng C.W., Tang C.S. 2006. Effect of polypropylene fibre and lime admixture on engineering properties of clayey soil. *Engineering Geology* 87(3), 230-240.
- [10] Fatahi B., Le T.M., Fatahi B., Khabbaz H. 2013. Shrinkage properties of soft clay treated with cement and geofibers. *Geotechnical and Geological Engineering* 31(5), 1421-1435.
- [11] Kaufmann J., Winnefeld F., Hesselbarth D. 2004. Effect of the addition of ultrafine cement and short fiber reinforcement on shrinkage, rheological and mechanical properties of portland cement pastes. *Cement and Concrete Composites* 26(5), 541-549.
- [12] Santoni R.L., Tingle J.S., Webster S.L. 2001. Engineering properties of sand-fiber mixtures for road construction. *Journal of geotechnical and geoenvironmental engineering* 127(3), 258-268.
- [13] Tang C., Shi B., Gao W., Chen F., Cai Y. 2007. Strength and mechanical behavior of short polypropylene fiber reinforced and cement stabilized clayey soil. *Geotextiles and Geomembranes* 25(3), 194-202.
- [14] Wirawan R., Sapuan S., Robiah Y., Khalina A. 2011. Elastic and viscoelastic properties of sugarcane bagasse-filled poly (vinyl chloride) composites. *Journal of thermal analysis and calorimetry* 103(3), 1047-1053.
- [15] Dexter A., Kroesbergen B. 1985. Methodology for determination of tensile strength of soil aggregates. *Journal of Agricultural Engineering Research* 31(2), 139-147.
- [16] Muntohar A.S., Widiyanti A., Hartono E., Diana W. 2012. Engineering properties of silty soil stabilized with lime and rice husk ash and reinforced with waste plastic fiber. *Journal of Materials in Civil Engineering* 25(9), 1260-1270.
- [17] Li M., Xi Chai S., Yuan Zhang H., Pu Du H., Wei L. 2012. Feasibility of saline soil reinforced with treated wheat straw and lime. *Soils and Foundations* 52(2), 228-238.
- [18] Sivakumar Babu G., Vasudevan A., Sayida M. 2008. Use of coir fibers for improving the engineering properties of expansive soils. *Journal of Natural Fibers* 5(1), 61-75.
- [19] Fatahi B., Khabbaz H., Fatahi B. 2012. Mechanical characteristics of soft clay treated with fibre and cement. *Geosynthetics International*, 19(3), 252-262.

NOVI RAČUNSKI MODEL ZA BOLJŠO NAPOVED KOMPRESIJSKEGA INDEKSA ZEMLJINE

Ahmet Demir

Osmaniye Korkut Ata University,
Civil Engineering Department
80000 Osmaniye, Turčija
E-pošta: ahmetdemir@osmaniye.edu.tr

Ključne besede

kompresijski indeks, statistična analiza, genetsko programiranje, ANFIS, empirične enačbe

Izvleček

Kompresijski indeks je eden od pomembnejših parametrov zemljine, ki je bistven za geotehnično projektiranje. Ker so laboratorijski in terenski preizkusi za določitev vrednosti kompresijskega indeksa (C_c) težavni, dolgotrajni in dragi, se za ta namen pogosto uporabljajo empirične enačbe na osnovi parametrov zemljin. V preteklih letih so bile predlagane številne empirične enačbe, ki podajajo relacijo med stisljivostjo in drugimi parametri zemljine, kot so naravna vlažnost, meja židkosti, indeks plastičnosti in specifična gravitacija. Te empirične enačbe zagotavljajo dobre rezultate za posamezne preizkusne nize, vendar ne morejo natančno ali zanesljivo napovedati vrednosti kompresijskega indeksa iz različnih preizkusnih nizov. Druga pomanjkljivost teh empiričnih enačb je, da uporabljajo en parameter za ocenitev kompresijskega indeksa (C_c), čeprav kaže C_c prostorske značilnosti, odvisne od več parametrov zemljin. Prispevek predstavlja možnost za genetsko programiranje (GEP) in Adaptive Neuro-Fuzzy (ANFIS) računski zgled za oceno kompresijskega indeksa iz parametrov zemljine kot so naravna vlažnost, meja židkosti, indeks plastičnosti, specifična gravitacija in količnik por. Skupno je bilo za razvoj modelov uporabljenih 299 podatkovnih nizov zbranih iz literature. Učinkovitost tako izdelanih modelov je bila celovito ocenjena z uporabo različnih statističnih verifikacijskih orodij. Napovedani rezultati so pokazali, da modela GEP in ANFIS omogočata dokaj obetavne pristope za napoved kompresijskega indeksa zemljin in sta lahko bolj učinkovita kot empirične enačbe..

NEW COMPUTATIONAL MODELS FOR BETTER PREDICTIONS OF THE SOIL-COMPRESSION INDEX

Ahmet Demir

Osmaniye Korkut Ata University,
Civil Engineering Department
80000 Osmaniye, Turkey
E-mail: ahmetdemir@osmaniye.edu.tr

Keywords

compression index, statistical analysis, genetic expression programming, adaptive neuro-fuzzy, empirical equations

Abstract

The compression index is one of the important soil parameters that are essential for geotechnical designs. Because laboratory and in-situ tests for determining the compression index (C_c) value are laborious, time consuming and costly, empirical formulas based on soil parameters are commonly used. Over the years a number of empirical formulas have been proposed to relate the compressibility to other soil parameters, such as the natural water content, the liquid limit, the plasticity index, the specific gravity. These empirical formulas provide good results for a specific test set, but cannot accurately or reliably predict the compression index from various test sets. The other disadvantage is that they tend to use a single parameter to estimate the compression index (C_c), even though C_c exhibits spatial characteristics depending on several soil parameters. This study presents the potential for Genetic Expression Programming (GEP) and the Adaptive Neuro-Fuzzy (ANFIS) computing paradigm to predict the compression index from soil parameters such as the natural water content, the liquid limit, the plastic index, the specific gravity and the void ratio. A total of 299 data sets collected from the literature were used to develop the models. The performance of the models was comprehensively evaluated using several statistical verification tools. The predicted results showed that the GEP and ANFIS models provided fairly promising approaches to the prediction of the compression index of soils and could provide a better performance than the empirical formulas.

1 INTRODUCTION

The settlement of a structure is the vertical, downward movement due to a volume decrease of the soil on which the structure is built. Geotechnical engineers have a responsibility to calculate the extent of the possible settlements as completely as possible for the safety of particular projects. So, a study of the consolidation characteristics of soft, compressible geo-environmental materials is very useful for forecasting the magnitude and time of the settlement of the structure. The desired use of the structure may be damaged and the design life of the structure may be reduced if the settlement is not kept within a tolerable limit. To evaluate the spatial distribution of the consolidation settlement (s_c) in a large coastal reclamation area, geotechnical engineers need to correctly access the spatial characteristics of the soil's properties. However, it is difficult to evaluate the exact spatial characteristics of the soil's properties because the amount of geotechnical investigation data is insufficient in most cases.

In particular, it is well known that when compressible geo-materials, like silt or clay layers, are subjected to a stress, an increase in the pore-water pressure occurs immediately. Because the hydraulic conductivity of these soils is very small, the excess pore-water pressure generated by loading gradually dissipates over a long period. Consequently, the associated volume change (consolidation) of the soil continues a long time after the completion of the structure. In geotechnical engineering, the change in the void ratio versus the change in the effective pressure compressibility of the soils is defined as the coefficient of the compressibility index (C_c), which is generally determined directly using the $e - \log p$ curve.

Oedometer tests of which testing procedures have been standardized by ASTM-D-2435-96 [1] are commonly used for experimental determinations of the compression index in the laboratory. However, these are laborious, time-consuming and costly methods. In order to obtain the C_c value for soils with less effort and more economically, empirical equations based on the fundamental soil parameters, as specified using simpler laboratory tests, are generally preferred [2-9]. However, most of them are developed using limited experimental data and do not provide satisfactory and precise predictions.

The other disadvantage of these equations is that they generally use a single soil parameter or use multivariable equations based on linear approaches to predict the compression index [9-11]. The soils have reasonably complex structures, imprecise physical properties and a spatial variability (i.e., heterogeneities) associated with their formation. Therefore, their mechanical and dynamic features show an uncertain behavior in contrast to most other engineering materials [12]. Alternative methods such as GEP, ANNs and ANFIS allow the modelling of spatially complex systems and have recently emerged as commonly used and promising approaches [13-17]. Their importance is also related in all engineering areas as a result of the high-speed development of information and computer technologies. These methods have a capability for pattern recognition, classification, speech recognition, design of structures, automatic control, manufacturing process control, and the modeling of material behavior [18-20].

In this paper new approaches based on GEP and ANFIS were introduced for the prediction of the compression index of soils. The data sets for training and testing were obtained from the literature. Five basic soil properties that are accepted to be substantial parameters in geotechnical engineering, such as the natural water content (w_n), the liquid limit (LL), the plasticity index (PI), the specific gravity (G_s) and the void ratio (e), were used for the GEP and ANFIS models as the input parameters.

2 OVERVIEW OF THE COMPRESSION INDEX OF SOILS

The compression index (C_c) shows the slope of the linear part of the curve of the void ratio versus the logarithm of the effective pressure (Fig. 1). In other words, it means a change in the void ratio due to the effective pressure change during the consolidation of soils.

For a layer of normally consolidated soil of thickness H , the initial void ratio e_0 , the compression index C_c , the effective overburden pressure P'_0 , and the total settlement S_t under an applied load Δp can be expressed as

$$S_t = \frac{C_c}{1 + e_0} H \log \frac{P'_0 + \Delta p}{P'_0} \quad (1)$$

where C_c is the slope of the virgin compression portion of the $e - \log p$ curve determined from a standard consolidation test on an undisturbed sample.

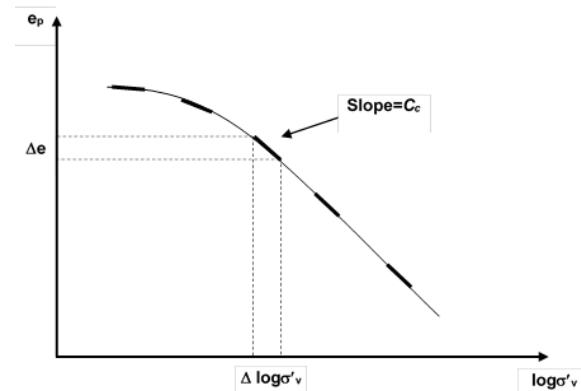


Figure 1. A typical $e_p - \log \sigma'_v$ curve for obtaining the value of C_c at any load increment.

3 BRIEF REVIEW OF GENETIC EXPRESSION PROGRAMMING (GEP)

Genetic Expression Programming (GEP), which is based on genetic algorithms (GAs) and genetic programming (GP), was developed for the first time by [21]. Its data-processing system is similar to the human genetic system and is a computer program encoded in linear chromosomes of fixed length. The fundamental concept of this approach is to find a mathematical function, defined as a chromosome with multi genes, by using the data presented to it. The mathematical expression is encoded as simple strings of fixed length, which are subsequently expressed as expression trees of different

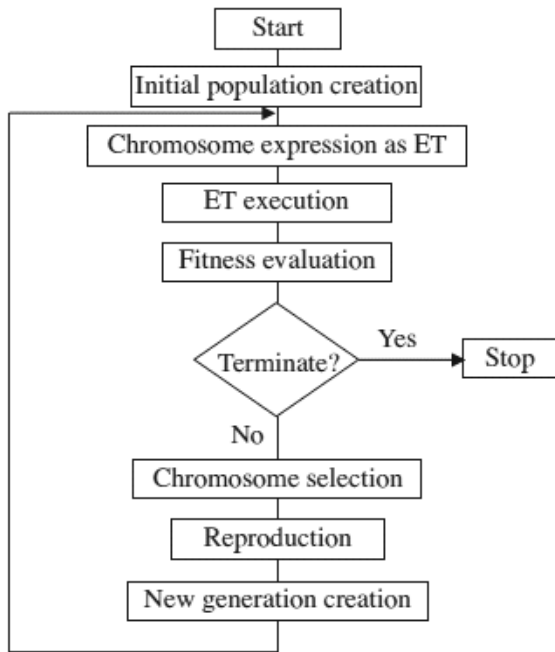


Figure 2. The algorithm of Genetic Expression Programming [25].

size and shape in GEP [22-24]. A typical GEP algorithm is sketched out in Fig. 2. Its processing initializes, selecting five elements, such as the function set, the terminal set, the fitness function, the control parameters and the stop condition. The GEP algorithm randomly generates an initial chromosome that symbolizes a mathematical function and then converts it into an expression tree (ET), as indicated in Fig. 3.

The later processing is to compare between the predicted values and the measured values. If the desired results are achieved using the initially selected error criteria, the GEP algorithm is terminated. When the expected results cannot be obtained, some chromosomes are selected by means of the method called roulette-wheel sampling. This method, with an elitism strategy, is employed by the GEP algorithm to select and copy the individuals. Single or several genetic operators, such as crossover, mutation and rotation, are used for introducing variations into the population. Note that the rotation operator rotates two subparts of the genome with respect to a randomly chosen point. Further descriptions of the GEP algorithm can be found in [21]. They are mutated to obtain new chromosomes. After the desired fitness score is obtained, this process terminates and then the knowledge coded in the genes in chromosomes is decoded for the best solution of the problem [25].

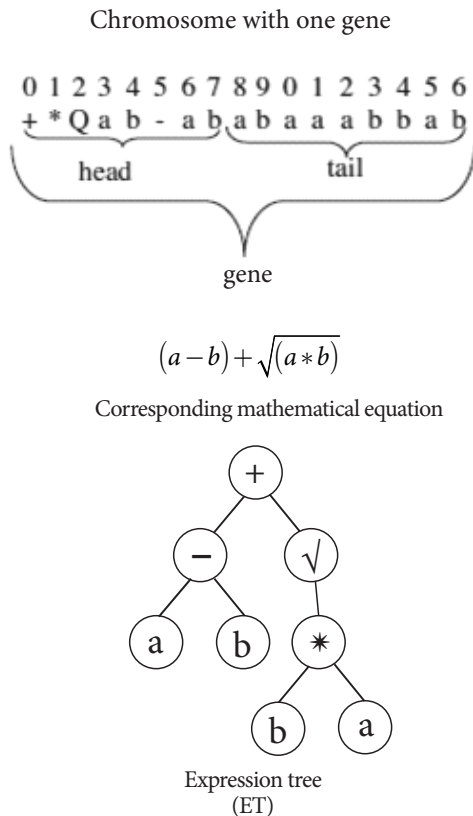


Figure 3. Schematic indication of a chromosome with one gene and its expression tree and the corresponding mathematical equation.

GEP has two main components that are defined as the chromosomes and the expression trees (ETs). The chromosomes that may have one or more genes are coded with some information using a special language about the problem. The mathematical information is translated to the ET using a bilingual and conclusive language called Karva Language (the language of the genes) and by means of the language of ETs. The genotype is accurately derived by using the Karva Language. The GEP genes are made up of two parts that are named as the head and the tail. The head of a gene includes the main variables needed to code any expression, such as some functions, variables and constants. The tail simply contains variables and constants, which may be required for additional terminal symbols. These symbols are used in the event that the variables in the head are insufficient to encipher a function. While the head of a gene contains arithmetic and trigonometric functions – like +, -, √, /, p, sin, cos – the tail includes the constants and the independent variables of the problem – like (1, a, b, c).

At the beginning of the model's construction the user specifies the length of the head (i.e., the number of symbols), which is the most significant parameter in the GEP process. The encoding process takes place by reading the ET from left to right in the top line of

the tree and from the top to the bottom, and the ET is converted to Karva Language. The GEP genes include a non-coding part similar to the coding and non-coding sequences of biological genes. There are four primary operators (such as selection, mutation, transposition, and cross-over) during the GEP processing. When the mathematical equation obtained from the GEP model is not suitable for the problem, the chromosomes should be modified by means of GEP operators to obtain the next generation. The operators given above are applied with the operator rate that shows a certain probability for a chromosome. The operator rates are specified by the user prior to the analysis. The mutation rate is generally used between 0.001 and 0.1. On the other hand, it is suggested that the transposition rate and cross-over rate are 0.1 and 0.4, respectively [25].

4 FUZZY INFERENCE SYSTEMS

Zadeh [26] proposed the first fuzzy approach. This method exhibits some differences from the traditional cluster theory (TCT), which is the crisp definition for an element belonging to a cluster. According to TCT, an element either belongs to a cluster or not. However, the fuzzy approach does not decide completely with respect to the belonging. This is because the degree of membership of an element is important for the fuzzy approach. It is defined partially by the continuous membership functions that take a value between 0 and 1 [27, 28]. Takagi and Sugeno [29] proposed two models known as the Mamdani and Tagagi-Sugeno (TS) models. There are, however, some differences between them. The Mamdani model employs human expertise and the linguistic knowledge's to build the membership functions and the if-then rules. However, in the TS model the optimization and adaptive techniques are used and it also uses a smaller number of if-then rules. So, the advantage of some aspects of the TS model is that it is more suitable for the mathematical and computational modeling, and therefore it is mostly preferred by researchers [14, 24]. The other advantage is that it also makes it possible to design the output function as either linear or constant [13, 30 and 31]. ANFIS is a kind of fuzzy-logic approach proposed by Jang [32]. It has more advanced properties than other fuzzy models, such as learning and parallelism, like that of ANNs, which allow the fuzzy rules and membership functions to be generated adaptively using a neural training process with the data set presented. In the Sugeno-type fuzzy approach, the if-then rules given below are used:

$$\text{If } x = A_1 \text{ and } y = B_1 \text{ then } f_{1(x,y)} = p_1x + q_1y + k_1 \quad (2)$$

$$\text{If } x = A_2 \text{ and } y = B_2 \text{ then } f_{2(x,y)} = p_2x + q_2y + k_2 \quad (3)$$

where x (or y) = the input node; i, p, q and k = the consequence parameters obtained from the training; A and B = are labels of the fuzzy set defining a suitable membership function. A backpropagation learning algorithm and a hybrid learning algorithm are utilized to update the membership functions during the fuzzy process [33]. In Fig. 4, the main concept of the ANFIS approach is illustrated. As shown, the computational process of the ANFIS is performed in five steps. The initial parameters that define the membership functions are specified in the first step. For example, the initial parameters of the generalized bell-shaped are widely used as a membership function, as given below:

$$\eta_A(X) = \frac{1}{1 + \left| \frac{x - c_i}{a_i} \right|^{2b}} \quad (4)$$

where η = the membership function; a, b and c = the parameter set known as the initial (or premise) parameters. In second step, every node in this layer is a fixed node labelled Π , representing the firing strength of each rule. The firing strength means the degree to which the antecedent part of the rule is satisfied. It represents the product of the incoming signals that is calculated using the following equation:

$$U_{2,i} = w_i = \eta A_i(x) \times \eta B_i(y) \quad i = 1, 2 \quad (5)$$

The firing strengths computed in the second step are normalized using the following equation in the third step,

$$U_{3,i} = \bar{w}_i = \frac{w_i}{w_1 + w_2} \quad i = 1, 2 \quad (6)$$

In the fourth step, the effect of each rule on the output is computed with an adaptive node function using the following equation:

$$U_{4,i} = \bar{w}_i f_i = \bar{w}_i (p_i x + q_i y + k_i) \quad (7)$$

where w is the normalized firing strength calculated in step 3; and $p_i, q_i,$ and k_i are the resulting parameters. The final output of the ANFIS model is found in the fifth step using the equation shown below:

$$U_{5,i} = \sum \bar{w}_i f_i = \frac{\sum_i w_i f_i}{\sum_i w_i} \quad (8)$$

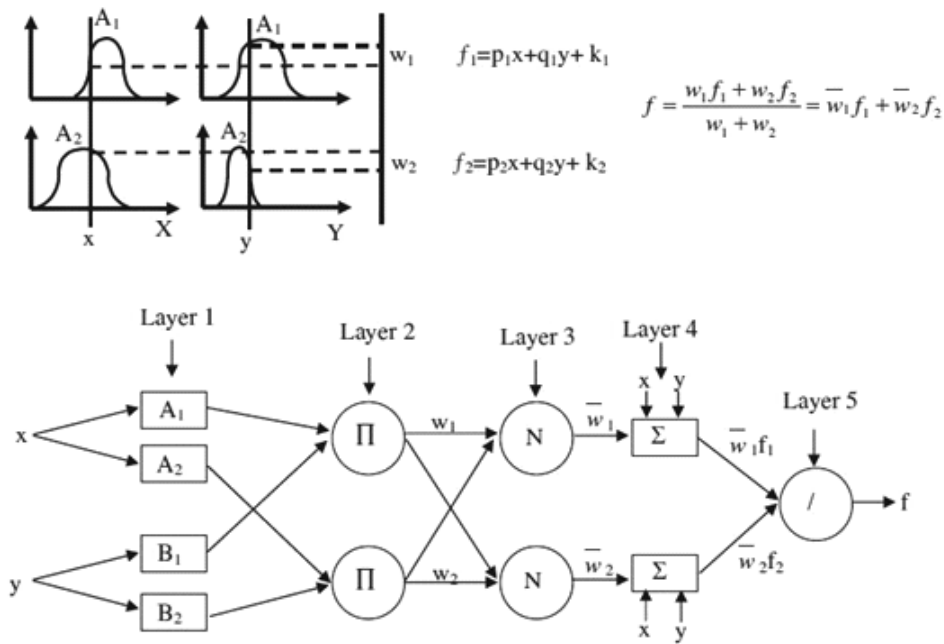


Figure 4. The simple ANFIS architecture [34].

5 DATA COLLECTION

This study aims to estimate the compression index by taking account of the physical properties of soils. The data sets used to develop the GEP and ANFIS models were obtained from Kalantary and Kordnaeij [35]. They reported on data from Iran and suggested an ANN model for the prediction of the compression index. The input parameters used herein were selected in such a manner that the phenomenon of the compression index is defined by these parameters in accordance with the

methods used extensively in practical engineering.

Therefore, the void ratio (e_o), the natural water content (ω_n), the liquid limit (LL), the plastic index (PI), and the specific gravity (G_s) were chosen as the input parameters. Also, based on the previous trend of studies, the compression index of the soils is assumed to be affected by them. Fig. 5 shows histograms of the inputs and the target parameters and, also, the statistical parameters of the input and output variables for each data set are given in Table 1. As is clear from Table 1, there is a high correlation between the input parameters (ω_n and e_o) and the target parameter (C_c).

Table 1. Statistical parameters of the input and output variables for each data set.

Data Set	Variable	x_{ort}	σ	C_v	C_{sx}	C_k	x_{maks}	x_{min}	Range	Correlation coefficient with the C_c
Training	ω_n	28.39	6.94	48.16	1.01	2.44	57.40	11.10	46.30	0.76
	LL	40.02	9.83	96.31	1.26	0.92	96.31	24.00	72.31	0.48
	PI	18.83	8.50	71.88	1.37	0.36	71.88	4.00	67.88	0.46
	e_o	0.76	0.15	0.02	0.72	4.95	4.95	0.41	4.54	0.85
	G_s	2.64	0.06	0.00	-9.77	0.50	2.80	2.43	0.37	-0.16
Testing	ω_n	28.93	6.80	46.28	0.46	-0.04	46.40	14.50	31.90	0.80
	LL	37.41	7.46	55.60	0.62	-0.40	57.00	25.00	32.00	0.30
	PI	16.53	6.79	46.07	0.44	-0.68	34.00	6.00	28.00	0.27
	e_o	0.77	0.15	0.02	0.68	0.63	1.23	0.48	0.76	0.87
	G_s	2.64	0.05	0.00	-0.70	1.29	2.74	2.49	0.25	0.00

C_v : variation coefficient, C_{sx} : skewness coefficient, C_k : kurtosis coefficient.

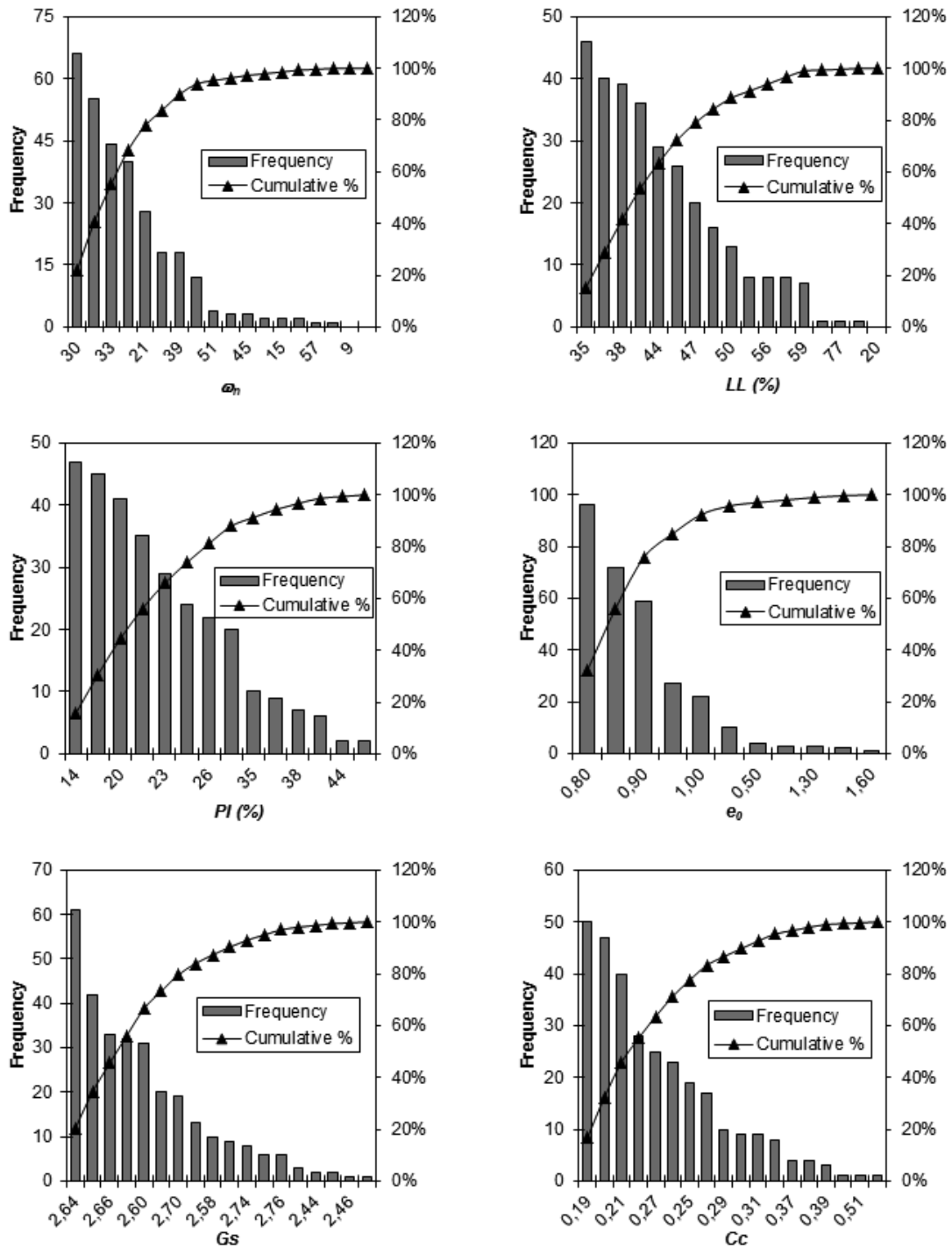


Figure 5. The histograms of the input variables and the output variable.

6 GEP MODEL DEVELOPMENT

The GEP models enhanced herein are mainly designed to generate mathematical functions for the prediction of the compression index of the soil. Three GEP models (GEP Model I, GEP Model II and GEP Model III) were

developed. Whilst five input parameters were selected, such as ω_n , LL , PI , e_o and G_s for the GEP Model I, three and two input parameters (LL , PI and e_o), (ω_n and e_o) were used in the GEP Model II and GEP Model III, respectively. In other words, the ω_n and G_s parameters were not taken into account for the inputs of the GEP

Model II. For that reason, three mathematical functions in the form $y = f(\omega_n, LL, PI, e_o \text{ and } G_s)$, $y = f(LL, PI \text{ and } e_o)$ and $y = f(\omega_n \text{ and } e_o)$ were generated for the prediction of the compression index of the soil. The model parameters used for both models are given in Table 2. DTREG software is used for the GEP algorithm [36]. The functions obtained from the GEP Models are given below:

Model I

$$C_c = \tan \left[\exp \left[\left(\tan (LL \times G_s)^{1/9} \right)^{1/3} \right]^2 \right. \\ \left. + \operatorname{atan} \left[\frac{\sin (\cos (G_s) \times (2e_o + G_s))}{\omega_n} \right] \right] \\ - \operatorname{atan} \left[\operatorname{atan} (\cot (LL) - 2LL) + (G_s - e_o)^{1/2} \right] \\ - \cos \left[\frac{\sec (PI)^3}{G_s^2 \times (G_s + G_s^3)} \right]$$

Model II

$$C_c = \cos \left[\ln \left(\sqrt{e_o \times LL} \right) + \operatorname{atan} (LL) \right] \\ + \sin \left[\sqrt{\ln \left[2.80 \left[2(LL) - (LL \times e_o) \right] \right]} \right] \\ + \operatorname{atan} \left[-1.88 \left(\ln \left[\sqrt{\frac{LL}{e_o}} \right] \right) \right] \\ + \operatorname{atan} \left[\sqrt{e_o \left[((PI - 3.44) \times e_o) \times (LL + 6.15) \right]} \right]$$

Model III

$$C_c = \cos \left[(\omega_n \times e_o + \omega_n) / \left(\sqrt{\omega_n} \times 2\omega_n \right) \right] \\ + \cos \left(\sqrt{\omega_n} \times e_o \right) \times \left[(e_o)^2 / 2\omega_n \right] + \frac{(e_o)^2}{(\omega_n \times e_o)^{1/3}}$$

7 ANFIS MODEL DEVELOPMENT

Three ANFIS Models (ANFIS Model I, ANFIS Model II and ANFIS Model III) were built using the same inputs as in the GEP. The membership functions of each of the input variables were generated using the grid-partition method. The triangular membership function was chosen for both models and the hybrid learning algorithm was executed for optimizing the parameters that can perform a rapid identification of the parameters, substantially reducing the time needed to reach convergence.

Table 2. GEP parameters of the developed models .

Population Size	50
Generation	194174
Number of The Genes	4
Length of The Gene Head	8
Max. Generation	227405
Linking Function	+
Function Set	+, -, *, /, √, exp, ln, sin, cos, atan
Mutation Rate	0.044
Inversion Rate	0.1
One-Point Recombination Rate	0.3
Two-Point Recombination Rate	0.3
Gene-Transposition Rate	0.1

In order to avoid over fitting, the stopping criterion was adopted as the minimum validation error. The ANFIS Model I has 243 linear parameters, 45 nonlinear parameters, 524 nodes and 243 fuzzy rules. On the other hand, ANFIS Model II has 64 linear parameters, 48 nonlinear parameters, 158 nodes and 64 fuzzy rules. Also, ANFIS Model III has 9 linear parameters, 18 nonlinear parameters, 35 nodes and 9 fuzzy rules. The fuzzy toolbox of the MATLAB computer-aided software was used for the model development [33].

8 RESULTS AND DISCUSSION

This paper, to a large extent, intends to investigate the potential use of GEP and ANFIS for the prediction of the compression index of soils, which has great significance for soil mechanics and foundation engineering. The results obtained from these approaches were comprehensively evaluated in terms of statistics for a quantitative assessment of the model's predictive abilities. Of the 299 data sets, 233 were used for training the models and 66, which are not used in training stage, were presented for the testing of the models. In order to learn the performance of the developed models, several statistical verification criteria were used, such as the coefficient of correlation (R), the root-mean-square error (RMSE) and the standard deviation (σ) of the errors. The definition of these evaluation criteria are given as follows:

$$R = \frac{\sum_{i=1}^n (u_i^m - \bar{u}^m)(u_i^c - \bar{u}^c)}{\sqrt{\sum_{i=1}^n (u_i^m - \bar{u}^m)^2} \sqrt{\sum_{i=1}^n (u_i^c - \bar{u}^c)^2}} \quad (12)$$

$$RMSE = \sqrt{\frac{\sum_{i=1}^N (u_i^m - u_i^c)^2}{N}} \quad (13)$$

$$\sigma = \sqrt{\frac{\sum_{i=1}^N (e - \bar{e})^2}{(N - 1)}} \quad (14)$$

where u_i^m and u_i^c are the measured and predicted values, respectively. \bar{u}^m and \bar{u}^c are the mean of the measured and predicted values, e is the absolute error ($|u_i^m - u_i^c|$), \bar{e} is the mean of the absolute error, and N is the size of the sample. The C_c values estimated from all the models through the training and testing process were graphically compared with the case records in Fig.6. It is clear from the figure that the results from the GEP and ANFIS are in good agreement with the case records. This also shows that all the models were found to be able to learn the complex relationship between the input parameters relating to soils and the value of C_c . Moreover, the statistical performances of the models are presented in Table 3. With respect to this table, all the models for compression index C_c give a satisfactory agreement in terms of the statistical evaluation criteria. The best results with regard to the R values were 0.910 and 0.900 for the GEP Model I and the ANFIS Model I, respectively. However, the GEP Model II and the ANFIS Model II give relatively high R values, i.e., 0.870 and 0.870, respectively. In statistics, the overall error performances of the relationship between the two groups can be interpreted from the R values. According to Smith (1986), if a proposed model gives $R > 0.8$, there is a strong correlation between the measured and the predicted values for all the data available in the database.

As the models are compared with regard to the RMSE, which is a measurement of the deviation around the regression line, it is clear that the lowest RMSE is obtained from Eq. (9) generated from GEP Model I, i.e., 0.029. On the other hand, Eq. (10) generated from GEP Model II gives an RMSE value of 0.034. The other models yield low RMSE values, ranging from 0.032 to 0.090. The RMSE value has great significance for the statistics in addition to the R value, because although the relationship provides a high R value, it may also give a high RMSE value.

As seen from Table 4, the predictability of the GEP and ANFIS models is also statistically compared with the empirical formulas, the mean and the standard deviation of the ratio $C_{c,pred}/C_{c,mea}$, which is often used for a statistical analysis. The mean (μ) and the standard deviation (σ) of $C_{c,pred}/C_{c,mea}$ are important indicators of

the accuracy and the precision of the prediction method. Under ideal conditions, an accurate and precise method gives a mean value of 1.0 and a standard deviation of 0. A μ value greater than 1.0 indicates an overestimation and an underestimation, otherwise. The best model is represented by a μ value close to 1.0 and a σ value close to 0. Based on the μ value, the GEP Model I shows a good prediction when using the soil parameters such as ω_n , LL , PI , e_o and G_s . Other empirical formulas yield a μ value in the range 0.820–14.574. This means that, on average, they considerably underestimate or overestimate the compression index. The value of σ is also found to be a minimum for the GEP Model I.

Table 3. Performance statistics of the models.

	GEP Models			ANFIS Models		
	I	II	III	I	II	III
R	0.910	0.870	0.866	0.900	0.870	0.852
RMSE	0.029	0.034	0.035	0.032	0.090	0.037
σ	0.018	0.023	0.024	0.021	0.081	0.026

Table 4. Statistical results for conventional empirical formulas.

Equation	Average, μ	Standard Deviation, σ	References
$C_c = 0.01\omega_n - 0.05$	1.154	0.224	Azzouz [4]
$C_c = 0.01\omega_n$	1.411	0.262	Koppula [37]
$C_c = 0.013\omega_n - 0.115$	0.820	0.206	Park and Lee [9]
$C_c = 0.54e_o - 0.19$	1.058	0.204	Nishida [38]
$C_c = 0.75e_o - 0.38$	0.874	0.352	Sowers [39]
$C_c = 0.006\omega_L - 0.054$	0.858	0.292	Azzouz [4]
$C_c = 0.009\omega_L - 0.090$	1.241	0.429	Terzaghi and Peck [3]
$C_c = 0.014\omega_L - 0.168$	1.786	0.642	Park and Lee [9]
$C_c = 0.2343(\omega_L/100)G_s$	1.167	0.352	Nagaraj and Murthy [5]
$C_c = 2.926(\omega_L/100)G_s$	14.574	4.399	Park and Lee [9]
$C_c = 0.009\omega_n + 0.005\omega_L$	2.216	0.443	Koppula [37]
GEP Model I	0.993	0.131	This study
GEP Model II	0.980	0.151	This study
GEP Model III	1.015	0.150	This study
ANFIS Model I	1.016	0.140	This study
ANFIS Model II	0.992	0.138	This study
ANFIS Model III	1.010	0.149	This study

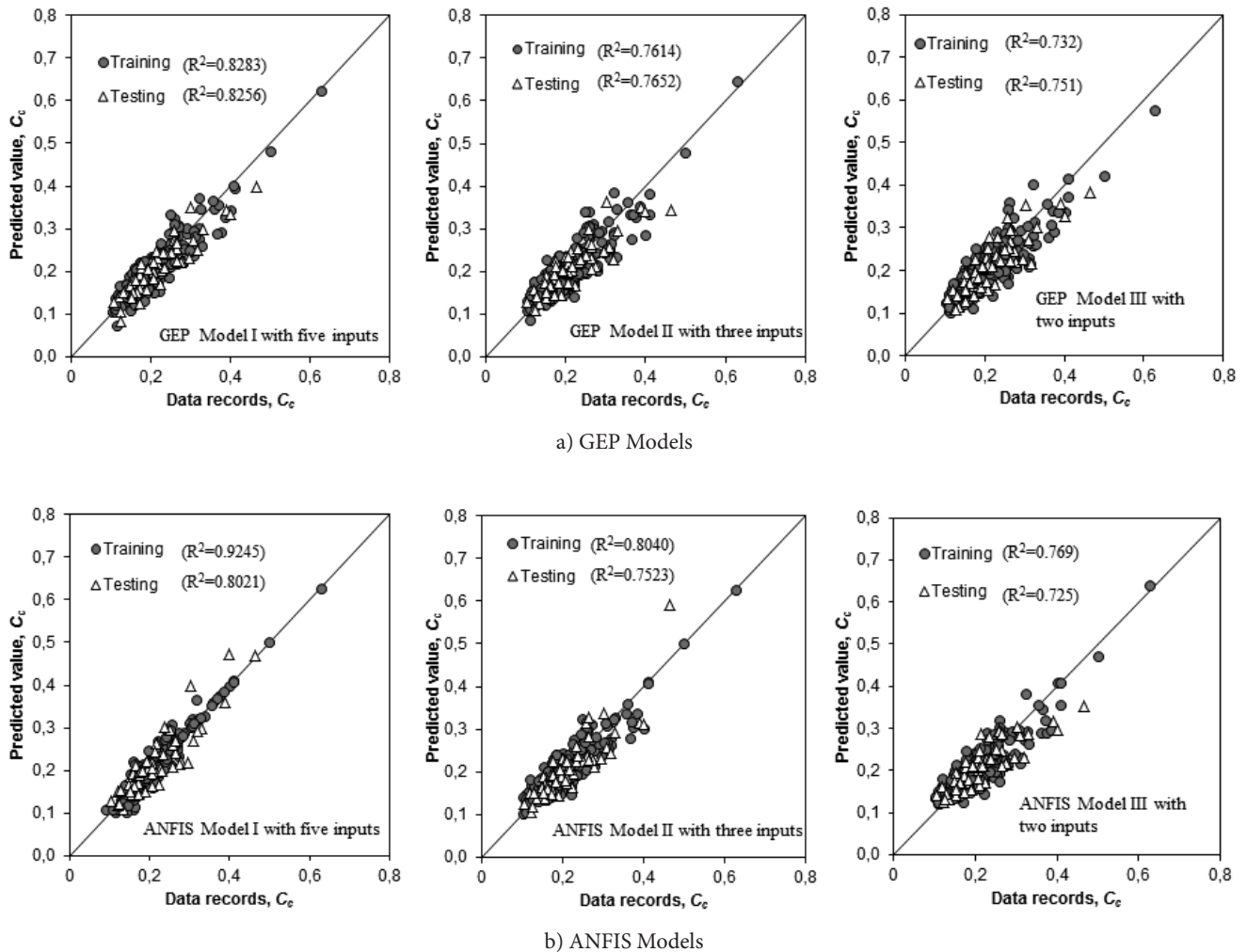


Figure 6. Comparison of the case records with the predicted C_c values from the GEP and ANFIS Models.

The evaluations given above clearly reveal that Eqs. (9), (10) and (11) generated by the GEP Models and the ANFIS Models have a good prediction ability. The prediction accuracy of the models appears to be statistically sufficient in terms of the prediction of C_c . Since the laboratory and the *in-situ* tests for the determination of the C_c value are laborious, time consuming and costly, it is better to use Eqs. (9), (10) and (11) to estimate the compression index (C_c) of soils.

9 CONCLUSIONS

This study looks at the capability of Genetic Expression Programming (GEP) and Adaptive Neuro-Fuzzy (ANFIS) for the prediction of the compression index (C_c) in soils. Data for the development and the testing of the models were obtained from the literature. At

the end of the analyses, three mathematical equations from the GEP and three ANFIS Models were developed for a better prediction of the soil-compression index. The results of these compression indexes of the soils predicted by the GEP Models are compared with those obtained from the ANFIS and the conventional empirical formulas.

The comparison between soft computing systems mentioned above indicated that the GEP Model I markedly outperformed the other models. The satisfactory agreement was obtained as a result of the testing procedures of Eqs. (1) and the GEP Models. This was evidenced by some statistical performance criteria used for evaluating the models. Eqs. (1) produced the GEP Model I and GEP Model II, respectively, and gave a high correlation coefficient (0.910 and 0.870, respectively) and low RMSE values (0.029 and 0.035). On the other hand, the ANFIS Models produced satisfactory results

with R values that are ranging from 0.900 to 0.850 and higher RMSE values ranging from 0.032 to 0.900 than the GEP Models. The overall evaluation of the results obtained throughout the paper revealed that the soft-computing techniques used herein are very encouraging for the cases tested.

It was also observed that the best results were obtained from Model I with five input parameters. The other models that were developed to see the effects of different soil properties also produced satisfactory results. It was concluded from all the findings herein that the use of basic soil properties, such as the void ratio (e_o), the natural water content (ω_n), the liquid limit (LL), the plastic index (PI), and the specific gravity (G_s), appears to be reasonable for the prediction of the compression index (C_c) of soils.

REFERENCES

- [1] ASTM D 2435-96 1998. Standard test method for one-dimensional consolidation properties of soils. Annual Book of ASTM standards. Vol. 04.08, Soil and Rock (I). Standard. Pennsylvania pp.207-216.
- [2] Helenelund K.V. 1951. On consolidation and settlement of loaded soil layers. Dissertation, Finland Technical Institute, Helsinki, Finland.
- [3] Terzaghi, K., Peck, R.B. 1967. Soil mechanics in engineering practice. 2nd ed. John Wiley & Sons Inc., New York.
- [4] Azzouz, A.S., Krizek R.J., Corotis, R.B. 1976. Regression analysis of soil compressibility. Soils Foundations 16, 2, 19-29.
- [5] Nagaraj, T.S., Murthy, B.R.S. 1986. A critical reappraisal of compression index equations. Geotechnique 36, 1, 27-32.
- [6] Nakase, A., Kamei, T., Kusakabe, O. 1988. Constitutive parameters estimated by plasticity index. Journal of Geotechnical Engineering, ASCE, 114, 844-858.
- [7] Sridharan, A. Nagaraj, H.B. 2000. Compressibility behaviour of remoulded, finegrained soils and correlation with index properties. Canadian Geotechnical Journal 37, 3, 712-722.
- [8] Giasi, C.I., Cherubini, C., Paccapelo, F. 2003. Evaluation of compression index of remoulded clays by means of Atterberg limits. Bull. Eng. Geol. Environ. 62, 4, 333-340.
- [9] Park, H.I., Lee, S.R. 2011. Evaluation of the compression index of soils using an artificial neural network. Computers and Geotechnics 38, 472-481.
- [10] Bowles, J. E. 1992. Engineering properties of soils and their measurement (fourth ed.). New York, NY: McGraw-Hill.
- [11] Yoon, G.L., Kim, B.T., Jeon, S.S. 2004. Empirical correlations of compression index for marine clay from regression analysis. Canadian Geotechnical Journal 41, 6, 1213-1221.
- [12] Jaksa, M. B. 1995. The influence of spatial variability on the geotechnical design properties of a stiff, overconsolidated clay. Ph.D. thesis, Faculty of Engineering, The University of Adelaide, 469 pp.
- [13] Shahin, M. A., Maier, H. R., Jaksa, M. B. 2003. Settlement prediction of shallow foundations on granular soils using B-spline neurofuzzy models. Computers and Geotechnics 30, 637-647.
- [14] Tutmez, B., Tercan, A. E. 2007. Spatial estimation of some mechanical properties of rocks by fuzzy modeling. Computers and Geotechnics 34, 10-18.
- [15] Cobaner, M., Haktanir, T., Kisi, O. 2008. Prediction of hydropower energy using ANN for the feasibility of hydropower plant installation to an existing irrigation dam. Water Resources Management 22, 6, 757-774.
- [16] Baykasoglu, A., Gullu, H., Canakci, H., Ozbakir, L.L. 2008. Prediction of compressive and tensile strength of limestone via genetic programming. Expert Systems with Applications 35, 111-123.
- [17] Kayadelen, C., Gunaydin, O., Fener, M., Demir, A., Ozvan, A. 2009. Modeling of the angle of shearing resistance of soils using soft computing systems. Expert Systems with Applications 36, 11814-11826.
- [18] Najjar, Y. M., Basheer, I. A. 1996. Discussion of stress-strain modelling of sands using artificial neural networks. Journal of Geotechnical Engineering 122, 11, 949-950.
- [19] Adam, E. G. 2003. Data-driven linguistic modeling using relational fuzzy rules. IEEE Transactions on Fuzzy Systems 11, 1, 121-134.
- [20] Kim, Y.S., Kim, B.T. 2008. Prediction of relative crest settlement of concrete-faced rockfill dams analyzed using an artificial neural network model. Computers and Geotechnics 35, 3, 313-322.
- [21] Ferreira, C. 2001. Gene expression programming: A new adaptive algorithm for solving problems. Complex Systems 13, 2, 87-129.
- [22] Munoz, D. G. 2005. Discovering unknown equations that describe large data sets using genetic programming techniques. Master thesis in electronic systems at Linkoping Institute of Technology, LITH-ISY-EX-05/3697.
- [23] Cevik, A. 2007. A new formulation for longitudinally stiffened webs subjected to patch loading. Journal of Constructional Steel Research 63, 1328-1340.

- [24] Kayadelen, C. 2011. Soil liquefaction modeling by Genetic Expression Programming and Neuro-Fuzzy. *Expert Systems with Applications* 38, 4080–4087.
- [25] Teodorescu, L., Sherwood, D. 2008. High energy physics event selection with gene expression programming. *Computer Physics Communications* 178, 409–419.
- [26] Zadeh, L. A. 1965. Fuzzy sets. *Information and Control* 8, 338–353.
- [27] Dubois, D., Prade, H. 1980. *Fuzzy sets and systems*. New York: Academic Press.
- [28] Topcu, I. B., Sarıdemir, M. 2007. Prediction of rubberized concrete properties using artificial neural network and fuzzy logic. *Construction and Building Materials*, in press
- [29] Takagi, T., Sugeno, M. 1985. Fuzzy identification of systems and its applications to modeling and control. *IEEE Transactions Systems, Man, and Cybernetics* 15, 116–132.
- [30] Abdulsamet, H., Mehmet, Y., Omer, C., Ismail, E. 2004. Adaptive neuro-fuzzy modeling of transient heat transfer in circular duct air flow. *International Journal of Thermal Sciences* 43, 1075–1090.
- [31] Yılmaz, Y., Mahmut, B. 2006. Adaptive neuro-fuzzy based modelling for prediction of air pollution daily levels in city of Zonguldak. *Chemosphere* 63, 1575–1582.
- [32] Jang, J. S. R. 1993. ANFIS: Adaptive-network-based fuzzy inference systems. *IEEE Transactions Systems, Man, and Cybernetics* 23, 3, 665–685.
- [33] Demuth, H., Beale, M. 2001. *Neural network toolbox for use with Matlab*. Natick, Mass: The MathWorks Inc. 840 pp.
- [34] Padmini, D., Ilamparuthi, K., Sudheer, K. P. 2008. Ultimate bearing capacity prediction of shallow foundations on cohesionless soils using neurofuzzy models. *Computers and Geotechnics* 35, 33–46.
- [35] Kalantary, F., Kordnaeij, A. 2012. Prediction of compression index using artificial neural network. *Scientific Research and Essays* 7, 31, 2835–2848.
- [36] Sherrod, P.H. 2008. DTREG predictive modeling software. <<http://www.dtreg.com/>>.
- [37] Koppula S.D. 1981. Statistical estimation of compression index. *Geotechnical Testing Journal* 4, 2, 68–73.
- [38] Nishida Y. 1956. A brief note on compression index of soils. *J SMFE Div. ASCE* 1, 14, 1027.
- [39] Sowers G.B. 1970. *Introductory soil mechanics and foundation*. 3rd ed. London: The Macmillan company of Collier-Macmillan Ltd., pp. 102.

NAVODILA AVTORJEM

Vsebina članka

Članek naj bo napisan v naslednji obliki:

- Naslov, ki primerno opisuje vsebino članka in ne presega 80 znakov.
- Izvleček, ki naj bo skrajšana oblika članka in naj ne presega 250 besed. Izvleček mora vsebovati osnove, jedro in cilje raziskave, uporabljeno metodologijo dela, povzetek izidov in osnovne sklepe.
- Največ 6 ključnih besed, ki bi morale biti napisane takoj po izvlečku.
- Uvod, v katerem naj bo pregled novejšega stanja in zadostne informacije za razumevanje ter pregled izidov dela, predstavljenih v članku.
- Teorija.
- Eksperimentalni del, ki naj vsebuje podatke o postavitvi preiskusa in metode, uporabljene pri pridobitvi izidov.
- Izidi, ki naj bodo jasno prikazani, po potrebi v obliki slik in preglednic.
- Razprava, v kateri naj bodo prikazane povezave in posplošitve, uporabljene za pridobitev izidov. Prikazana naj bo tudi pomembnost izidov in primerjava s poprej objavljenimi deli.
- Sklepi, v katerih naj bo prikazan en ali več sklepov, ki izhajajo iz izidov in razprave.
- Vse navedbe v besedilu morajo biti na koncu zbrane v seznamu literature, in obratno.

Dodatne zahteve

- Vrstice morajo biti zaporedno oštevilčene.
- Predložen članek ne sme imeti več kot 18 strani (brez tabel, legend in literature); velikost črk 12, dvojni razmik med vrsticami. V članek je lahko vključenih največ 10 slik. Isti rezultati so lahko prikazani v tabelah ali na slikah, ne pa na oba načina.
- Potrebno je priložiti imena, naslove in elektronske naslove štirih potencialnih recenzentov članka. Urednik ima izključno pravico do odločitve, ali bo te predloge upošteval.

Enote in okrajšave

V besedilu, preglednicah in slikah uporabljajte le standardne označbe in okrajšave SI. Simbole fizikalnih veličin v besedilu pišite poševno (npr. v , T itn.). Simbole enot, ki so sestavljene iz črk, pa pokončno (npr. Pa, m itn.). Vse okrajšave naj bodo, ko se prvič pojavijo, izpisane v celoti.

Slike

Slike morajo biti zaporedno oštevilčene in označene, v besedilu in podnaslovu, kot sl. 1, sl. 2 itn. Posnete naj bodo v katerem koli od razširjenih formatov, npr. BMP, JPG, GIF. Za pripravo diagramov in risb priporočamo CDR format (CorelDraw), saj so slike v njem vektorske in jih lahko pri končni obdelavi preprosto povečujemo ali pomanjšujemo.

Pri označevanju osi v diagramih, kadar je le mogoče, uporabite označbe veličin (npr. v , T itn.). V diagramih z več krivuljami mora biti vsaka krivulja označena. Pomen oznake mora biti razložen v podnapisu slike.

Za vse slike po fotografskih posnetkih je treba priložiti izvirne fotografije ali kakovostno narejen posnetek.

Preglednice

Preglednice morajo biti zaporedno oštevilčene in označene, v besedilu in podnaslovu, kot preglednica 1, preglednica 2 itn. V preglednicah ne uporabljajte izpisanih imen veličin, ampak samo ustrezne simbole. K fizikalnim količinam, npr. t (pisano poševno), pripišite enote (pisano pokončno) v novo vrsto brez oklepajev. Vse opombe naj bodo označene z uporabo dvignjene številke¹.

Seznam literature

Navedba v besedilu

Vsaka navedba, na katero se sklicujete v besedilu, mora biti v seznamu literature (in obratno). Neobjavljeni rezultati in osebne komunikacije se ne priporočajo v seznamu literature, navedejo pa se lahko v besedilu, če je nujno potrebno.

Oblika navajanja literature

V besedilu: Navedite reference zaporedno po številkah v oglatih oklepajih v skladu z besedilom. Dejanski avtorji so lahko navedeni, vendar mora obvezno biti podana referenčna številka.

Primer: »..... kot je razvidno [1,2]. Brandl and Blovsky [4], sta pridobila drugačen rezultat...«

V seznamu: Literaturni viri so oštevilčeni po vrstnem redu, kakor se pojavijo v članku. Označimo jih s številkami v oglatih oklepajih.

Sklicevanje na objave v revijah:

- [1] Jelušič, P., Žlender, B. 2013. Soil-nail wall stability analysis using ANFIS. Acta Geotechnica Slovenica 10(1), 61-73.

Sklicevanje na knjigo:

- [2] Šuklje, L. 1969. Rheological aspects of soil mechanics. Wiley-Interscience, London

Sklicevanje na poglavje v monografiji:

- [3] Mitchel, J.K. 1992. Characteristics and mechanisms of clay creep and creep rupture, in N. Guven, R.M. Pollastro (eds.), Clay-Water Interface and Its Rheological Implications, CMS Workshop Lectures, Vol. 4, The clay minerals Society, USA, pp. 212-244..

Sklicevanje na objave v zbornikih konferenc:

- [4] Brandl, H., Blovsky, S. 2005. Slope stabilization with socket walls using the observational method. Proc. Int. conf. on Soil Mechanics and Geotechnical Engineering, Bratislava, pp. 2485-2488.

Sklicevanje na spletne objave:

- [5] Kot najmanj, je potrebno podati celoten URL. Če so poznani drugi podatki (DOI, imena avtorjev, datumi, sklicevanje na izvirno literaturo), se naj prav tako dodajo.

INSTRUCTIONS FOR AUTHORS

Format of the paper

The paper should have the following structure:

- A Title, which adequately describes the content of the paper and should not exceed 80 characters;
- An Abstract, which should be viewed as a mini version of the paper and should not exceed 250 words. The Abstract should state the principal objectives and the scope of the investigation and the methodology employed; it should also summarise the results and state the principal conclusions;
- Immediately after the abstract, provide a maximum of 6 keywords;
- An Introduction, which should provide a review of recent literature and sufficient background information to allow the results of the paper to be understood and evaluated;
- A Theoretical section;
- An Experimental section, which should provide details of the experimental set-up and the methods used to obtain the results;
- A Results section, which should clearly and concisely present the data, using figures and tables where appropriate;
- A Discussion section, which should describe the relationships shown and the generalisations made possible by the results and discuss the significance

Podatki o avtorjih

Članku priložite tudi podatke o avtorjih: imena, nazive, popolne poštne naslove, številke telefona in faksa, naslove elektronske pošte. Navedite kontaktno osebo.

Sprejem člankov in avtorske pravice

Uredništvo si pridržuje pravico do odločanja o sprejemu članka za objavo, strokovno oceno mednarodnih recenzentov in morebitnem predlogu za krajšanje ali izpopolnitev ter terminološke in jezikovne korekture. Z objavo preidejo avtorske pravice na revijo ACTA GEOTECHNICA SLOVENICA. Pri morebitnih kasnejših objavah mora biti AGS navedena kot vir.

Vsa nadaljnja pojasnila daje:

Uredništvo
ACTA GEOTECHNICA SLOVENICA
Univerza v Mariboru,
Fakulteta za gradbeništvo
Smetanova ulica 17, 2000 Maribor, Slovenija
E-pošta: ags@uni-mb.si

- of the results, making comparisons with previously published work;
- Conclusions, which should present one or more conclusions that have been drawn from the results and subsequent discussion;
- A list of References, which comprises all the references cited in the text, and vice versa.

Additional Requirements for Manuscripts

- Use double line-spacing.
- Insert continuous line numbering.
- The submitted text of Research Papers should cover no more than 18 pages (without Tables, Legends, and References, style: font size 12, double line spacing). The number of illustrations should not exceed 10. Results may be shown in tables or figures, but not in both of them.
- Please submit, with the manuscript, the names, addresses and e-mail addresses of four potential referees. Note that the editor retains the sole right to decide whether or not the suggested reviewers are used.

Units and abbreviations

Only standard SI symbols and abbreviations should be used in the text, tables and figures. Symbols for physical quantities in the text should be written in *Italics* (e.g. ν , T , etc.). Symbols for units that consist of letters should

be in plain text (e.g. Pa, m, etc.).

All abbreviations should be spelt out in full on first appearance.

Figures

Figures must be cited in consecutive numerical order in the text and referred to in both the text and the caption as Fig. 1, Fig. 2, etc. Figures may be saved in any common format, e.g. BMP, JPG, GIF. However, the use of CDR format (CorelDraw) is recommended for graphs and line drawings, since vector images can be easily reduced or enlarged during final processing of the paper.

When labelling axes, physical quantities (e.g. v , T , etc.) should be used whenever possible. Multi-curve graphs should have individual curves marked with a symbol; the meaning of the symbol should be explained in the figure caption. Good quality black-and-white photographs or scanned images should be supplied for the illustrations.

Tables

Tables must be cited in consecutive numerical order in the text and referred to in both the text and the caption as Table 1, Table 2, etc. The use of names for quantities in tables should be avoided if possible: corresponding symbols are preferred. In addition to the physical quantity, e.g. t (in Italics), units (normal text), should be added on a new line without brackets.

Any footnotes should be indicated by the use of the superscript¹.

LIST OF REFERENCES

Citation in text

Please ensure that every reference cited in the text is also present in the reference list (and vice versa). Any references cited in the abstract must be given in full. Unpublished results and personal communications are not recommended in the reference list, but may be mentioned in the text, if necessary.

Reference style

Text: Indicate references by number(s) in square brackets consecutively in line with the text. The actual authors can be referred to, but the reference number(s) must always be given:

Example: "... as demonstrated [1,2]. Brandl and Blovsky [4] obtained a different result ..."

List: Number the references (numbers in square brackets) in the list in the order in which they appear in the text.

Reference to a journal publication:

- [1] Jelušič, P., Žlender, B. 2013. Soil-nail wall stability analysis using ANFIS. *Acta Geotechnica Slovenica* 10(1), 61-73.

Reference to a book:

- [2] Šuklje, L. 1969. Rheological aspects of soil mechanics. Wiley-Interscience, London

Reference to a chapter in an edited book:

- [3] Mitchel, J.K. 1992. Characteristics and mechanisms of clay creep and creep rupture, in N. Guven, R.M. Pollastro (eds.), *Clay-Water Interface and Its Rheological Implications*, CMS Workshop Lectures, Vol. 4, The clay minerals Society, USA, pp. 212-244.

Conference proceedings:

- [4] Brandl, H., Blovsky, S. 2005. Slope stabilization with socket walls using the observational method. *Proc. Int. conf. on Soil Mechanics and Geotechnical Engineering*, Bratislava, pp. 2485-2488.

Web references:

- [5] As a minimum, the full URL should be given and the date when the reference was last accessed. Any further information, if known (DOI, author names, dates, reference to a source publication, etc.), should also be given.

Author information

The following information about the authors should be enclosed with the paper: names, complete postal addresses, telephone and fax numbers and E-mail addresses. Indicate the name of the corresponding author.

Acceptance of papers and copyright

The Editorial Committee of the Slovenian Geotechnical Review reserves the right to decide whether a paper is acceptable for publication, to obtain peer reviews for the submitted papers, and if necessary, to require changes in the content, length or language.

On publication, copyright for the paper shall pass to the ACTA GEOTECHNICA SLOVENICA. The AGS must be stated as a source in all later publication.

For further information contact:

Editorial Board

ACTA GEOTECHNICA SLOVENICA

University of Maribor,

Faculty of Civil Engineering

Smetanova ulica 17, 2000 Maribor, Slovenia

E-mail: ags@uni-mb.si

NAMEN REVIJE

Namen revije ACTA GEOTECHNICA SLOVENICA je objavljane kakovostnih teoretičnih člankov z novih pomembnih področij geomehanike in geotehnike, ki bodo dolgoročno vplivali na temeljne in praktične vidike teh področij.

ACTA GEOTECHNICA SLOVENICA objavlja članke s področij: mehanika zemljin in kamnin, inženirska geologija, okoljska geotehnika, geosintetika, geotehnične konstrukcije, numerične in analitične metode, računalniško modeliranje, optimizacija geotehničnih konstrukcij, terenske in laboratorijske preiskave.

Revija redno izhaja dvakrat letno.

AVTORSKE PRAVICE

Ko uredništvo prejme članek v objavo, prosi avtorja(je), da prenese(jo) avtorske pravice za članek na izdajatelja, da bi zagotovili kar se da obsežno razširjanje informacij. Naša revija in posamezni prispevki so zaščiteni z avtorskimi pravicami izdajatelja in zanje veljajo naslednji pogoji:

Fotokopiranje

V skladu z našimi zakoni o zaščiti avtorskih pravic je dovoljeno narediti eno kopijo posameznega članka za osebno uporabo. Za naslednje fotokopije, vključno z večkratnim fotokopiranjem, sistematičnim fotokopiranjem, kopiranjem za reklamne ali predstavitvene namene, nadaljnjo prodajo in vsemi oblikami nedobičkonosne uporabe je treba pridobiti dovoljenje izdajatelja in plačati določen znesek.

Naročniki revije smejo kopirati kazalo z vsebino revije ali pripraviti seznam člankov z izvlečki za rabo v svojih ustanovah.

Elektronsko shranjevanje

Za elektronsko shranjevanje vsakršnega gradiva iz revije, vključno z vsemi članki ali deli članka, je potrebno dovoljenje izdajatelja.

ODGOVORNOST

Revija ne prevzame nobene odgovornosti za poškodbe in/ali škodo na osebah in na lastnini na podlagi odgovornosti za izdelke, zaradi malomarnosti ali drugače, ali zaradi uporabe kakršnekoli metode, izdelka, navodil ali zamisli, ki so opisani v njej.

AIMS AND SCOPE

ACTA GEOTECHNICA SLOVENICA aims to play an important role in publishing high-quality, theoretical papers from important and emerging areas that will have a lasting impact on fundamental and practical aspects of geomechanics and geotechnical engineering.

ACTA GEOTECHNICA SLOVENICA publishes papers from the following areas: soil and rock mechanics, engineering geology, environmental geotechnics, geosynthetic, geotechnical structures, numerical and analytical methods, computer modelling, optimization of geotechnical structures, field and laboratory testing.

The journal is published twice a year.

COPYRIGHT

Upon acceptance of an article by the Editorial Board, the author(s) will be asked to transfer copyright for the article to the publisher. This transfer will ensure the widest possible dissemination of information. This review and the individual contributions contained in it are protected by publisher's copyright, and the following terms and conditions apply to their use:

Photocopying

Single photocopies of single articles may be made for personal use, as allowed by national copyright laws. Permission of the publisher and payment of a fee are required for all other photocopying, including multiple or systematic copying, copying for advertising or promotional purposes, resale, and all forms of document delivery.

Subscribers may reproduce tables of contents or prepare lists of papers, including abstracts for internal circulation, within their institutions.

Electronic Storage

Permission of the publisher is required to store electronically any material contained in this review, including any paper or part of the paper.

RESPONSIBILITY

No responsibility is assumed by the publisher for any injury and/or damage to persons or property as a matter of product liability, negligence or otherwise, or from any use or operation of any methods, products, instructions or ideas contained in the material herein.



Univerza v Mariboru

www.fg.um.si

Univerza
v Ljubljani



Fakulteta
za gradbeništvo
in geodezijo
Naravoslovnotehniška
Fakulteta

www.fgg.uni-lj.si
www.ntf.uni-lj.si



www.sloged.si

SLOVENSKO DRUŠTVO ZA
PODZEMNE GRADNJE
SLOVENIAN SOCIETY FOR
UNDERGROUND STRUCTURES

www.ita-slovenia.si